

TWC

# University of Utah

## Department of Chemical Engineering

1972-0407

72-0407

THE RESPONSE OF A BURNING SOLID PROPELLANT  
SURFACE TO THERMAL RADIATION

by

C. Max Muhlfeith, Alva D. Baer, and Norman W. Ryan

Grant No. AFOSR-1656-69

August 1, 1971

"APPROVED FOR PUBLIC RELEASE: DISTRIBUTION UNLIMITED"



JAN 18 1972

RECEIVED

AD 736 049

Salt Lake City, Utah

Distribution of this document is unlimited.

Distribution Statement A:  
Approved for public release;  
distribution is unlimited.

F21205

**Private STINET**[Home](#) | [Collections](#)[View Saved Searches](#) | [View Shopping Cart](#) | [View Orders](#)[Add to Shopping Cart](#)

Other items on page 1 of your search results: 1

[View XML](#)

Citation Format: Full Citation (1F)

**Accession Number:**

AD0736049

**Citation Status:**

Active

**Citation Classification:**

Unclassified

**SBI Site Holding Symbol:**

TAV

**Fields and Groups:**

210200 - Combustion and Ignition

210902 - Solid Rocket Propellants

**Corporate Author:**

UTAH UNIV SALT LAKE CITY DEPT OF CHEMICAL ENGINEERING

**Unclassified Title:**

(U) The Response of a Burning Solid Propellant Surface to Thermal Radiation.

**Title Classification:**

Unclassified

**Descriptive Note:**

Technical rept.,

**Personal Author(s):**

Mihlfeith, C Max

Baer, Alva D

Ryan, Norman W

**Report Date:**

01 Aug 1971

**Media Count:**

158 Page(s)

**Cost:**

\$14.60

**Contract Number:**

AF-AFOSR-1656-69

**Report Number(s):**

AFOSR-TR-71-2664

**Project Number:**

AF-9711

**Task Number:**

971101

**Monitor Acronym:**

AFOSR

**Monitor Series:**

TR-71-2664

**Report Classification:**

Unclassified

**Descriptors:**

(U) (\*SOLID ROCKET PROPELLANTS, THERMAL ANALYSIS), (\*SOLID PROPELLANT ROCKET ENGINES, INTERIOR BALLISTICS), COMBUSTION, BURNING RATE, THERMAL RADIATION, HEAT FLUX, MATHEMATICAL MODELS, EXPERIMENTAL DATA

**Identifiers:**

(U) L BURNERS, T BURNERS

**Identifier Classification:**

Unclassified

**Abstract:**

(U) A new technique for the study of processes related to propellant combustion instability has been employed in which burning rate variations produced by a periodic radiant heat flux are measured. The phase angle between the perturbing flux and the burning rate response and the dependence of the magnitude of the response on the driving frequency are obtained. As the frequency of the perturbing flux increases, magnitude of the reaction is observed to first increase and then to pass through a maximum. In general, the experimental results tend to confirm the theoretical models for transient burning rate response, although the observed maximums in the response functions appear to occur at higher frequencies than is predicted by the simpler gas-phase models. (Author)

**Abstract Classification:**

Unclassified

**Distribution Limitation(s):**

01 - APPROVED FOR PUBLIC RELEASE

**Source Code:**

363025

**Document Location:**

DTIC AND NTIS



---

[Privacy & Security Notice](#) | [Web Accessibility](#)

[private-stinet@dtic.mil](mailto:private-stinet@dtic.mil)



UNIVERSITY OF UTAH

DEPARTMENT OF CHEMICAL ENGINEERING

*Technical Report*

on

THE RESPONSE OF A BURNING SOLID PROPELLANT  
SURFACE TO THERMAL RADIATION

by

C. Max Muhlfeith, Alva D. Baer, and Norman W. Ryan

Grant No. AFOSR-1656-69

August 1, 1971

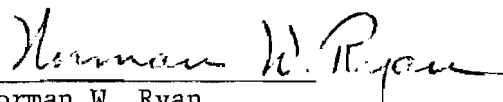
"APPROVED FOR PUBLIC RELEASE: DISTRIBUTION UNLIMITED"

This research under Grant AF AFOSR 69-1656, for the period October, 1968, through September, 1971, was sponsored by the Air Force Office of Scientific Research, Office of Aerospace Research, United States Air Force.

The Technical Supervisor for this program is Lt. Col. Richard W. Haffner, Project Scientist, Energetics Division, Directorate of Engineering Sciences, Air Force Office of Scientific Research (AFSC).

This report was prepared by C. M. Muhlfeith, Alva D. Baer, and Norman W. Ryan.

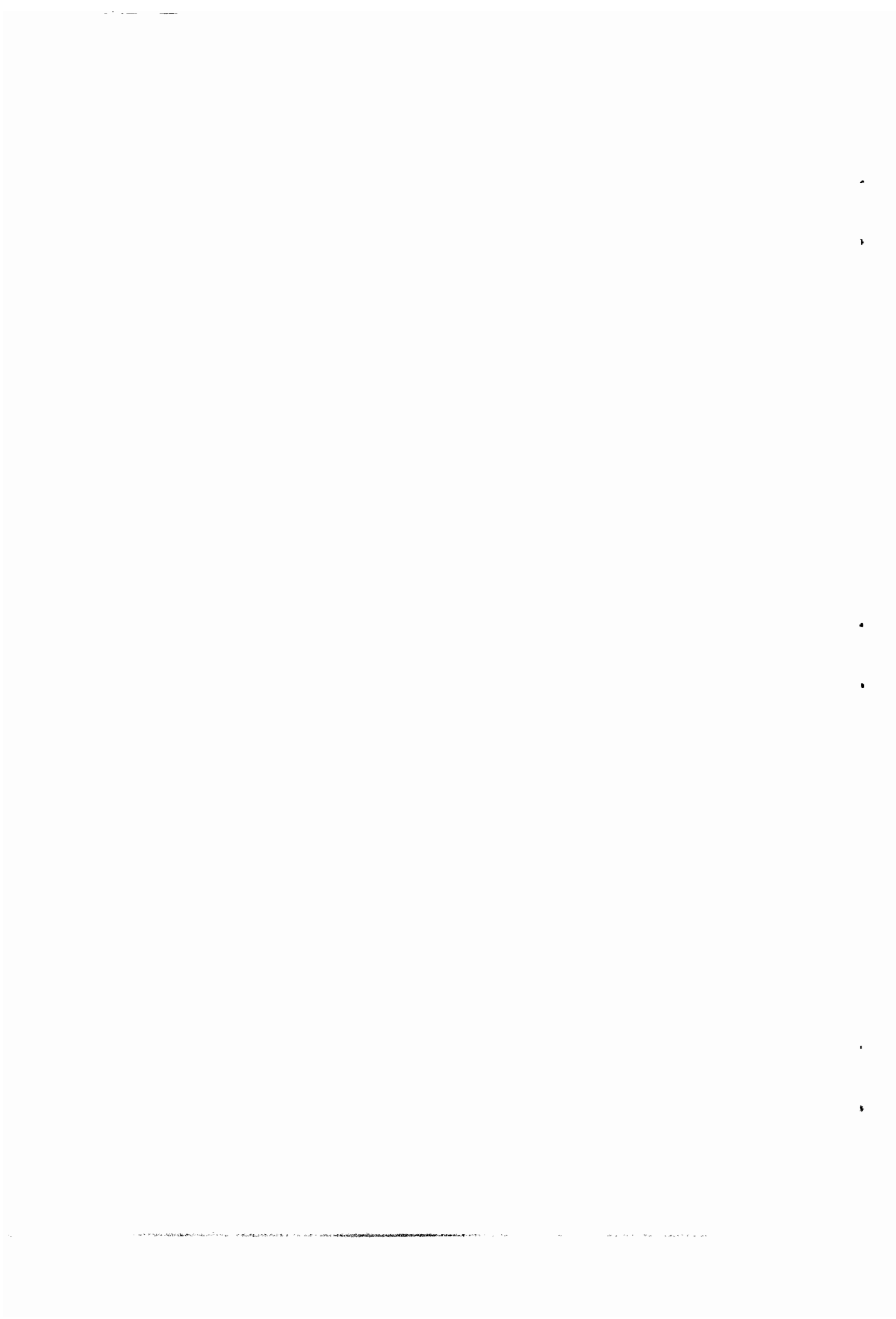
Report approved by

  
Norman W. Ryan  
Principal Investigator



## TABLE OF CONTENTS

Acknowledgements - - - - -	iii
Abstract - - - - -	vi
List of Figures - - - - -	ix
CHAPTER I: INTRODUCTION - - - - -	1
CHAPTER II: DISCUSSION OF RELATED EXPERIMENTS - - - - -	4
CHAPTER III: THEORETICAL CONSIDERATIONS - - - - -	10
A. Surface and Condensed Phase Energy Sources - - - - -	10
B. Mass Efflux at a Burning Surface - - - - -	15
C. Response of a Burning Solid Propellant to Pressure Perturbations - - - - -	16
D. Propellant Response to Radiant Heat Flux Perturbations - - - - -	21
1. Gas Phase Analysis - - - - -	22
2. Analysis of the Solid Phase of an Opaque Propellant - - - - -	24
3. Matching Conditions at the Solid-Gas Interface - - - - -	26
4. Burning Rate Response of an Opaque Propellant -	28
5. Analysis of the Solid Phase for a Translucent Propellant - - - - -	29
6. Matching Conditions and Burning Rate Response for a Translucent Propellant - - - - -	33
E. Burning Rate Response to Pressure Perturbations - - -	34
F. Relationship Between Mass Flux Perturbations and the Transient Force - - - - -	35
G. Results of a Parametric Study of the Burning Rate Model - - - - -	37
CHAPTER IV: APPARATUS GENERAL FEATURES - - - - -	44
A. Radiant Source Unit - - - - -	45
B. Measurement of the Flux Profile - - - - -	46
C. Combustion Chamber - - - - -	49



CHAPTER V: THERMAL RADIATION AUGMENTATION OF AP COMPOSITE PROPELLANT BURNING	52
A. Burning Rate Measurements	53
B. Procedure for Measuring Steady Burning Rates	54
C. Absorption of Radiation Due to the Propellant Flame	56
D. Data from Steady Burning Rate Experiments	58
E. Factors Influencing the Net Heat Effect	63
CHAPTER VI: TRANSIENT BURNING RATE EXPERIMENTS	67
A. Equipment: Microphone Adapted as a Transient Force Transducer	67
B. Propellant Used for the Transient Burning Rate Experiments	71
C. Procedure for Transient Burning Rate Experiments	73
D. Data Acquisition and Reduction	75
E. Polyurethane Propellants	84
F. Polybutadiene Propellants	91
G. Phase Angle Measurements	96
H. Comparison with L*-Burner and T-Burner Data	104
CHAPTER VII: CONCLUSIONS AND RECOMMENDATIONS	110
A. Radiation Augmentation of Composite Propellant Combustion	110
B. Transient Burning Rate Experiments	110
REFERENCES:	113
APPENDIX A: NOMENCLATURE	121
APPENDIX B: RADIANT HEAT FLUX PROFILES FOR RADIATION FURNACE	124
APPENDIX C: SUMMARY TABLE OF DATA	128



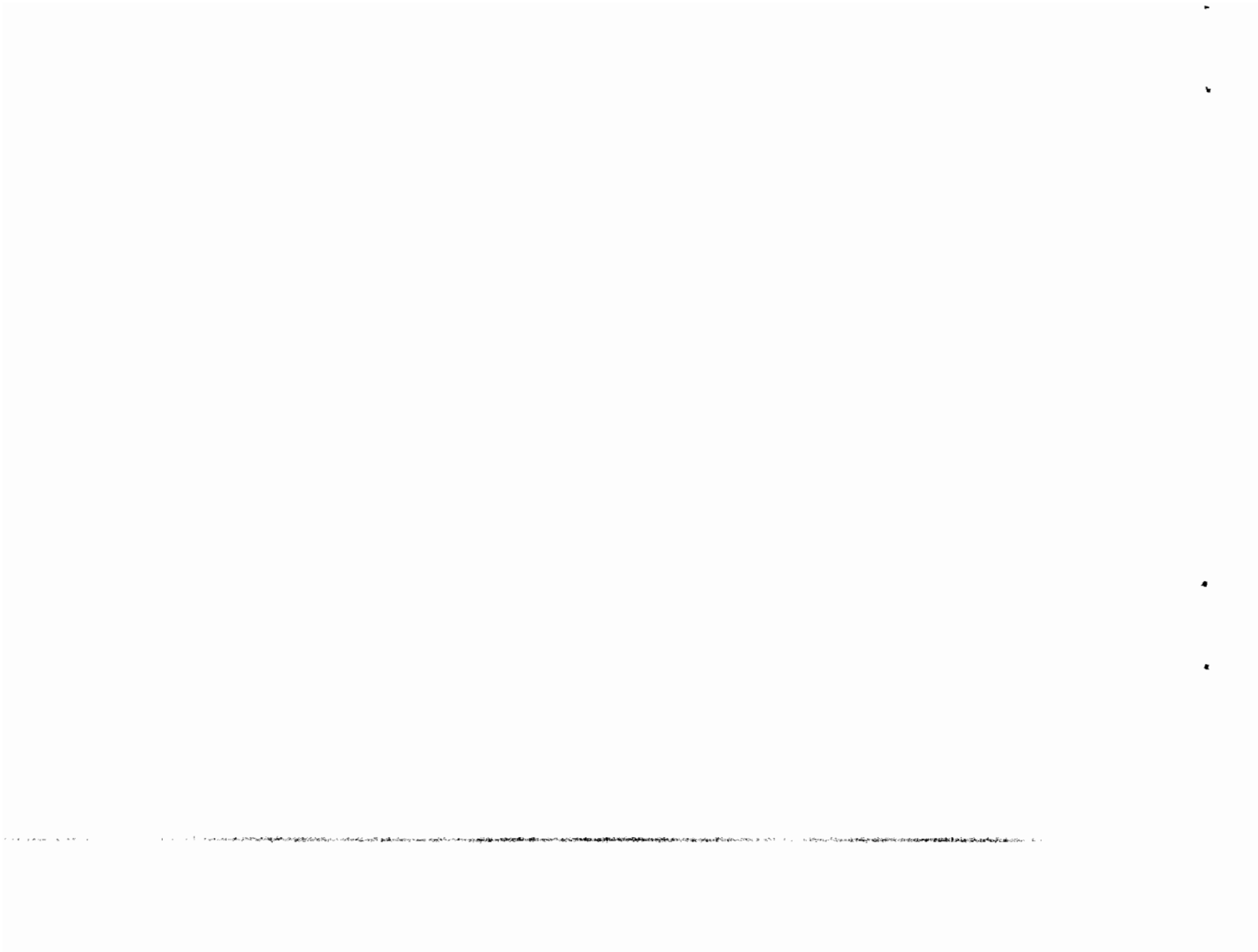


## ABSTRACT

*Start*

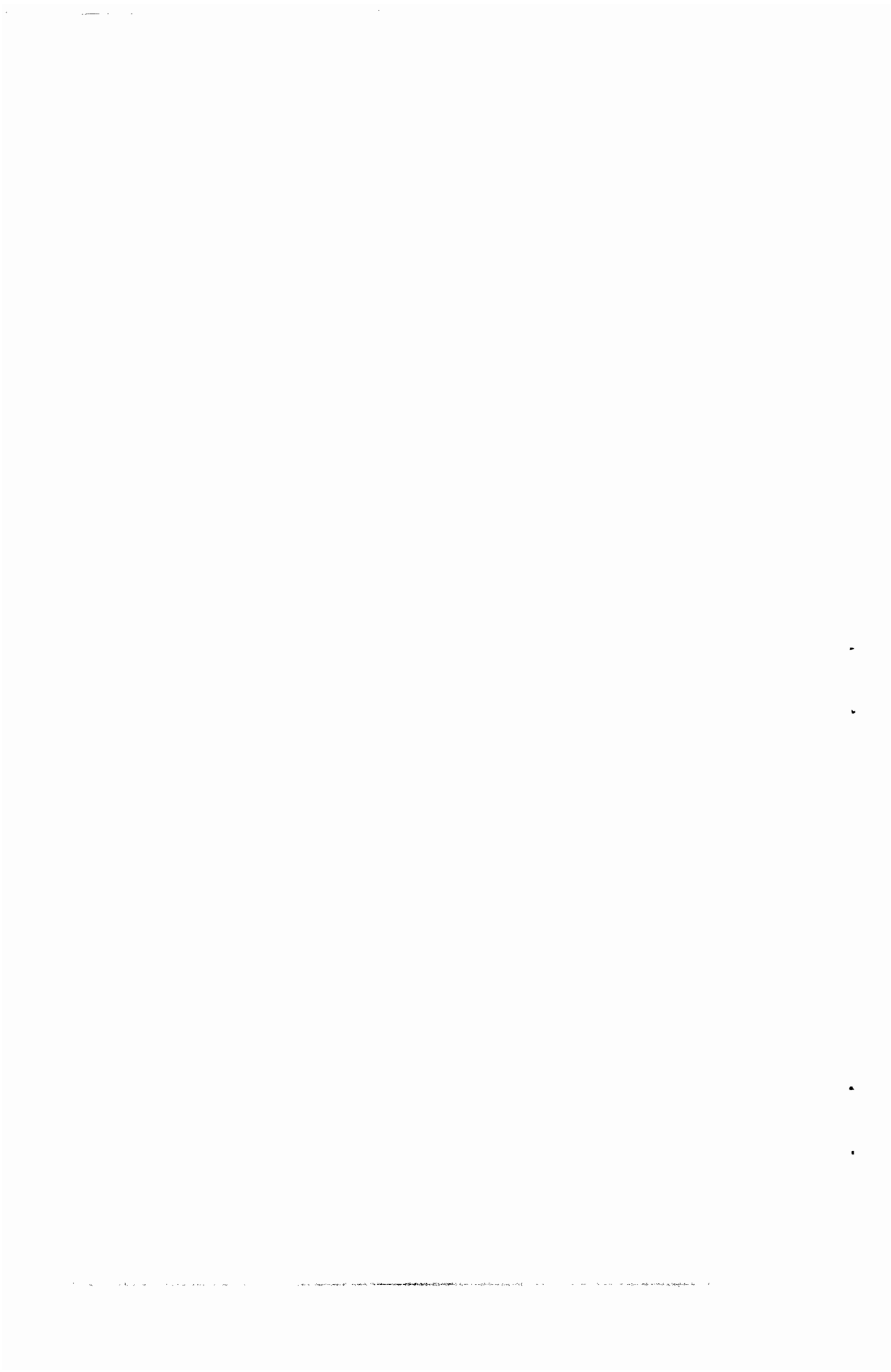
A direct measurement was made of the dynamic response of burning solid-propellant strands to an externally imposed radiant heat flux. Burning rate changes were determined for both steady and periodic energy fluxes at atmospheric pressure. The strands were mounted at the secondary focus of an elliptical mirror system, and flux levels to  $15 \text{ cal/}(\text{sec})(\text{cm}^2)$  were obtained by use of a 5kw Xenon-Mercury lamp. Steady-state burning rates were obtained by a photographic technique, and the periodic variations in mass evolution rates were detected by measurement of the recoil force on the strands. A quartz-crystal microphone was used as a micro-force transducer.

The heat flux response function, defined as  $(m'/\bar{m})(F'/\bar{F})$  where  $m$  and  $F$  are mass rate and heat flux respectively and the prime and overbar denote perturbed and steady-state quantities, which was measured in this experiment, is closely related to the pressure,  $p$ , response function,  $(m'/\bar{m})(p'/\bar{p})$  which is important to the combustion stability of a solid propellant in an engine. The approximate correspondence of these two response functions was demonstrated by calculations based upon current transient combustion theories. The sharp flame front model was employed for the gas phase, and the usual assumptions of a homogeneous, passive solid with energy release at the surface and an Arrhenius type regression law were employed. Both response functions were calculated as a function of the dimensionless



perturbing frequency ( $\Omega = \omega \alpha / \bar{r}^2$  where  $\omega$  is the radiant frequency,  $\alpha$  the propellant thermal diffusivity and  $\bar{r}$  the mean burning rate) for the same fixed parameters. At low frequencies, the response functions are essentially identical and both exhibit maxima in the response at nearly the same frequency in the range of dimensionless frequencies of 6-50. At high frequencies, the pressure response is higher than the flux-driven response apparently because of the effect of rapidly responding gas-phase processes. For the opaque propellant, the correspondence is close enough that values of the flux-driven response are relatable to the more practically important pressure-coupled response.

Response functions were experimentally determined for several ammonium perchlorate oxidized composite propellants. A strong effect of propellant transmissivity was theoretically predicted and experimentally observed. Semi-transparent propellants showed little response to periodic heat fluxes; and as the opacity of a propellant system was increased, both the magnitude of the response and the frequency of the maximum in the response function increased. The response functions of the opaque, polyurethane-fueled propellants exhibited maxima in the dimensionless frequency range of 10-40, while the response functions of the polybutadiene-acrylic-acid co-polymer-fueled propellants were uniformly high without significant maximum. The measured responses were reproducible and moderate changes in the propellant formulation could be detected by changes in the response.



This experimental technique holds promise as a sensitive method for evaluation of the combustion stability characteristics of solid propellants.

In general, the experimental data were in qualitative agreement with the theoretical predictions; and the essential validity of the current concepts of the nature of the burning surface response to perturbations has been supported. For a given system, the observed behavior can be described by appropriate adjustment of the parameters in the phenomenological models; although in the same cases, the physical interpretation of the values of these parameters is clouded. Because it is now possible to measure directly the response over a wide range of frequencies, it should be possible to evaluate combustion instability theories on the basis of the reasonableness of the parameter values required to describe the observed response functions.

*J. H. (H. W.)*

■

■

■

■

## LIST OF FIGURES

<u>Figure</u>	<u>Title</u>	<u>Page</u>
3-1	Schematic Diagram of a Burning Solid Propellant Interface	12
3-2	Effect of Surface Reaction Activation Energy on the Response Function.	38
3-3	Effect of Surface Temperature on the Response Function	39
3-4	Effect of the Heat of Vaporization on the Response Function	40
3-5	Effect of the Extinction Coefficient on the Response Function	41
3-6	Effect of the Heat of Vaporization on the Phase Angle Between the Imposed Flux and the Mass Flux Perturbation	42
4-1	General View of the Radiation Furnace, Combustion Chamber, and Data Acquisition Equipment	48
4-2	Closeup View of the Data Acquisition and Data Processing Equipment	48
4-3	Attachments for Various Experiments	50
4-4	Combustion Chamber and the Three-axis Positioning Stages	50
5-1	Combustion Chamber with the Mount Used in the Burning Rate Experiments	55
5-2	The Effect of External Thermal Radiation on Composite Propellant Burning Rates	59
5-3	The Effect of Surface Temperature on the Net Heat of Gasification	66





6-1	Micro-Force Transducer and Propellant Mount for Transient Burning Rate Experiments	69
6-2	Block Diagram of Data Acquisition and Data Analysis Procedure for Transient Burning Rate Experiments	76
6-3	Typical Output for Transient Burning Rate Experiments	77
6-4	Strip Chart Record of Micro-Force Transducer Signal	79
6-5	Strip Chart Record of Micro-Force Transducer Signal	80
6-6	Mean Value of Transducer Signal for Propellant UBU	85
6-7	Mean Value of Transducer Signal for Propellant UAX	86
6-8	Mean Value of Transducer Signal for Propellant UCX	87
6-9	Normalized Value of Transducer Signal for PU-AP Propellants	90
6-10	Mean Value of Transducer Signal for Propellant UCV	92
6-11	Mean Value of Transducer Signal for Propellant UCW	93
6-12	Normalized Value of Transducer Signal for PBAA-AP Propellants	95
6-13	Phase Angle for Propellant UBU	97
6-14	Phase Angle for Propellant UAX	98
6-15	Phase Angle for Propellant UCX	99
6-16	Phase Angle for Propellant UCV	100
6-17	Phase Angel for Propellant UCW	101
6-18	Phase Angle Lag for PU Propellants	102
6-19	Phase Angle Lag for PBAA Propellants	103
6-20	Comparison Between Transducer Signal, L*-Burner and T-Burner Data	108



## CHAPTER I: INTRODUCTION

Solid rockets have been employed extensively since the early 1940's as propulsive devices for weapons systems and the instrument packages of a wide variety of scientific investigations. The present methods used in the design of rockets are adequate to insure production of reliable rockets for a great variety of specific missions. However, truly optimal design requires a detailed understanding of the many processes involved in the operation of the solid propellant motor. Ultimately, the propulsion engineer would like to be able to predict both steady state and transient burning rates from a knowledge of the thermochemistry of the ingredients, the chamber pressure, and the appropriate chemical reaction rates. Such a goal is presently far from being realized, primarily due to a lack of fundamental knowledge concerning the combustion dynamics and energy release rates. Further information on the propellant combustion processes and its dependence on physiochemical factors such as the extent of solid phase chemical reaction, the influence of gas phase energy release, and the effect of acoustic fields within the gas cavity is highly desirable. It is the task of laboratory research to supply such knowledge, and the objective of the present study was to generate this type of information.

In the past, laboratory studies have characterized the overall nature of the combustion process both in the steady state and under transient conditions. Further development of our understanding now

requires more detailed mechanistic studies; and because of the complex nature of the combustion processes, new and unique experimental procedures must be used. It was believed that currently available devices for studying transient and steady state combustion processes, *i.e.*, strand bombs, T-burners, L\*-burners and thermochemical kinetic methods have been exploited to the point where little information fundamentally different from published results could be obtained. The decision to attempt some completely different experiments was made with the anticipation of developing a new approach from which a more complete understanding of composite propellant combustion processes could be gained. Specifically, external thermal radiant energy was used to drive the combustion process and to modify steady and transient burning rates.

The study described below is an investigation of some new and hopefully constructive experimental techniques directed at gaining a quantitative evaluation of: (1) the influence of steady thermal radiation on propellant burning rates, and (2) the magnitude and frequency dependence of combustion irregularities (mass efflux) which are induced by periodic variations in heat fluxes to the surface.

The experiments were designed to avoid modification of the combustion process to unrealistic conditions, and attention was centered on processes occurring near the solid-gas interface.

This presentation is divided into a discussion of related previous experiments, theoretical considerations relevant to the results of

experiments successfully completed and finally a description of the experimental results and their significance. The experiments fall naturally into two distinct, but related, categories and are discussed in separate chapters. These categories are: (1) the thermal radiation augmentation of steady propellant burning, (2) the dynamic response of burning to periodic variations of the heat flux.

Conclusions drawn from the analysis of the results are presented along with recommendations for further studies, in the final chapter. Reference [56] presents a discussion of several other studies which were done and are related to the main theme of this work. Short tables and figures are included in the text and are labeled with the appropriate chapter number. Detailed tables of data are in Appendix C.

## CHAPTER II: DISCUSSION OF RELATED EXPERIMENTS

Logically, any discussion of transient combustion effects should start with a discussion of steady burning. The results of the empirical observations of steady burning are easily correlated. The burning rate is a simple function of pressure and initial propellant temperature. However, the calculation of burning rates from heat transfer and reaction rate data has not been totally satisfactory. Some partially successful attempts have been made to predict steady state combustion rates from standard laboratory thermochemical measurements. Physiochemical data required in the proposed burning rate models such as activation energies, pre-exponential factors, decomposition kinetics and energy effects, are assumed to be determinable by slow heating devices such as DTA and TGA units [54,78]. For example, it has been shown by Waesche and Wenograd [78] that the burning rate of an AP-PBAA composite propellant can be estimated from the decomposition kinetics of the condensed phase. Their estimates are low by a factor of two or three when compared to the burning rates determined in a strand bomb. The difference is likely the result of additional energy available from the flame when the propellants are actually burned. Experiments employing a self heating calorimeter [38], hot wire ignition [2], [4], and ignition initiated by radiant energy [60] have also been used to determine the activation energy and energy release rates, but the results of such tests have not been successfully applied to the burning process.

Reviews of the theory of thermal explosions and associated experimental techniques as methods for formal kinetic studies in the condensed phase are available [1,55]. However, use of such experimental techniques requires the application of non-linear curve fitting schemes for the interpretation of the data. It would appear that the techniques currently being exploited yield only qualitative information relevant to the steady state burning rate.

Either because the attempts to predict steady burning rates from first principles or from the results of independent laboratory tests have not been very successful or because of the practical importance of transient combustion problems, a greater effort has been expended on an attempt to understand the unsteady state processes even though the steady state phenomenon is not completely understood. The emphasis of the present study is influenced by such considerations, and in particular, the major effort was made to elucidate the processes which are important during oscillatory combustion.

In the prior studies of oscillatory solid propellant combustion, the frequency and rate of increasing magnitude of the gas cavity pressure oscillations were used to characterize the stability of the propellant combustion. Often the observed frequencies can be associated with the acoustic modes of the chamber, and the growth of the periodic pressure disturbances is termed acoustic instability. Various simple geometry burners have been designed to study unstable combustion under reasonably well-defined conditions similar to



conditions existing in a rocket motor. A cylindrical cavity with burning propellant discs at each end and vented at the center, 'T-burner,' has become a widely accepted device for studying the stability of solid propellants. Operation of such a unit depends primarily on the growth and/or decay of self-excited oscillatory pressures [13,32,59,66]. Many experimental studies have been completed during the past decade, but the successful application of these results to motor design remains to be demonstrated [14]. The studies have included effects of aluminum [59], burning rate retardants [7], total pressure, *i.e.*, burning rate [34] and composition variables [32], but there still remains the problem of transforming the T-burner data into relationships which the rocket motor designer could apply. Normally, the logarithmic growth rate of pressure oscillations in the T-burner is related to the response function of the burning surface after correcting for acoustic losses. The response function is assumed to be a property of the propellant and of pressure, and constancy of this function is required to transform results between the T-burner and the rocket motor. A problem with this approach is the *a priori* assumption of the existence of the acoustic response function. No one has ever made a direct measurement of the mass efflux-pressure coupled response of the propellant, and all published characteristics of such functions are inferred from T-burner type measurements. Further knowledge of the combustion process is required to evaluate this point.

Another type of combustion instability often observed occurs at

non-acoustic frequencies. This phenomenon seems to be related to gas phase combustion inefficiencies inside the combustion chamber and the solid-phase thermal wave fluctuations. Such instability is normally observed at low values for the ratio of the rocket nozzle area to the chamber volume ( $L^*$ ). Special small motors have been built to study this phenomenon. Studies have been made with respect to stability limits as set by burner area, pressure and oxidizer particle size [81]. Adequate theories to predict the stability limits have been developed, but certain physiochemical processes such as vaporization rate and its dependence on particle size and surface temperature, and the heat of vaporization require further consideration.

The T-burner and  $L^*$ -burners are only two of many bench scale devices designed to simulate real motor environments and operating conditions. Both the T-burner and low  $L^*$ -burner are used to generate data which can be employed to calculate the propellant response function. One set of experiments yields data for the low frequency regime, while the other T-burner tests, yields the data necessary for computing the high-frequency portion of the response function. In each case, an apparent coupling exists between the combustion chamber gas dynamics and the propellant burning rate response. The low  $L^*$ -burner is limited to a small range of low frequencies since the propellant thermal wave fluctuations, which are of significant magnitude only at low frequencies, drive the pressure. In the higher frequency region, where the T-burner operates, one witnesses primarily

the acoustic pressure coupling with the burning surface and the relative importance of the effects of gas-phase kinetics becomes greater than that of solid-phase thermal fluctuations.

Likely, no complete understanding of the combustion processes which lead to instability can be accomplished without the separate study of the controlling processes. A gas fired T-burner, recently developed at the University of Utah, enables one to study the gas-phase processes to determine the effect of mass flow rate and the chemical kinetics on the growth of sinusoidal oscillations [73]. This apparatus will hopefully permit the investigation of the interaction between chemical kinetics and acoustics. Other experimental work which was used to attempt to isolate the various steps are the propellant ingredient decomposition studies [10,11,12,22, 40,41,64], the use of pulsing or driven chambers [59] and the study of extinguishment by pressure decay [24,52].

The above discussion of composite propellant combustion experiments has been presented in order to place the present investigation in perspective with past experimental work. The most significant result of this review is the recognition that the present test devices do not yield data over a wide enough range of test conditions to completely describe the anticipated response function. There is an obvious need for data obtained over a wider range of frequencies. A direct measurement of the response is also required. One must conclude that in order to continue studies of solid propellant combustion, some new experimental technique needs to be developed.

Any results deduced by a new technique can, of course, be compared with the conclusions drawn from the more widely used methods.

The conditions under which the tests are made should also closely simulate the motor conditions; at least retention of the high heat flux from the natural flame is desirable. Since combustion irregularities are coupled to energy feedback from the gas phase, a disturbance in energy feedback of known magnitude should be useful in determining the magnitude of the propellant burning rate response. It is therefore desirable to perturb a 'steadily' burning propellant with an energy pulse great enough to modify the burning, but not great enough to modify the mode of burning.

In the present study, the natural energy feedback from the propellant flame was supplemented by use of a steady state or a periodic variation of thermal radiation focused on the burning propellant. The burning rate for the steady state radiation augmentation was measured using motion pictures. A high quality microphone was adapted as a force transducer for use in measuring the transient burning rates. Before discussing these experiments, consideration is now given to the theoretical aspects of combustion instability and of thermal radiation augmentation of the feedback heat flux.

### CHAPTER III: THEORETICAL CONSIDERATIONS

Two topics are discussed in this chapter: (1) the effect of solid phase or interfacial energy sources on propellant burning, and (2) the response of burning solid propellants to pressure and surface heat flux perturbations. The possibility of subsurface reactions within a burning solid propellant is considered and possible methods for deducing this heat effect are discussed. Unsteady burning of solid propellants is discussed in terms of the response function and a model of unsteady burning is discussed along with supporting computations. Generalizations drawn from a parametric study of the model are used in the discussion of data presented in later chapters. An equation for the propellant response to variations in the surface heat flux is also derived and discussed in relationship to pressure-driven oscillatory burning.

#### A: SURFACE AND CONDENSED PHASE ENERGY SOURCES

The current development of combustion models involves questions concerning the possibility of condensed phase reactions or reactions which influence the boundary conditions needed for matching the thermal energy equation at the solid-gas interface. It has been demonstrated theoretically by Marxman, *et al.*, [53] and theoretically, with supporting experimental data, by Brown, *et al.*, [7,8] that the

inclusion of an energy source term in the interfacial zone can produce broader pressure-frequency stability limits than the simpler model given by Denison and Baum [23].

Adiabatic calorimeters specially designed for testing propellants have also provided some evidence of subsurface and/or solid phase reactions [36]. Recent theoretical work treats the effect of subsurface reactions in the normal combustion of ammonium perchlorate propellants [10,11]. Ignition experiments have suggested the presence of an interfacial energy source [4], however, conclusive experimental evidence for such a thermal effect during normal burning has yet to be presented.

However, the pre-ignition thermal effect detected during ignition tests and the heat effects observed in adiabatic calorimetry as well as subsurface temperature measurements using fine thermocouples [67] are not necessarily valid evidence for near-surface heat effects suspected of existing during normal deflagration.

An idealization of the interfacial zone is depicted in Figure 3-1. A detailed thermal energy balance at the interface can be written with allowance for surface energy source terms. Since there is no adequate way to measure the energy feedback from the gas flame, although it has been attempted [67], one must admit the existence of the gas phase feedback heat flux and account for it in the surface energy balance [63,68].

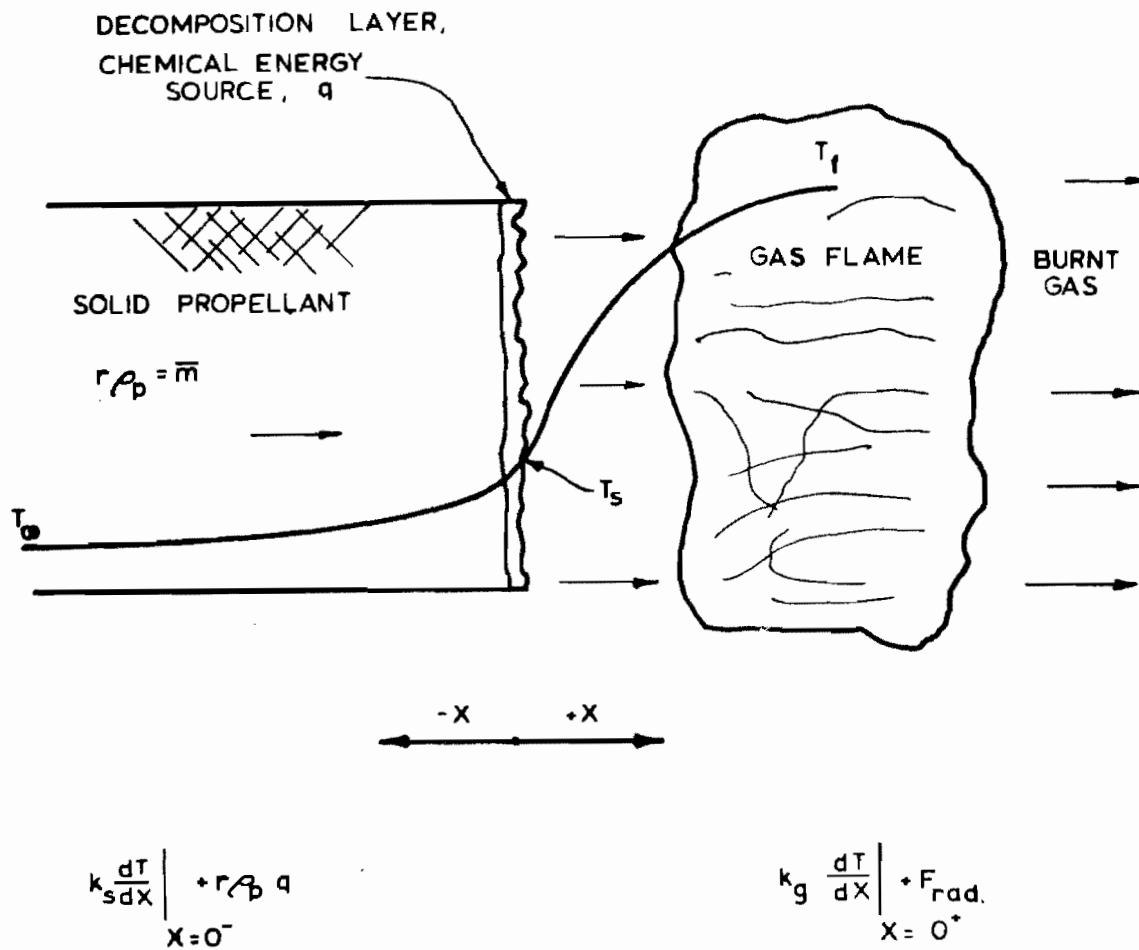


FIG. 3-1. Schematic Diagram of a Burning Solid Propellant Interface.

It can be shown that the thermal energy balance at the solid-gas interface of a solid propellant can be written as,

$$F = \rho r [C(T_s - T_{-\infty}) + q_s], \quad (3.1)$$

where

$F$  = total heat flux entering the solid phase,

$C$  = heat capacity of the solid phase,

$q_s$  = net heat effect of phase changes and chemical reactions occurring near the interface,

$\rho r = \dot{m}$  = mass burning rate.

In the following development,  $q_s$  is assumed to be a constant characteristic of the propellant, and is called the net heat of gasification.

Under the influence of a step input of heat flux, one observes a linear increase in burning rate which can be used to estimate the net heat of gasification,

$$\left(\frac{\partial r}{\partial F}\right)_{T_s, T_{-\infty}, q_s} = \frac{1}{\rho [C(T_s - T_{-\infty}) + q_s]}, \quad (3.2)$$

or

$$q_s = \frac{1}{\rho (\partial r / \partial F)_{T_s, T_{-\infty}, q_s}} - C(T_s - T_{-\infty}). \quad (3.3)$$

Equation 3.3 can be used to estimate the combustion parameter,  $q_s$ ,



from steady state radiation augmentation data. Such results are listed in Table 5-1 of Chapter V. It is also possible to estimate the value of  $q_s$  from rarefaction extinguishment tests [52] and from the effect of initial strand temperature on the steady state burning rate [49]; however, additional assumptions are required.

For the non-adiabatic situation employed in the present experiment, the flame temperature could be increased by partial absorption of the external radiant energy. However, the external flux was only a small fraction of the total energy release from the flame, so the flame temperature change would be negligible.

It has been postulated that  $q_s$  is perhaps a function of the propellant surface temperature, the oxidizer particle diameter, and the ambient pressure level [60]. Presumably, the burning rate dependence on the gasification process is treated since  $q_s$  is the energy per unit mass consumed. The current prejudice is that  $q_s$  may also be a function of the assumptions required by the measurement technique used.

Once it was demonstrated experimentally that a relatively small feedback flux would modify the linear burning rate of several composite propellants, the more interesting question of the transient burning, or dynamic response, was investigated. First, however, some consideration of the unsteady burning phenomenon must be presented.

## B: MASS EFFLUX AT A BURNING SURFACE

In this section, the relationship between a burning rate change and the physical reaction caused by this change is discussed. A possible method for determining this correspondence involves measuring the change in normal force generated at the surface when the burning rate of a propellant is modified by an external thermal energy source.

The total steady force,  $f$ , due to the combustion of a propellant strand is given by the steady state momentum equation,

$$f = r \rho A_b (v_e - \bar{r}) + A_b (P_o - P_\infty) . \quad (3.4)$$

The first term in equation 3.4 is the recoil force of the gases leaving the burning surface. Stationary laboratory coordinates are taken as the reference frame. The average regression rate,  $\bar{r}$ , is much less than the velocity of the combustion product,  $v_e$ , and can be neglected.

The pressure difference in equation 3.4 was approximated by the relationship,

$$P_o - P_f = \bar{m}^2 \frac{R}{PM} [\bar{T}_f - \bar{T}_o] , \quad (3.5)$$

where

$P_o$  = pressure near the propellant surface,

$P, P_f$  = pressure far from the propellant surface,

$M$  = average molecular weight of the gas phase,

$\bar{T}_f$  = average flame temperature,

$\bar{T}_o$  = gas temperature near the surface.

The total recoil force per unit area created by the mass efflux from the burning surface is given by equation 3.6,

$$f(t) = [m(t)]^2 \frac{RT_f}{PM} \quad (3.6)$$

The perturbed form of equation 3.6 is given in section F, page 35 in connection with the equations for the real part of the response function.

#### C: RESPONSE OF A SOLID PROPELLANT TO PRESSURE PERTURBATIONS

Much effort has been spent in the past on theoretical models for combustion instability observed in solid rockets. An early detailed model is that due to Hart and McClure [28]. More recent models of instability incorporate gas-phase effects [16] in order to treat the time delay features of gas-phase reactions. A very readable review and discussion of combustion instability is given by Culick [15] in which strong emphasis is given to interfacial conditions, with and without source terms, and distributed chemical energy release in the gas phase. One common feature of most theoretical models is that the level of sophistication implied by the analysis

is so great that direct evaluation of the models from simple experiments is unlikely.

All of the models previously developed treat the solid phase in the same manner. The differences which exist between the various models is due primarily to differences in the gas phase model and to considerations of surface-coupled reactions. A recent, relatively complete theory was given by Denison and Baum [23]. Since their work was presented, others have adapted their approach and attempted to apply it to similar types of unstable combustion. Marxman and Wooldridge [53] allow for surface-coupled reactions and present essentially the same result as Denison and Baum *via* transformations into three parameters, representing eight independent variables. Their analysis was used to rationalize the results of pressurization and depressurization experiments where interfacial sources tend to determine the extinguishment boundary. Brown, Muzzy and Stienle [8] develop a similar analysis and apply it to T-burner response functions in an effort to rationalize the shift in the response curve as additives supposedly modify the interfacial thermal energy sources. Their principal thesis is that since nearly all analysis result in a two-parameter equation for the response function, as claimed by Culick [15], one need only to determine these parameters and the response function is established for all conditions. The model presented by Krier, T'ien, Sirignano, and Summerfield [48] includes a linearized pyrolysis law and an improved gas phase model.

However, the final conclusions drawn are essentially the same as previous studies. The results from the theoretical study by Friedly and Petersen [26], wherein each of six variables were varied independently, predict that the resonance point is determined primarily by the surface reaction activation energy and surface temperature, *i.e.*, parameter A in the response function expression. The pre-exponential factor for surface-coupled reactions is eliminated from the results of the analysis so its importance can not be accessed.

A reportedly different approach which treats solid phase reactions has been advanced by Culick [20]. Instead of treating the effects of decomposition totally in the boundary condition, a finite region of solid-phase reactions is allowed. Decomposition within this layer is dependent on the temperature, but not the pressure. A simplified model for the gas phase, although somewhat improved over the model by Denison and Baum, leads to a relatively simple expression for the solution of the gas-phase conservation equations. Whereas Marxman and Wooldridge assume constant heat release in the gas phase, Culick's model permits a fluctuation of the gas-phase energy release which is temperature and pressure dependent. This is accomplished by developing the assumption that the release rate depends linearly upon the temperature and pressure fluctuations. Solution of the energy equation in the solid phase is accomplished by the usual perturbation scheme for the specified inert and reactive regions. The matching of the temperature at the junction between the

two solid phase regions yields an expression for the fluctuating surface heat flux in terms of fluctuating surface temperature and fluctuating pressure. Continuity of the heat flux from the gas phase to the solid phase yields the relationship between pressure and mass burning rate. The real part of the solution of this expression is, by definition, the response function. Numerical results determined using a range of values for the large number of input parameters leads to the following conclusions:

1. The maximum in the response function as a function of frequency occurs at a higher frequency as the activation energy of the surface pyrolysis is increased.
2. When decomposition reactions are included, reasonable response functions are obtained only for decomposition reactions which are exothermic. This seems to be a general result for all models, regardless of the values assigned to other parameters.
3. There is only a weak dependence of the response function on the temperature sensitivity of the decomposition reactions in the solid phase. Evidently the importance of the solid phase decomposition lies mainly in its effect on the mean temperature profile, which in turn affects the heat transfer away from the solid-gas interface both in the steady state and when the surface position oscillates due to oscillatory burning.

A model of combustion instability has been advanced by Cantrell, McClure and Hart [9] which included the effect of thermal radiation

on the acoustic response of solid propellants. Their concern was that the natural radiation from the flame zone might be an appreciable fraction of the heat flux to the propellant and would modify the response function. The results from this theoretical model were not useful in the present investigation where radiation was the principal disturbance, since the final response function presented by Cantrell, McClure and Hart was in terms of pressure and not heat flux fluctuations.

The mass-burning rate pressure response function for a composite propellant can be deduced from oscillatory combustion data taken in a T-burner or a L\*-burner. Most of the results of theoretical models can be cast into the form [15],

$$\frac{m'/\bar{m}}{p'/\bar{p}} = \frac{nAB}{[\lambda + \frac{A}{\lambda} - (1 + A) + AB]}, \quad (3.7)$$

where  $\lambda$  is a complex function of the dimensionless frequency,  $\Omega$  is the dimensionless frequency ( $\alpha\omega/\bar{r}^2$ ),  $\alpha$  is the thermal diffusivity of the solid,  $\omega$  is the angular frequency,  $\bar{r}$  is the mean burning rate, and the pressure index,  $n$ , in the burning rate law  $r = a p^n$ . The values of  $A$  commonly used to fit experimental data are from 10 to 30. The parameter  $B$  generally lies in the range 0.7 to 1.2 and depends on the model for the gas-phase reactions. The real part of equation 3.7 is called the pressure response function. In most theories  $A$  is equal to  $\frac{E_s}{R\bar{T}_s} \frac{(\bar{T}_s - T_i)}{\bar{T}_s}$  while  $B$  is determined by the

model used for the gas phase conservation equation. If the parameters A and B were known, one would have the complete response function. As discussed by Culick [15], it is actually the correspondence between the surface heat flux fluctuations and the mass burning rate which is needed in striking an energy and material balance at the solid-gas interface. However, these quantities are not easily determined. The pressure entered the analysis through the burning rate law and in most experiments is a much easier variable to measure than the surface heat flux. Thus, the pressure and/or pressure oscillation growth rates are used in the interpretation of experimental results.

From a somewhat more fundamental aspect however, if the surface heat flux were known and its dependence on pressure could be computed, the form of the response function could be changed into one containing the surface heat flux and its fluctuations with pressure. Before one can hope to accomplish such a task, a greater understanding of the relationship between the surface heat flux and its fluctuations and the corresponding burning-rate perturbation must be achieved.

#### D: PROPELLANT RESPONSE TO RADIANT HEAT FLUX PERTURBATIONS

The purpose of the discussion which follows is to describe the predicted response of a burning propellant to radiant flux variations and to show the similarities and differences to be



expected for the pressure-driven and heat flux-driven cases. Relationships are developed for the response, first, of the opaque propellant and then of the translucent propellant. Finally, the predicted pressure-driven response for the same gas-phase model is developed and compared to the predicted flux-driven response.

In the following analysis the steady state position of the surface of the solid propellant is assumed to be at  $X = 0$  and the solid moves from  $X = -\infty$  at a velocity of  $\bar{r}$ , the propellant burning rate. The position  $0^-$  and  $0^+$  are on either side of the origin. An inertial coordinate system is used. Thus, periodic variations of the distance,  $X_s$ , between the propellant surface and the origin occur. The positions  $S^+$  and  $S^-$  are respectively in the gas and the solid phase.

### 1. Gas Phase Analysis

The existence of an intense flame over the propellant surface must be accounted for in writing the energy equation for the gas phase. The steady state conductive heat flux from the gas phase is given by equation 3.8 as,

$$(k_g \frac{d\bar{T}}{dX})_{s^+} = m [Q_f - C_p (\bar{T}_f - \bar{T}_s)]. \quad (3.8)$$

A convenient form of the gas phase burning velocity is,

$$m_f = K_1 P^{v_1} \bar{T}_f^{v_2} \left[ 1 - \frac{C_p}{Q_f} (\bar{T}_f - \bar{T}_s) \right]^{\frac{1}{2}} e^{-E_f/2R\bar{T}_f} . \quad (3.9)$$

Equation 3.9 is based on the sharp flame front model [21].

The perturbed form of equation 3.8 is,

$$\left( k_g \frac{dT'}{dX} \right)_{s+} = m' [Q_f - C_p (\bar{T}_f - \bar{T}_s)] - \bar{m} C_p (T'_f - T'_s) . \quad (3.10)$$

The flame temperature fluctuation appearing in equation 3.10 can be expressed in terms of the surface temperature fluctuation and the gas phase burning velocity by perturbing equation 3.9. The assumption of isobaric conditions is convenient for the interpretation of data, *i.e.*,  $v_1 = 0$ . For additional convenience, and for the lack of detailed information, the coefficient  $v_2$  will also be taken as zero. The flame temperature fluctuation needed in equation 3.10 becomes,

$$\frac{T'_f}{\bar{T}_s} = C_4 \frac{m'_f}{\bar{m}} - C_5 \frac{T'_s}{\bar{T}_s} , \quad (3.11)$$

where

$$C_1 = \frac{C_p \bar{T}_s}{2C_2} ,$$

$$C_2 = Q_f - C_p (\bar{T}_f - \bar{T}_s) ,$$

$$C_3 = \frac{E_f}{2R\bar{T}_f} \frac{\bar{T}_s}{\bar{T}_f} - C_1 ,$$

$$C_4 = \frac{1}{C_3} ,$$

$$C_5 = \frac{C_1}{C_3} .$$

The results from the analysis of the conductive flux fluctuation from the gas phase is given by equation 3.12,

$$(k_g \frac{dT'}{dX})_s + = \frac{m'_f}{\bar{m}} \bar{m} C_2 - \bar{m} C_p \bar{T}_s (C_4 \frac{m'_f}{\bar{m}} - C_5 \frac{T'_s}{\bar{T}_s}) + \bar{m} C_p \bar{T}_s \frac{T'_s}{\bar{T}_s} . \quad (3.12)$$

Equation 3.12 will be used later in connection with the matching conditions between the gas phase and the solid phase.

## 2. Analysis of the Solid Phase of an Opaque Propellant

A perfectly opaque propellant will absorb all of the imposed radiation at the surface. Such a material does not exist, but it is convenient mathematical invention. The thermal energy equation for an opaque, chemically inert solid is,

$$\alpha \frac{d^2 T}{dX^2} - r \frac{dT}{dX} = 0 , \quad (3.13)$$

in the coordinate system shown in Figure 3.1. The possibility of chemical reactions could be considered in the boundary condition or as a distributed energy release term in equation 3.13. For the present case, all chemical reactions associated with polymer and AP decomposition will be treated as a boundary condition. The solution of equation 3.13 with the boundary conditions,  $X = 0$ ,

$\bar{T} = \bar{T}_s$  and  $\bar{T} \rightarrow \bar{T}_{-\infty}$  as  $X \rightarrow -\infty$ , is,

$$\bar{T} - \bar{T}_{-\infty} = (\bar{T}_s - \bar{T}_{-\infty}) e^{rX/\alpha}. \quad (3.14)$$

The complete temperature field must be found for the matching conditions. It is convenient to separate the steady and unsteady temperature fields as given by equation 3.15,

$$T(X,t) = \bar{T}(X) + T'(X) e^{i\omega t}. \quad (3.15)$$

Equation 3.15 is used in the unsteady heat conduction equation, and the result is a separation into the steady and time dependent parts. The steady state solution is given by equation 3.14. The equation for the temperature fluctuations is found from equation 3.16,

$$\alpha \frac{d^2 T'}{dX^2} - r \frac{dT'}{dX} - T' i\omega = 0. \quad (3.16)$$

The characteristic equation for equation 3.16 has roots,

$$\lambda_1, \lambda_2 = \frac{1}{2} \left( 1 \pm \sqrt{1 + 4 \frac{i\omega\alpha}{r^2}} \right), \quad (3.17)$$

of which only the one with the positive sign yields finite solutions as  $X \rightarrow -\infty$ . This root can be separated into real and imaginary

parts,

$$\lambda_r = \frac{1}{2} \left( 1 + \frac{1}{\sqrt{2}} [(1 + 16\Omega^2)^{\frac{1}{2}} + 1]^{\frac{1}{2}} \right), \quad (3.18)$$

$$\lambda_i = \frac{1}{2\sqrt{2}} [(1 + 16\Omega^2)^{\frac{1}{2}} - 1]^{\frac{1}{2}}. \quad (3.19)$$

The general solution to equation 3.16 is,

$$T' = T'_0 e^{\lambda_r X / \alpha}, \quad (3.20)$$

since  $T' = T'_0$  at  $X = 0$ . The required temperature profile for the solid is now known for the opaque solid and can be used in the boundary condition at the solid-gas interface.

$$\left( -k \frac{dT'}{dX} \right)_{s-} = \left( -k_g \frac{dT'}{dX} \right)_{s+} + m' q_s - F'_r. \quad (3.21)$$

However, equation 3.21 requires the gradient at the propellant surface but equation 3.20 yields the gradient only at the coordinate system origin. The solid-gas interface matching conditions must be considered.

### 3. Matching Conditions at the Solid-Gas Interface

The equations derived for the temperature for the solid phase were for the coordinate system origin, not the propellant surface.

Culick [16] has shown that a simple way to get the surface conditions, which will be valid for small perturbations, is to expand the temperature fluctuation and the temperature gradient in a Taylor series about the coordinate system origin. This procedure yields the result that,

$$T'_{s\pm} = T'_{o\pm} + \left(\frac{dT}{dX}\right)_{o\pm} X_s, \quad (3.22)$$

$$\left(\frac{dT'}{dX}\right)_{s\pm} = \left(\frac{dT'}{dX}\right)_{o\pm} + \left(\frac{d^2T}{dX^2}\right)_{o\pm} X_s. \quad (3.23)$$

The equivalence of the use of equation 3.22 and 3.23 and the result for the heat transfer rate as deduced when the coordinate system is attached to the oscillating burning propellant has been demonstrated by Culick [17]. There it is also shown that,

$$X_s = -\frac{1}{i\omega} \frac{m'}{\rho}, \quad (3.24)$$

so the matching condition can be used to write the burning rate response equation. Within the framework of the quasi static treatment of the gas phase, only the solid phase conditions must be used in equation 3.22 and 3.23. Under the experimental conditions of this investigation the gas phase should exhibit quasi static behavior.

#### 4. Burning Rate Response of an Opaque Propellant

The burning rate response of an opaque propellant to a disturbance in the thermal radiant energy flux can now be written by use of equations 3.22, 3.23, 3.24, 3.21 and the perturbed pyrolysis law. The normal pyrolysis law states that,

$$m_s = K_2 P^n e^{-E_s/RT_s} . \quad (3.25)$$

Which, for constant pressure, yields the result that,

$$\frac{m'_s}{\bar{m}_s} = -\frac{E_s}{RT_s^2} \frac{T'_s}{\bar{T}_s} . \quad (3.26)$$

The fluctuations in the surface temperature gradient becomes,

$$\left(k \frac{dT'}{dX}\right)_{s-} = \bar{m} C \lambda T'_s + \frac{C(\bar{T}_s - \bar{T}_{-\infty})}{\lambda} m' . \quad (3.27)$$

Equation 3.11 and 3.26 can be used to eliminate the flame temperature fluctuation and the surface temperature fluctuation, and since  $m'_s = m'_f = m'_g$ , the gas side conductive heat transfer fluctuation can be expressed in terms of the mass flux fluctuation and steady state combustion parameters. The result is given as equation 3.28.

$$\frac{m'_r}{F_r} = \frac{\frac{E_s}{RT_s^2} \frac{1}{C\bar{T}_s}}{\lambda + \frac{A}{\lambda} + AH - C_2 \frac{E_s}{RT_s^2} \frac{1}{C\bar{T}_s} + C_6} , \quad (3.28)$$

where

$$A = \frac{E_s}{RT_s} \left( \frac{\bar{T}_s - \bar{T}_{-\infty}}{\bar{T}_s} \right)$$

$$H = \frac{q_s}{C (\bar{T}_s - \bar{T}_{-\infty})}$$

and

$$C_6 = \frac{C_p}{C} \frac{E_s}{RT_s} C_4 - \frac{C_p}{C} C_5 - \frac{C_p}{C} .$$

The real part of equation 3.28 was computed for a range of parameters similar to those used in the case of pressure-driven oscillatory burning. The results are shown in the following figures, after normalization to the zero frequency limit. Figure 3.5, 3.6 and 3.7 shows the influence of the heat of gasification on the response function. Figure 3.3 shows the influence of the surface temperature on the response function. Figures 3.5, 3.6 and 3.7 also show the influence of propellant opacity on the response. In all cases, the response at low frequency is low with a steadily rising value as the frequency increases. At the frequencies greater than the frequency of maximum response, the response decreases rapidly with frequency.

## 5. Analysis of the Solid Phase for a Translucent Propellant

Since radiant energy was used as the driving energy stimulus, any in-depth adsorption of radiant energy will modify the burning



rate response. This difference in response shows up in the boundary conditions required for the steady state and for the perturbed thermal energy equation. The thermal energy equation in this case is,

$$\alpha \frac{d^2 \bar{T}}{dX^2} - r \frac{d\bar{T}}{dX} + \frac{\gamma \bar{F}_{or}}{\rho c} e^{\gamma X} = 0 , \quad (3.29)$$

where  $\gamma$  is the Beer's law absorption coefficient and  $\bar{F}_{or}$  is the natural radiation from the flame. The other terms in equation 3.29 have their usual significance. The same coordinate system as for the analysis of the opaque solid is used. The thermal energy equation is linear in temperature, so it can be separated into two temperatures. This makes it possible to separate equation 3.29 into two equations,

$$\alpha \frac{d^2 \bar{T}_c}{dX^2} - r \frac{d\bar{T}_c}{dX} = 0 , \quad (3.30)$$

and

$$\alpha \frac{d^2 \bar{T}_r}{dX^2} - r \frac{d\bar{T}_r}{dX} + \frac{\gamma \bar{F}_{or}}{\rho c} e^{\gamma X} = 0 . \quad (3.31)$$

Equation 3.30 and 3.31 must be satisfied using different boundary conditions. For equation 3.30, the boundary conditions are the same as were used for equation 3.13. The solution is equation 3.14. The temperature profile due to radiant energy can be found from equation 3.31 by using the following boundary conditions,

$$\begin{aligned} \frac{d\bar{T}_r}{dX} &= 0 & \text{at} & & X = 0, \\ \bar{T}_r &\rightarrow 0 & \text{as} & & X \rightarrow -\infty. \end{aligned}$$

The complete solution to equation 3.31 becomes,

$$\bar{T}_r = \frac{\gamma \bar{F}_{or}}{(\alpha \gamma^2 - r \gamma) \rho c} \left[ \frac{\gamma \alpha}{r} e^{rX/\alpha} - e^{\gamma X} \right]. \quad (3.34)$$

The complete steady state temperature field within the translucent solid becomes,

$$\bar{T} = \bar{T}_{-\infty} + (\bar{T}_s - \bar{T}_{-\infty}) e^{rX/\alpha} + \frac{\gamma \bar{F}_{or}}{(\alpha \gamma^2 - r \gamma) \rho c} \left[ \frac{\gamma \alpha}{r} e^{rX/\alpha} - e^{\gamma X} \right]. \quad (3.35)$$

Equation 3.35 can be used to form the matching conditions at the solid-gas interface for the burning surface. Clearly, as the extinction coefficient,  $\gamma$ , becomes very large, the steady state temperature profile converges to the temperature profile for an opaque propellant, equation 3.14.

It is necessary to first develop the solution to the perturbed temperature field in a translucent solid. Consider the equation for unsteady heat conduction into a translucent solid,

$$\alpha \frac{\partial^2 T}{\partial X^2} - r \frac{\partial T}{\partial X} - \frac{\partial T}{\partial t} + \frac{\gamma F_r}{\rho c} e^{\gamma X} = 0. \quad (3.36)$$

The temperature field can be separated into a steady state and an

unsteady contribution,

$$T(X,t) = \bar{T}(X) + T'(X) e^{i\omega t} . \quad (3.37)$$

The spacial fluctuation in temperature can be separated into a conduction and radiation contribution.

$$T'(X) = T'_c(X) + T'_r(X) . \quad (3.38)$$

The imposed flux can also be considered to be a harmonic function in phase with the temperature.

$$F_r = \bar{F}_r + F'_r e^{i\omega t} . \quad (3.39)$$

Substituting, equation 3.37 and 3.39 into equation 3.36 yields two equations to be solved,

$$\alpha \frac{d^2 T'_c}{dX^2} - r \frac{dT'_c}{dX} - i\omega T'_c = 0 , \quad (3.40)$$

and

$$\alpha \frac{d^2 T'_r}{dX^2} - r \frac{dT'_r}{dX} - i\omega T'_r = \frac{\gamma F'_r}{\rho c} e^{\gamma X} = 0 . \quad (3.41)$$

Equation 3.40 must be solved using the following boundary conditions,

$$\begin{array}{lll} T'_c \rightarrow 0 & \text{as} & X \rightarrow -\infty \\ T'_c = T'_{co} & \text{at} & X = 0 . \end{array} \quad (3.42)$$

Equation 3.40 must be solved using the following boundary conditions,

$$\begin{aligned} T'_r &\rightarrow 0 && \text{as} && X \rightarrow -\infty, \\ \left(\frac{dT'_r}{dX}\right) &= 0 && \text{at} && X = 0. \end{aligned} \quad (3.43)$$

In general, the unsteady temperature field is,

$$T' = T'_{co} e^{\lambda r X / \alpha} + \frac{\beta'}{(\alpha \gamma^2 - r \gamma - i \omega)} \left[ \frac{\gamma \alpha}{\lambda r} e^{\lambda r X / \alpha} - e^{\gamma X} \right], \quad (3.44)$$

where

$$\beta' = \frac{\gamma F'_r}{\rho c}.$$

#### 6. Matching Conditions and Burning Rate Response for a Translucent Propellant

The matching conditions at the solid-gas interface between the translucent propellant surface and the gas phase is given by equation 3.45,

$$\left(k_g \frac{dT'}{dX}\right)_{s+} = \left(k \frac{dT'}{dX}\right)_{s-} + m' q_s. \quad (3.45)$$

The conductive heat flux from the gas phase is given by equation 3.12. The temperature gradients needed in equation 3.45 are at the propellant surface, not at the coordinate system origin. As in the case of the opaque propellant, equations 3.22 and 3.23 can

be used to determine the surface conditions from the solutions which are valid at the coordinate system origin and, after the use of equation 3.45, lead to the burning rate response for a translucent propellant when  $\kappa = \gamma\alpha/\bar{r}$ .

$$\frac{\bar{m}'}{\bar{F}'_r} = \frac{\frac{E_s}{RT_s} \frac{1}{CT_s} \frac{(\kappa - \lambda) \kappa}{[\kappa^2 - \kappa - \lambda(\lambda - 1)]}}{\lambda + \frac{A}{\lambda} + AH - \frac{E_s}{RT_s} \frac{1}{CT_s} C_2 + C_6} \quad (3.46)$$

As the opacity of the propellant increases, the response function for the translucent propellant, converges to the same value as for the opaque propellant. The steady state value,  $\omega = 0$ , of the response was used to normalize the burning rate response.

#### E: BURNING RATE RESPONSE TO PRESSURE FLUCTUATIONS

A direct comparison of the predicted response to pressure and flux perturbations is possible if the same gas phase model as employed to develop the response functions. Culich [15] shows that the pressure-driven response function can be written as,

$$\frac{\bar{m}'/\bar{m}}{p'/\bar{p}} = \frac{EW - n_s (V - \lambda)}{\lambda + \frac{A}{\lambda} + LE - V} \quad (3.47)$$

where the solid-phase parameters,

$$A = (1 - T_{-\infty}/\bar{T}_s) (E_s/RT_s)$$

$$L = q_s / \bar{RT}_s, \text{ and } E = E_s / \bar{RT}_s.$$

For the sharp flame front model,

$$V = \frac{E_s}{\bar{RT}_s^2} \left( \frac{C_2}{C} \right) - \frac{C_p}{C} \left( \frac{E_s}{\bar{RT}_s C_3} - C_5 - 1 \right),$$

$$W = \left( \frac{C_p}{C} \right) \left( \frac{n}{C_3} \right), \text{ and}$$

the other constants are defined under Eq. (3.11). Since the pressure driven response function should equal  $n$  at low frequencies ( $\lambda \rightarrow 1$ ),  $n_s$  may be evaluated to insure this limiting condition, or

$$n_s = n + \frac{nA + E(nL - W)}{1 - V}.$$

#### F: RELATIONSHIP BETWEEN MASS FLUX PERTURBATIONS AND THE TRANSIENT FORCE

The steady state recoil force which results from the mass leaving the burning surface is given by equation 3.6. The transient force due to mass flux, flame temperature and pressure fluctuations can be found from a first-order perturbation of appropriate terms in equation 3.6. The result is equation 3.48,

$$f'(t) = 2\bar{m} m'(t) \frac{\bar{RT}_f}{P_M} + \bar{m}^2 \frac{RT_f'}{P_M} - \bar{m}^2 \frac{\bar{RT}_f}{P_M^2} p' . \quad (3.48)$$

The first term in equation 3.48 is on the order of 200, the second 10, and the third, 1. Using the equations which were derived earlier for the mass flux and for the flame temperature fluctuation and neglecting pressure fluctuations, the transient force can be written in terms of the kinetic parameters. Abbreviating the real part of equation 3.28 by  $R_{op}$ , and using equation 3.11, the transient force due to the mass flux and flame temperature fluctuations can be written,

$$f'(t) = 2\bar{m} \frac{RT_f}{PM} R_{op} F'_r + \bar{m}^2 \frac{RT_s}{PM} (C_4 - C_5 \frac{RT_s}{E_s}) R_{op} F'_r . \quad (3.49)$$

For the case of a translucent propellant, the transient force is given by,

$$f'(t) = 2\bar{m} \frac{RT_f}{PM} R_{TR} F'_r + \bar{m}^2 \frac{RT_s}{PM} (C_4 - C_5 \frac{RT_s}{E_s}) R_{TR} F'_r , \quad (3.50)$$

where the right hand side of equation 3.46 is abbreviated as  $R_{TR}$ .

From both equation 3.49 and 3.50 it can be seen that the force is directly proportional to the mass burning rate response function. It now becomes a simple matter to also compute the surface temperature and flame temperature fluctuations from equation 3.26 and 3.11 respectively, if desired.

### G: RESULT OF A PARAMETRIC STUDY OF THE RESPONSE FUNCTIONS

Values of the heat-flux-driven response function for the translucent propellant given by equation 3.46, were computed for various values of the input parameters. The objective of these calculations was to demonstrate the qualitative similarities between experimental results and calculations and to aid in selection of parameters to describe the response the actual propellants tested. The following plots are in terms of the real part of the response function normalized to the steady-state or zero frequency value.

Figure 3.2 illustrates the effect of variation of the activation energy of the surface pyrolysis reaction,  $E_s$  for an opaque propellant. Higher values of  $E_s$  increase the response relative to the zero frequency value and also increase the frequency at which the maximum in the response function occurs. Variation of  $E_s$  was found to be the only effective method for significantly changing the position of the maximum in the response functions. To a good approximation, the experimentally observed position of the maximum could be used to determine  $E_s$  if, of course, it is assumed that the model is adequate.

Figure 3.3 shows the effect of variations in the steady-state surface temperature. The response is apparently insensitive to variations in  $\bar{T}_s$ , and most calculations were made for a fixed value of  $\bar{T}_s = 850^\circ\text{K}$ .

The magnitude of the heat release at the propellant surface,  $q_s$ , profoundly affected the predicted response; and Figure 3.4 shows an example of this effect. In general, large energy release at the surface produces high response function maximums. However, for some values of the parameters, large  $E_s$  for example, as the magnitude of  $-q_s$  increases, the effect is found to pass through a maximum and then decrease.



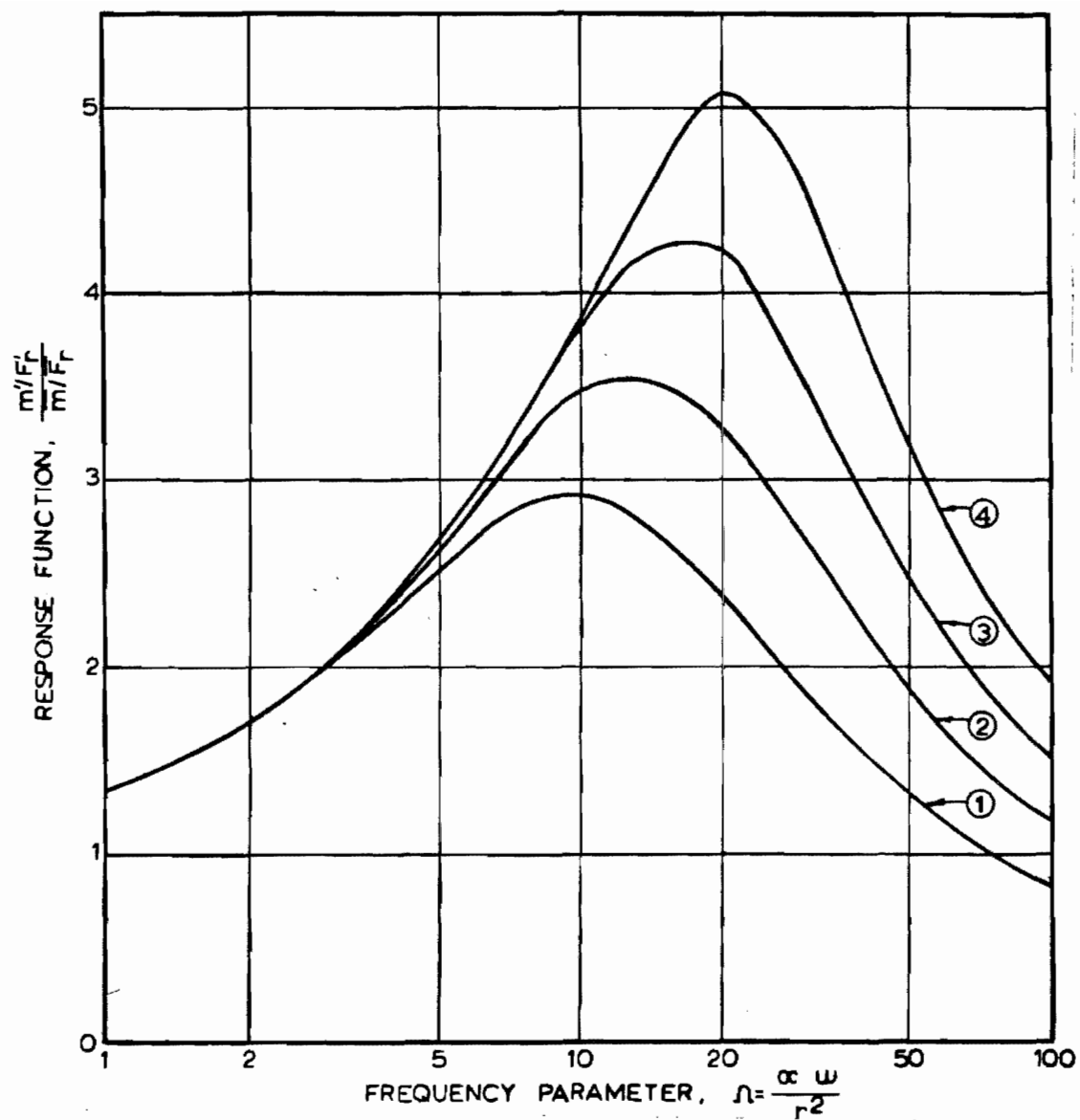


FIG. 3-2.

1.  $T_s = 850^\circ\text{K}$ ,  $T_f = 2500^\circ\text{K}$   
 $q_s = -25 \text{ cal/gm}$   
 $E_s = 30,000 \text{ cal/gmole}^\circ\text{K}$   
 $E_f = 40,000 \text{ cal/gmole}^\circ\text{K}$
2.  $E_s = 40,000 \text{ cal/gmole}^\circ\text{K}$
3.  $E_s = 50,000 \text{ cal/gmole}^\circ\text{K}$
4.  $E_s = 60,000 \text{ cal/gmole}^\circ\text{K}$

FIG. 3-2. Effect of Surface Reaction Activation Energy on the Response Function.

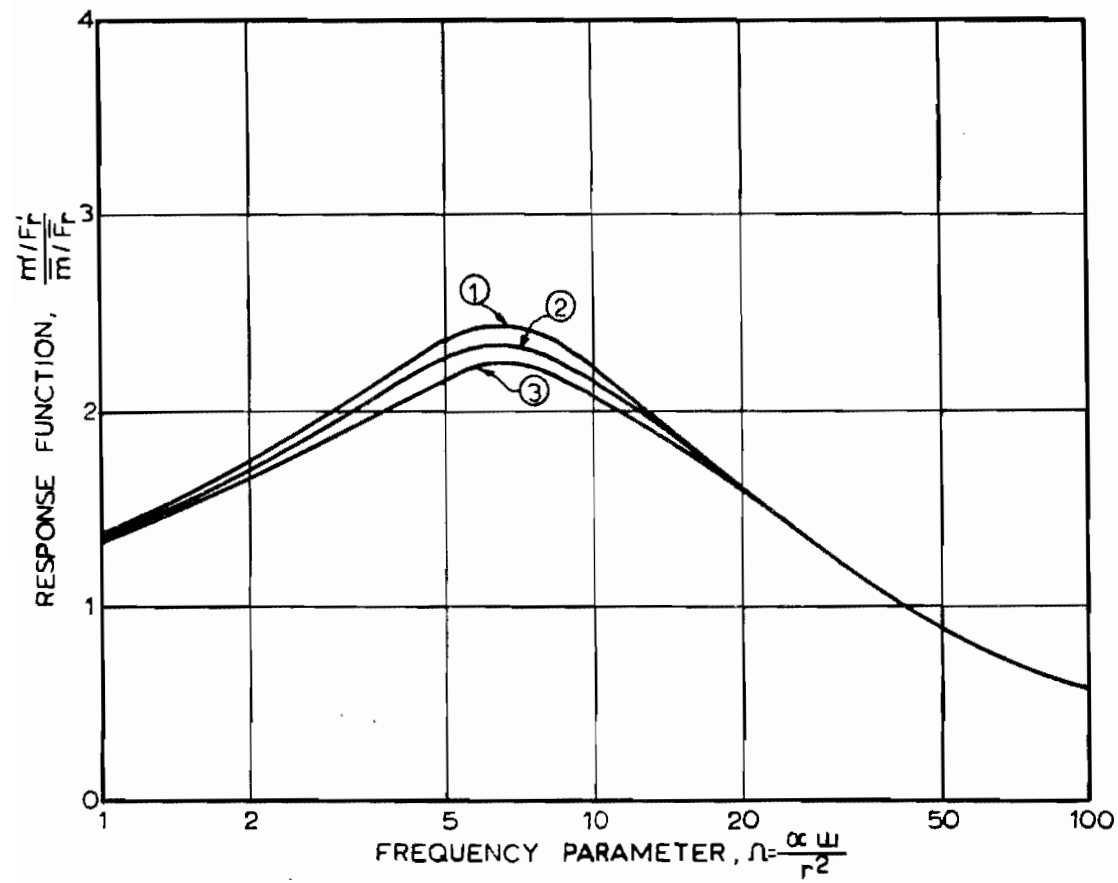


FIG. 3-3.

1.  $T_s = 750^\circ\text{K}$ ,  $T_f = 2500^\circ\text{K}$   
 $q_s = -25 \text{ cal/gm}$   
 $E_s = 20,000 \text{ cal/gmole}^\circ\text{K}$   
 $E_f = 40,000 \text{ cal/gmole}^\circ\text{K}$
2.  $T_s = 800^\circ\text{K}$
3.  $T_s = 850^\circ\text{K}$

FIG. 3-3. Effect of Surface Temperature on the Response Function.

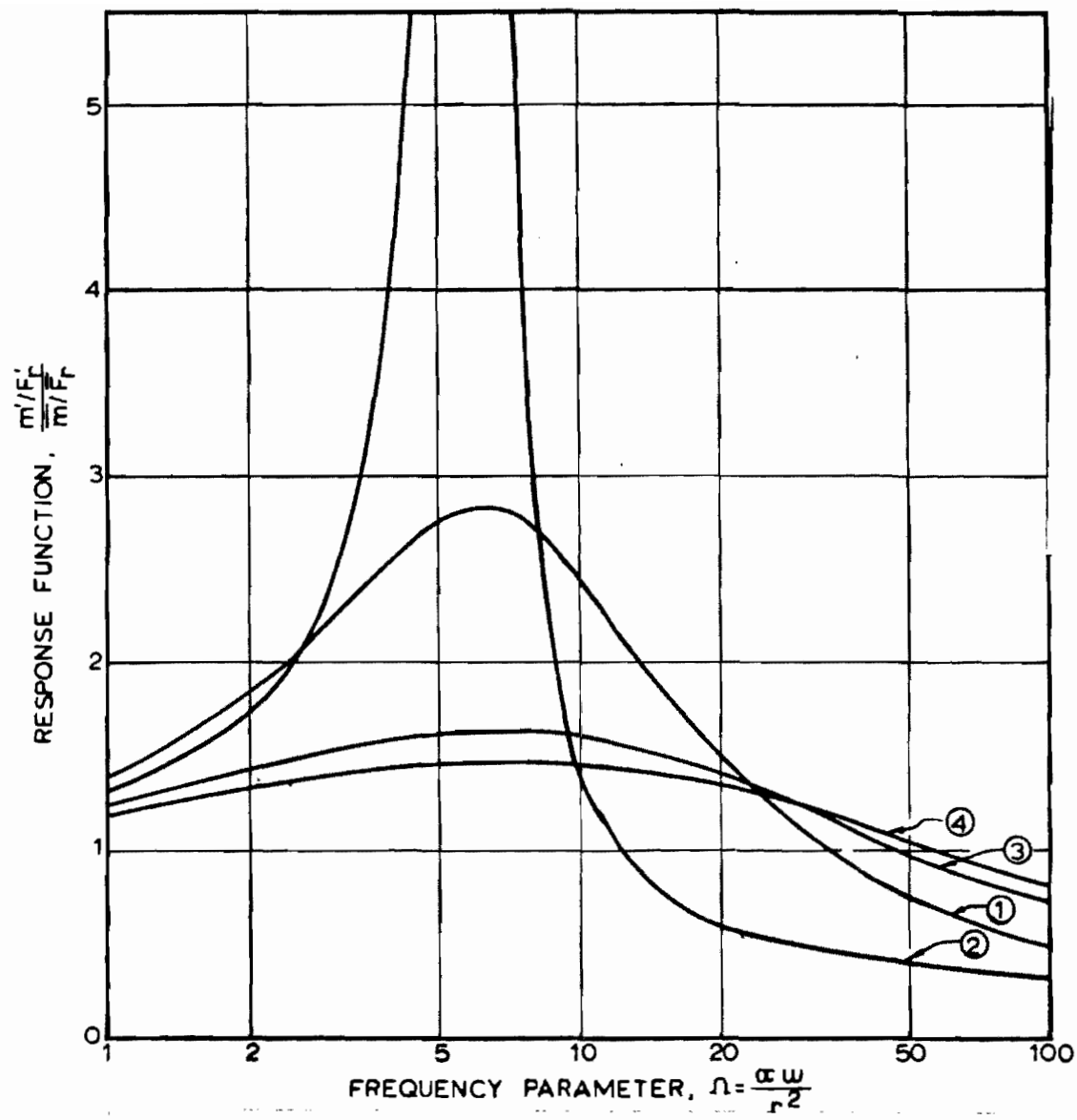


FIG. 3-4.

1.  $T_s = 850^\circ\text{K}$ ,  $T_f = 2500^\circ\text{K}$   
 $q_s = -50$  cal/gm  
 $E_s = 20,000$  cal/gmole $^\circ\text{K}$   
 $E_f = 40,000$  cal/gmole $^\circ\text{K}$
2.  $q_s = -100$  cal/gm
3.  $q_s = +50$  cal/gm
4.  $q_s = +100$  cal/gm

FIG. 3-4. Effect of the Heat of Vaporization of the Response Function.

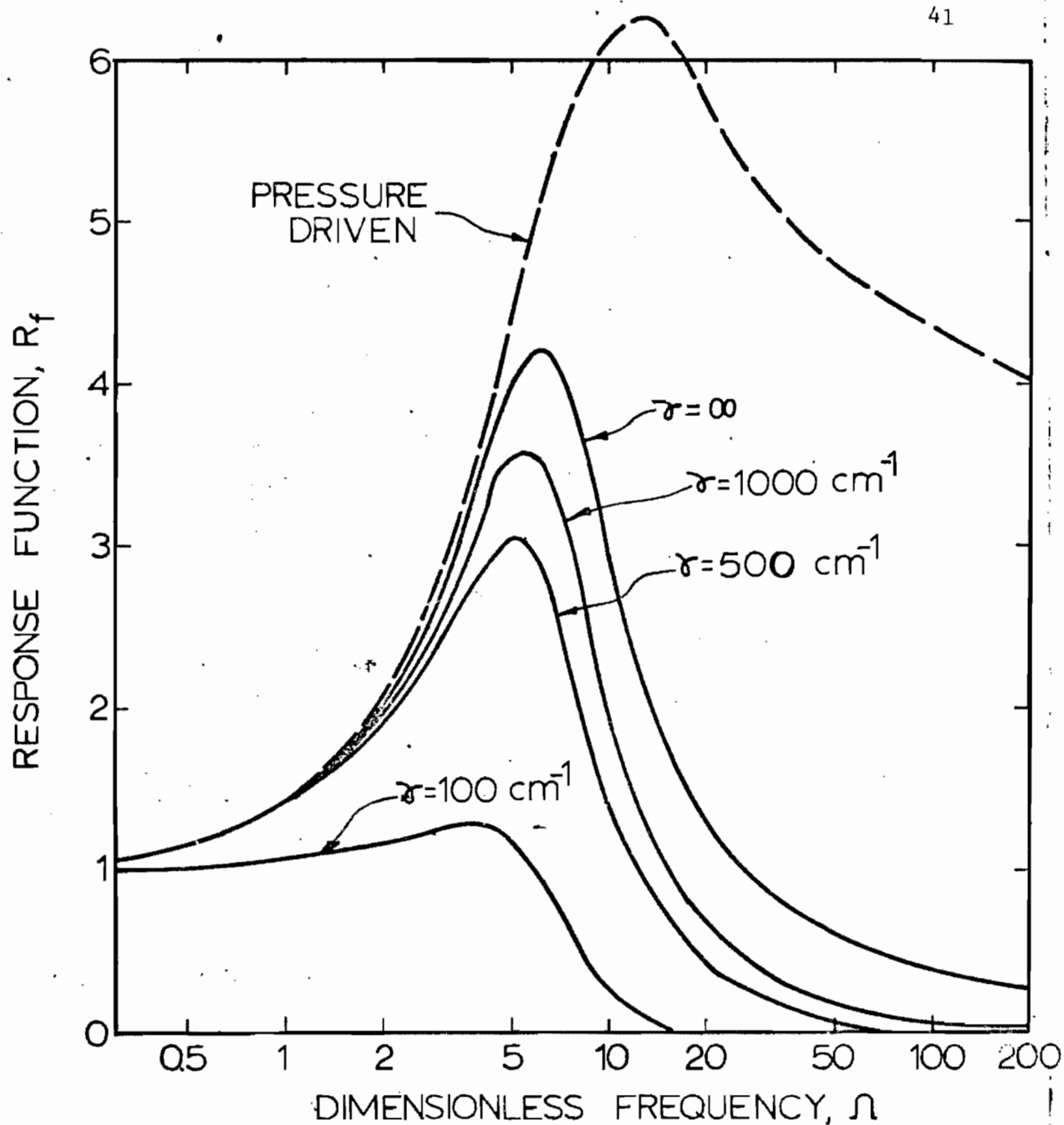


FIG. 3-5 A comparison is shown here of the real part of the response functions for the pressure and heat flux-driven oscillations of a burning solid propellant. The same parameters were used in each case.

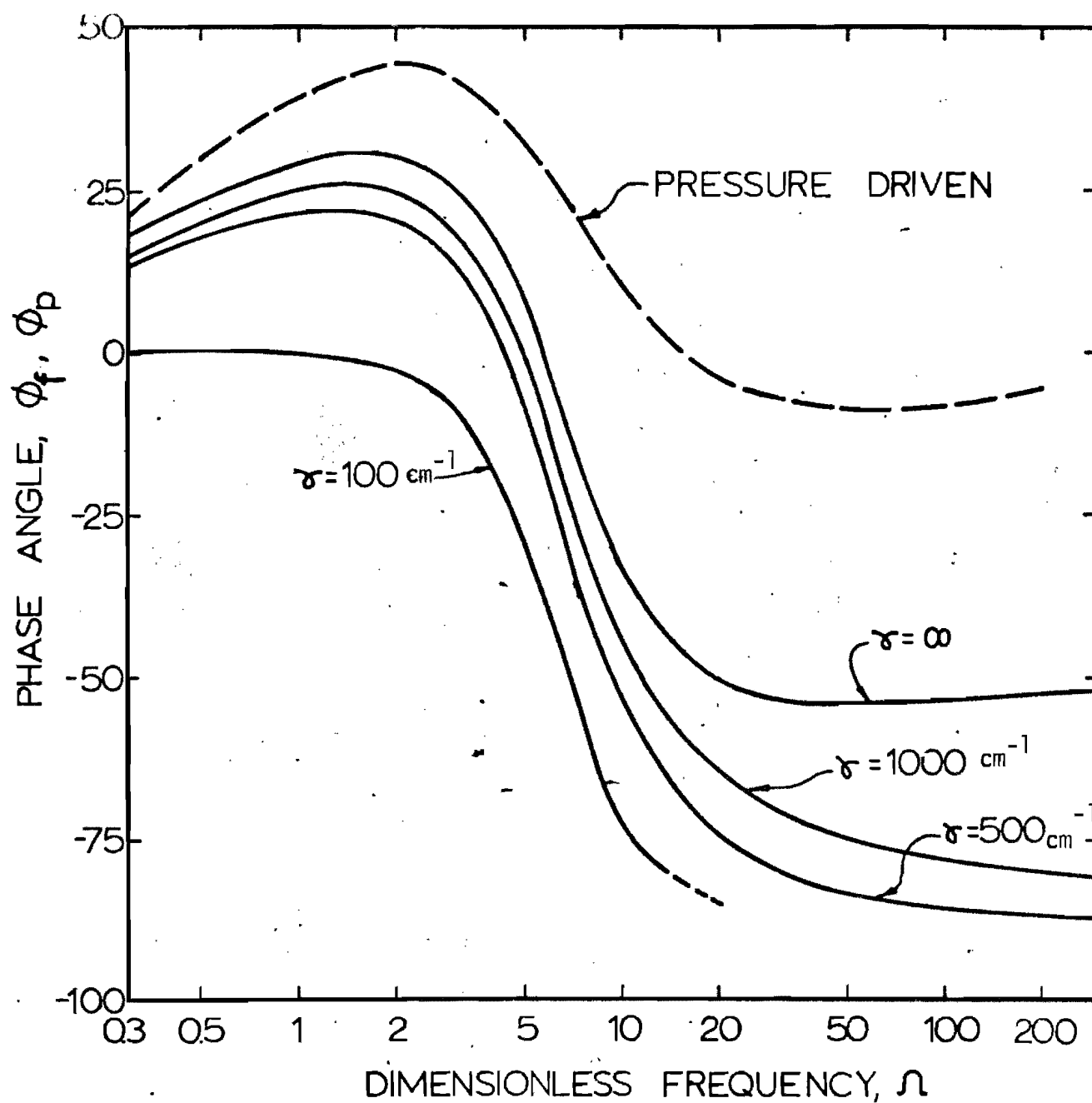


FIG. 3-6 A comparison is shown here of the phase angle for the pressure and heat flux-driven oscillations of a burning solid propellant. The same parameters were used in each case.

Figure 3.5 shows the effect of propellant opacity,  $\gamma$ , on the flux-driven response. For a  $\gamma$  of  $10^4 \text{ cm}^{-1}$  the opaque and translucent responses are essentially identical. Significant effects are noted at high frequencies even for  $\gamma$  greater than 1000 which would represent a very opaque propellant. For many practical propellants  $\gamma$  approximately  $100 \text{ cm}^{-1}$ , and their response to radiant flux would be expected to be dominated by transmissivity effects. Experimentally, this effect was noted; very transparent propellants were found to be insensitive to high frequency radiation perturbations.

Figure 3.5 also shows a comparison of the pressure-coupled model results, equation 3.47 to the flux-driven case for the same values of the combustion parameters. The response functions are not identical, but the qualitative similarity is great enough to encourage the effort to obtain the pressure-driven functions by measurement of the flux-driven case. Parameters which yield high relative response to the radiant flux show strong response to pressure fluctuations although the frequency of the response function maximum is somewhat greater for the pressure-driven case, and the high frequency effects are also greater. If  $n_s$  in equation 3.25 is taken to be equal to zero, as is often assumed, the resulting response function differs from equation 3.46 only by a constant.

Figure 3.6 represents the calculated phase angle between the input flux and the mass efflux response for the parameters of Figure 3.5. In general, the prediction is for a phase lead at low frequencies, a zero phase angle near the maximum in the response function, and a high frequency asymptote from  $-50$  to  $-90^\circ$ . For some values of the parameters (large values of  $E_s$ ,  $E_j$ , and  $-q_s$ ) the phase angle is predicted to shift discontinuously from a lead to  $90^\circ$  lag at the response function maximum and to then approach a smaller lag angle at high frequencies. This particular type of behavior was never observed experimentally.

## CHAPTER IV: APPARATUS - GENERAL FEATURES

Radiant energy focused on the burning surface of a solid propellant strand was used as a means of perturbing the burning rate. Several sources of thermal radiant energy were considered after the criteria for the energy source were set. These criteria are: (1) a flux great enough to perturb the reaction zone was required; (2) a uniform flux was needed over a region large enough to get an average response, *i.e.*, hot spots from the source should be much larger than the individual AP particles; (3) an appreciable depth of field in the focal volume of the energy flux was necessary so that the sample would be exposed to a uniform flux as the interface regressed since fixed position strands were employed; and, (4) the heat flux produced by the energy source should be reproducible over periods of several months and be steady throughout the test time of a few seconds.

A gas laser source was considered because commercial equipment met criteria number three and four very well. However, the energy is concentrated into such small areas that an average response could be difficult to achieve. Results from recent propellant ignition and combustion studies employing laser radiation confirm this suspicion [31,72]. Thermal radiation sources appeared to be the only practical devices, and arc sources appeared to be most applicable. A thermal radiation furnace powered by a high-pressure-

compact arc, Mercury-Xenon lamp was chosen as the energy source as the best compromise of requirements and availability. The voltage-current requirements of the Mercury-Xenon lamp were easily supplied by an existing power supply.

#### A: RADIANT SOURCE UNIT

A radiation furnace was constructed with the arc lamp at the primary focus and a combustion chamber at the secondary focus of a 21-inch diameter elliptical mirror. The housing for the arc lamp was made from steel channels welded into a 32 x 48 x 36 inch rectangular frame and covered with 3/8 inch transite. Doors on the sides and the back facilitate easy access to the lamp and reflector inside the lamphouse. A 21-inch elliptical reflector, Model 2100-2 from Heyer-Schultz, Inc., was mounted on three-axis adjustable frames to allow for focusing the system. Three adjustment screws on the ring holding the reflector provide another degree of freedom. The framework supporting the high-pressure lamp, (Hanovia Model 932 B-39 5 Kw D.C.) compact arc lamp purchased from Engelhard Hanovia, was also adjustable. Three blowers forced air into the lamphouse to insure adequate cooling of the lamp and reflector.

An 8.0-inch diameter two-leaf shutter operated by an air piston was used to control the exposure interval for the ignition and steady burning tests. The shutter mechanism was mounted on a trolly assembly and could be completely removed from the radiation



beam. This feature permitted easier access to the combustion chamber. Two water-cooled steel plates, mounted on a trolley assembly and opening like a curtain, doused the beam of radiation and prevented thermal damage to the shutter. Two multiflex Eagle Signal timers HXS-141 were used to control the exposure time to ignite the sample and to reopen the shutter to augment the burning after ignition had occurred. A second shutter assembly was used for the dynamic response experiments. This shutter, which could be inserted on the same trolley assembly as a leaf shutter, consisted of a 24-inch diameter chopper wheel with six equal open areas and six uncut sections on the periphery of the wheel. The chopper was driven by a 7/16 hp, 26 volt D.C. motor. The power for driving the motor was supplied by a pair of high capacity alkaline rechargeable batteries. Speed control of the motor was accomplished by use of a heavy-duty rheostat. The chopper speed, actually the period of exposure, was measured by a Berkley Model 7250 time interval meter which was triggered by a photo diode. Radiation from the furnace passed through an 8.5-inch diameter opening over the chopper. A manually-operated slide shutter between the arc lamp and the chopper protected the chopper wheel blades while the wheel was brought up to speed.

#### B: MEASUREMENT OF THE FLUX PROFILE

In order to insure that the surface of the burning strands were always uniformly exposed to radiation, it was necessary to

generate a three-dimensional map of the secondary focal volume of the furnace. This was most conveniently done by use of the transient, rate-of-rise type calorimeter in which a small hole in a metal disc was used to define the area of measurement. A number of calorimeters were built as adaptations of the basic design by Beyer, McCulley and Evans [5]. Both an error analysis and experience with this type of calorimeter indicate that when properly assembled and used, the measured heat flux values are in error by no more than 5 percent. In the present study, relative values of the heat flux were most important, and such a maximum error was considered tolerable. Figures B-1, B-2 and B-3 show the result of this focal volume heat flux measurement. A cylindrical region in which the maximum flux variation was less than 10 percent existed for 2.5 cm in the axial direction and was 0.6 cm in diameter. The size of this region of essentially constant heat flux was more than adequate for tests with the 0.6 cm strands burned for sample lengths of less than 1.0 cm.

A Hy-Cal Model C-1301-A-120-072 calorimeter whose calibration was traceable to the National Bureau of Standards was purchased for calibration of the rate-of-rise calorimeters. However, with the available sources of radiation in the laboratory, it was not possible to make direct comparison of the calorimeters without use of radiation shields on the Hy-Cal unit. Because the uncertainties introduced by use of these shields were as great as the maximum

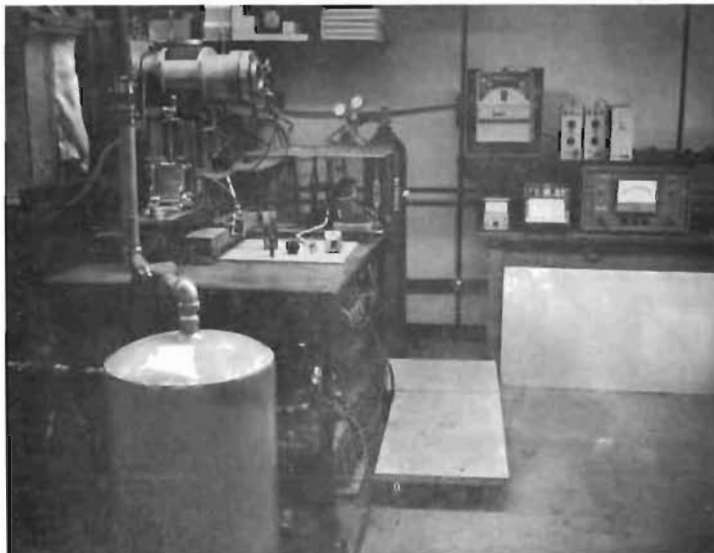


Fig. 4-1. General View of the Radiation Furnace, Combustion Chamber and Data Acquisition Equipment.



Fig. 4-2. Closeup View of the Data Acquisition and Data Processing Equipment. Tape-recorder, RMS Voltmeter, Phase Angle Meter, Amplifiers and Recorder.

possible errors associated with the rate-of-rise calorimeters, no improvement in accuracy of the flux measurement could be achieved by use of the Hy-Cal calorimeter.

#### C: COMBUSTION CHAMBER

The combustion chamber, shown in Figure 4-4, was a 6 inch by 18 inch aluminum cylinder closed at one end by a cover plate with a 3-inch view window and closed at the front by a 0.75 inch by 6 inch quartz window. Stainless steel tubing connections were installed in the back plate to introduce cooling water and window flushing gas. Electrical connections for ignition leads and power for back lighting the sample were also installed in this back plate. Windows placed around the cylindrical walls of the chamber permitted viewing the sample from either side and from above. The entire chamber was mounted on two adjustable stages to facilitate three-axis positioning of test areas at the secondary focus of the elliptical mirror. A water-cooled triangular block was installed inside the chamber. A 1.06-inch diameter axial hole in this block was used to support the rate-of-rise calorimeters, a drill chuck which served to hold propellant samples used in the burning rate study, a force transducer used during dynamic response tests, and various other attachments used in the supplementary tests. Four 1/4 inch openings around the 6-inch diameter window were used to permit the introduction of nitrogen for flushing the window. A

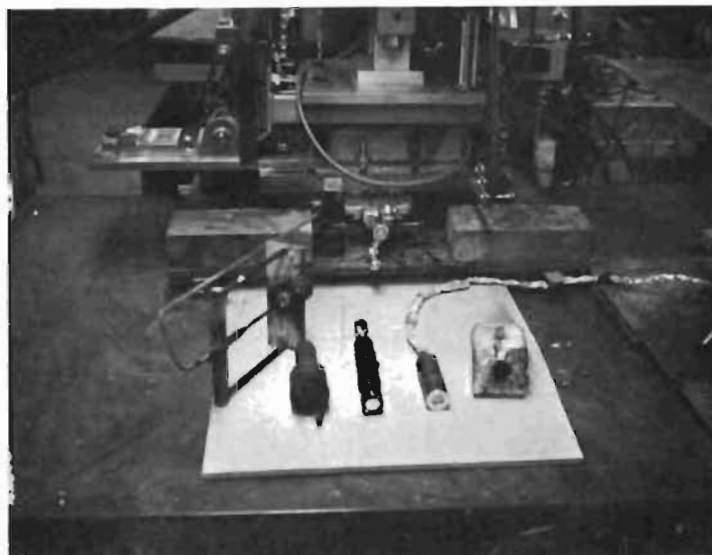


Fig. 4-3. Attachments for Various Experiments. Left to Right: Ignition with surface cooling, holder for burning rate tests, rate-of-rise calorimeter, micro-force transducer and the sample mount for transient burning rate experiments.

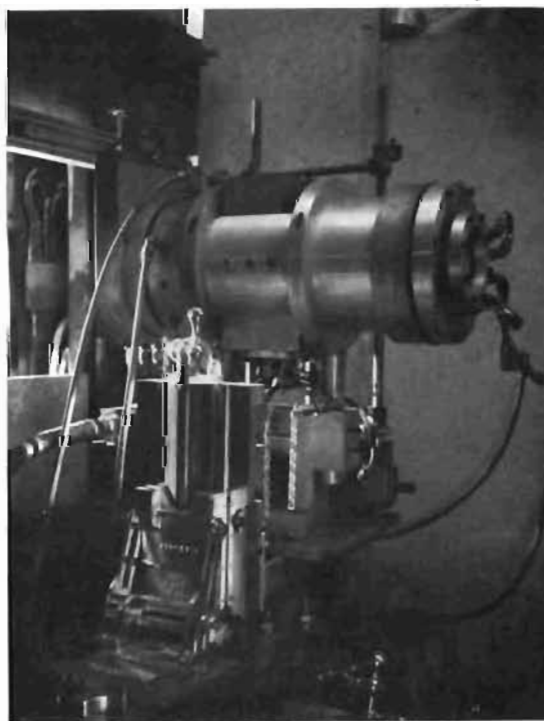


Fig. 4-4. Combustion Chamber and the Three-axis Positioning Stages.

120-liter surge tank was connected to the chamber by a 2-inch diameter rubber hose which served to maintain essentially constant pressure in the chamber. The combustion chamber was operable from full vacuum to 5 atms pressure.

## CHAPTER V: THERMAL RADIATION AUGMENTATION OF AP COMPOSITE PROPELLANT BURNING

The considerations presented in Chapter III indicate the desirability of knowing the effect of a thermal energy disturbance on the burning rate of a composite propellant. This chapter contains a discussion of the determination of the influence of an external radiant heat flux on the steady burning rate and an estimate of the thermal radiation absorbed by the propellant flame. Values of the apparent heat of gasification of a series of propellants are presented based upon the results of this determination.

Several other research groups have tried to determine the effect of thermal radiation on propellant burning rates [51,60]. Ohlemiller and Summerfield [60] advanced a propellant sample in the focus of an arc furnace to maintain a nearly constant imposed flux at the burning surface. The depth of field of the arc image furnace they used was small so advancing the sample was necessary. The results of their work were not useful for the present study since all tests were made at pressures below the propellant deflagration limit. Levy and Friedman [51] considered the burning rates of pressed strands of AP during exposure to radiation. They were able to demonstrate that the burning rate could be increased by use of external radiation. Because the AP strands burned slowly, manual advancement of the regressing interface to maintain focus

was satisfactory. In the present study, since the flux at the secondary focus was fairly uniform, and the burning rate was considered to be too fast to accurately advance the samples, the strands could be held in a fixed position at the secondary focus of the optical system.

#### A: BURNING RATE MEASUREMENTS

It was not possible to generate a radiant heat flux of sufficient intensity to greatly increase the burning rate. Typically, the increase was only 5 to 10 percent of the steady regression rate. Thus, accurate measurement of the linear burning rate was necessary, and this requirement was satisfied by using a photographic technique. Several alternate methods of measuring the increase in burning rate were attempted. The accuracy of the conventional technique for measuring burning rates by the use of imbedded timing wires was found to be about equal to the maximum change produced by the external radiation. In some tests, the regression rate was measured by continuously weighing the burning strand. The strand was mounted at the free end of a flexible, cantilever metal strip, and the strand weight was determined by measurement of the beam deflection with a fiber optics position sensor. Unfortunately, for configurations with sufficient sensitivity and adequate response times, the natural frequency of the systems was in the range of the low frequency (20 to 40Hz) combustion noise, and the resonant coupling produced spurious signals which completely obscured the desired



information. An attempt was made to measure the changes in burning rate by the measurement of the rate-of-change of the transmitted radiation intensity as the samples regressed. A high and low modulation of the radiation from the arc lamp was employed to obtain the transmitted light signal which was detected using a vacuum photodiode. The changes in the burning rate measured for a single strand as a result of the high-low flux variation were consistent, but the run-to-run reproducibility was not satisfactory. Useful data were obtained from scaled motion pictures taken of back-lighted burning strands.

#### B: PROCEDURE FOR MEASURING STEADY BURNING RATES

Cylindrical samples 3 cm long and 1 cm in diameter were cut from slabs of cured propellant and were held in the jaws of a drill chuck mounted in the triangular block inside the combustion chamber. Figure 5-1 shows the sample mounting arrangement. A thin layer of Kel-F grease on the non-burning sides of the samples was used as an inhibitor. About 2.5 cm of the original sample extended beyond the jaws of the chuck. A small scale which was mounted on the drill chuck was visible on the film and was used to determine the magnification. A 16 mm movie camera, Kodak Cine Special with external lenses, was focused on the center of the cylindrically-shaped samples and operated continuously at 20 frames per second during an ignition period, a steady non-radiated period, and a

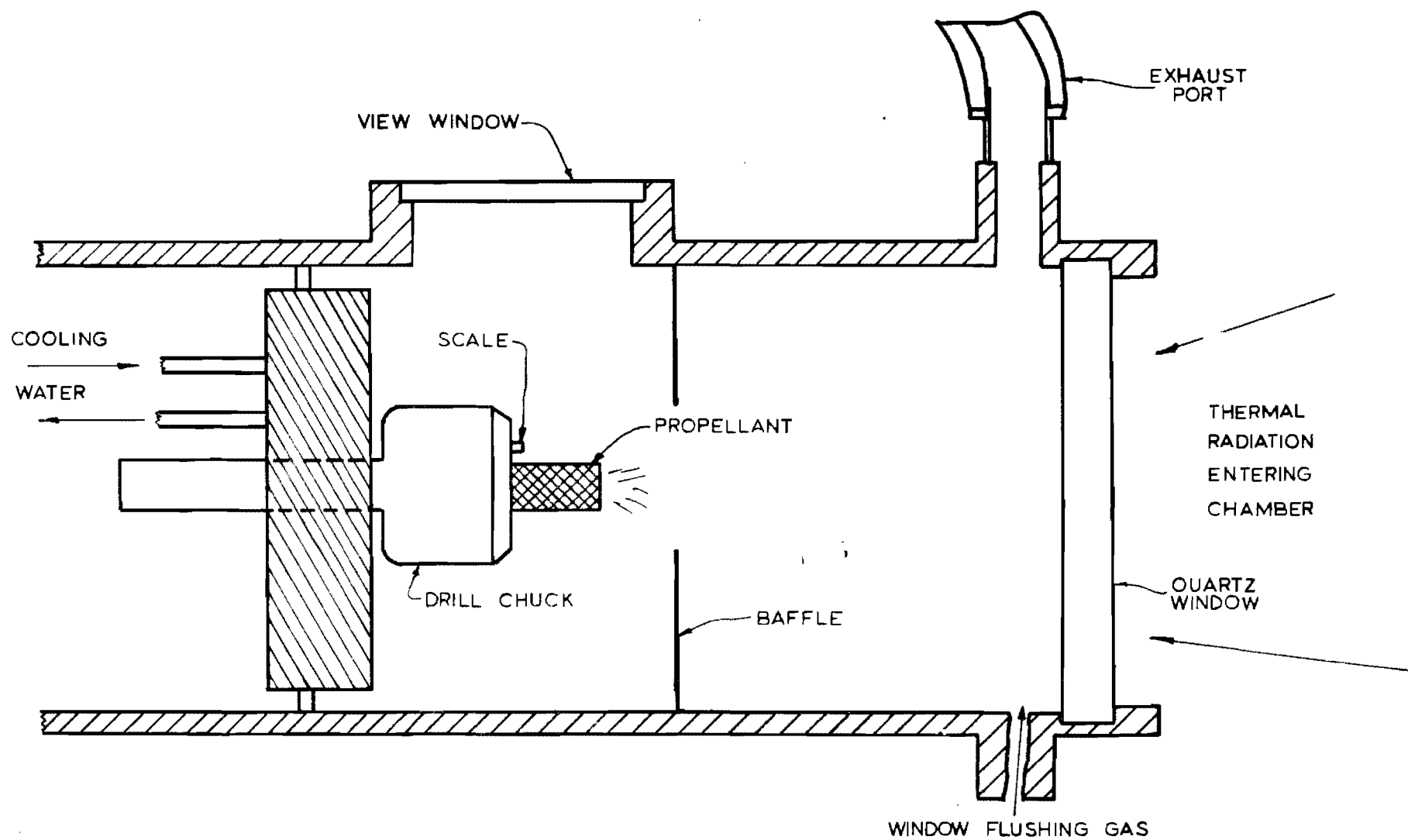


FIG. 5-1. Combustion Chamber with the Mount Used in the Burning Rate Experiments.

radiated period obtained by controlling the shutter.

Two timers were used to control the radiation furnace shutter sequence. The initial exposure was about 1.5 times the known ignition time and was sufficient to insure consistent ignition. The shutter was then closed for one or two seconds to obtain a period of undisturbed steady burning. It is shown in Chapter VI, that the steady-state burning rate is obtained in less than 50 milliseconds after changes in flux for all propellants considered. The shutter was then reopened and the strand exposed to radiation until near sample burnout. Finally, a manual override switch was used to close the shutter. The framing speed of the camera was assumed to be constant during the exposure of each roll. The framing speed of the camera was determined by photographing the digital display of a Hewlett-Packard electronic counter, Model 7250.

The developed film was studied by displaying it on a single frame film reader. Overall magnification varied slightly from run to run and averaged about 8.25. From 10 to 25 runs could be recorded on 100 feet of film. The sample length as a function of time was determined from the photographs for each run, and these data were used to determine the linear burning rate during the test sequence.

### C: ABSORPTION OF RADIATION DUE TO THE PROPELLANT FLAME

Estimates of the imposed radiation losses in the flame were needed in the interpretation of the transient and steady-state burning rate data. Tests designed to yield such estimates are briefly mentioned here and discussed in detail in reference [56]. The methods used to estimate the radiation loss lead naturally to several other experiments involving the transmission of radiation by propellants and the effect of temperature on this partial transparency which are described in reference [56].

Two methods were used for estimating the fraction of the radiation from the arc-lamp which was absorbed by the flame. Both methods gave equivalent results. Each technique, required the use of an RCA 1P42 vacuum photo diode to measure low level heat fluxes. The photo diode output is proportional to the intensity of radiation with peak spectral response at  $0.5\mu\text{m}$  which is near the maximum in the intensity of energy from the xenon-mercury lamp. All systems considered which used the photo diode as a heat-flux indicator were shown to be grey absorbers. The photo diode was calibrated against the type of calorimeter described in Reference [5] at very low flux levels.

The primary technique used for estimating the flame attenuation required the insertion of 0.3mm diameter, thin wall tubes down the axis of the 1.65cm long x 0.65cm diameter samples. The end of the tube on the side of the sample exposed to the radiation extended 1mm beyond the sample surface. The photo diode monitored the radiation through the opposite end of the tube and the decrease in photo cell signal which resulted as the flame was established was assumed to be the result of energy absorption in the flame.

The second technique which was applicable only to translucent propellants, involved monitoring the intensity of lamp radiation which passed through the strand and noting the drop in the photo cell output during the end of the ignition transient.

Table 5.1 summarized the results of this study. The clean burning, polyurethane propellant flame absorbed about 20 percent of the incident energy while for the formulations containing 1 to 2 percent aluminum and solid burning rate catalysts as little as 20 percent of the incident energy reached the propellant surface.

#### D: DATA FROM STEADY BURNING RATE EXPERIMENTS

One advantage of the photographic technique was evident from tests on the various propellants. Anomalous behavior, particularly non-uniform regression, could be recognized and the data from such a test were rejected. The results of the radiation augmentation burning rate studies are summarized in Figure 5-2. The detailed data are tabulated in Appendix C. In all tests, the maximum heat flux from the arc image furnace was  $14.85 \text{ cal/cm}^2\text{sec}$  (uncorrected for losses due to the flame).

With the exception of the low AP loading propellant UBU, all steady-rate burning rates were found to increase linearly with the external heat flux. Propellant UBU was burning near its deflagration limit, for the  $0.80 \text{ cm}^2$  cross-sectional area used in this test, and external radiation was required to sustain combustion. For the larger diameter samples of UBU ( $1.65 \text{ cm}^2$ ) used in the tests described in Chapter VI, the supplementary energy was not required. These burning

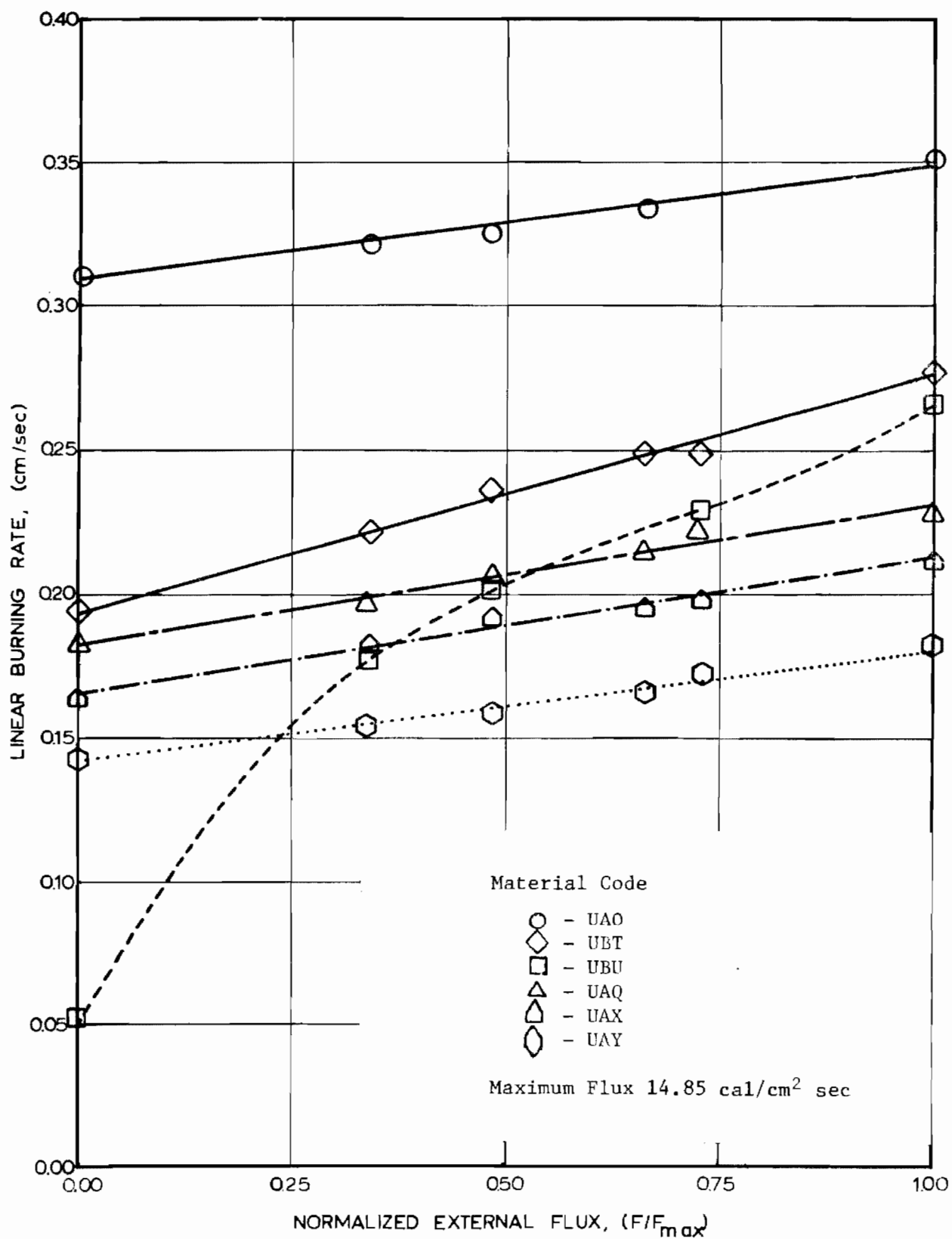


FIG. 5-2. The Effect of External Thermal Radiation on Composite Propellant Burning Rates.

TABLE 5-1  
LOSS OF IMPOSED RADIATION DUE TO THE  
PROPELLANT FLAME

Propellant Code	Average Percent Radiation Loss <sup>1</sup> Through the Propellant Flame
UAO	50 - 60%
UAQ	25 - 35%
UAP <sup>2</sup>	70 - 80%
UBT	15 - 25%
UAZ	15 - 25%
UAY	15 - 25%
UBU	15 - 25%

1 Average range of fractional losses for both the view through a small tube and the direct view through translucent propellants.

2 UAP contains 2% aluminum.

rate data were used to estimate the net heat of gasification.

Table 5-2 contains the net heats of gasification as calculated by using equation 3.11. Note that only general trends with respect to fuel-binder and oxidizer concentration can be drawn.

A possible explanation for the net heat being exothermic is the presence of a very intense flame from the burning of ammonia and perchloric acid which is known to be exothermic [40]. The protrusion of ammonium perchlorate particles above the mean surface of the propellant flame which in turn supply the thermal energy necessary to pyrolyze the fuel-binder. It has been shown that the net heat effect should be exothermic as a consequence of the heat from the ammonia/perchloric acid flame [40]. Estimates of  $q_s$  based on an equation given in the literature[74], yield exotherms for all propellants used in this study.

The principal conclusion of these results is that, because of required assumptions and experimental uncertainties, only order of magnitude values of  $q_s$  may be determined by this technique.



TABLE 5-2  
NET HEAT OF GASIFICATION OF VARIOUS PROPELLANTS ESTIMATED  
FROM RADIATION AUGMENTATION BURNING RATE DATA

Propellant Code	Corrected Slope $\partial r / \partial F$	Net Heat Effect <sup>1,2</sup> $q_1$ cal/q
UAO	$5.98 \times 10^{-3}$	- 64
UBU	$14.6 \times 10^{-3}$	-140
UBT	$6.94 \times 10^{-3}$	- 78
UAX	$3.7 \times 10^{-3}$	0
UAY	$3.28 \times 10^{-3}$	+ 20
UAQ	$3.6 \times 10^{-3}$	0

<sup>1</sup> Initial temperature of the propellant, 2500°K.

Surface temperature of the propellant, 850°K.

Propellant heat capacity, 0.33 cal/g °K.

Propellant density, 1.65 g/cm<sup>3</sup>.

<sup>2</sup>

$$q = \frac{1}{\rho \left( \frac{\partial r}{\partial F} \right)_{T_s, T_\infty}} - c_p (\bar{T}_s - T_\infty) .$$

### E: FACTORS INFLUENCING THE NET HEAT EFFECT

A re-examination of equation 3.3 for the net heat of gasification yields some suggestions for alternate experiments which are related to the consequences of thermal effects near the solid-gas interface.

$$F = m [C_p (T_s - T_{-\infty}) + q_s] . \quad (3.3)$$

If the relationship between heat transfer from the gas phase, conductive and convective, and gas phase burning velocity is ignored and a thermal radiant energy perturbation is treated as being equivalent to a conductive or convective flux perturbation, then equation 3.3 is a valid expression relating a heat flux disturbance, burning rate change and net heat of gasification. To a first approximation this assumption of equivalence between thermal radiant energy and conductive heat flux disturbances is likely valid. In the case of small burning rate fluctuations affected by the flux perturbations, as in this study, the errors arising from the impreciseness of this statement are undoubtedly smaller than the errors in the experiment. It should be recalled that equation 3.25 for the radiation-driven, propellant-response function incorporates the inevitable consequences of forced mass efflux and gas flame adjustments, albeit only for laminar flames. Thus, within the framework of the assumptions incorporated in the interfacial thermal

energy balance, and for small burning rate perturbations, equation 3.3 can be used to estimate the net heat of gasification.

Beginning with the above equation, equation 3.9, the net heat of gasification can be shown to depend on imposed radiant flux, surface temperature and initial temperature as follows,

$$q = \frac{1}{dm/dF} - C \frac{1}{\frac{d \ln(m)}{dT_s}} + C \frac{1}{\frac{d \ln(m)}{dT_{-\infty}}} - C (T_s - T_{\infty}) . \quad (5.1)$$

The first term in equation 5.1, as measured in the present study, is comparatively large, nearly equal to the fourth term. Measurements of the surface temperature of ammonium perchlorate propellants, using IR detection schemes, shows that over a limited pressure range, the surface temperature is constant [41] and in the range from 500°C to 550°C. It has been shown that decomposing ammonium perchlorate exhibits a temperature sensitivity similar to that given by an Arrhenius expression [40,41], with an activation energy of about 30,000 cal/gmole °K. Presumably, ammonium perchlorate-oxidized propellants should follow a similar Arrhenius expression,  $m = B \exp (-E/RT)$ , which yields,

$$\frac{d \ln(m)}{dT_s} = \frac{E_s}{RT_s^2} . \quad (5.2)$$

The effect of initial temperature on propellant burning rates has been shown to be of the form,

$$\frac{m}{m_{\text{ref}}} = a \left( \frac{T_{-\infty}}{T_{-\infty, \text{ref}}} \right)^b \quad (5.3)$$

where  $m_{\text{ref}}$  is the mass burning rate corresponding to the reference initial temperature and  $a$  and  $b$  are positive constants [35].

$$\frac{d \ln(m)}{dT_{-\infty}} = \frac{b}{T_{-\infty}} \quad (5.4)$$

Combining equation 5.1, 5.2 and 5.4, the result is,

$$q = \frac{1}{dm/dF} - C T_s \left( \frac{RT_s}{E} + 1 \right) + C T_{-\infty} \left( \frac{1}{b} + 1 \right). \quad (5.5)$$

Equation 5.5 indicates that increasing the initial temperature yields higher net heats of gasification. High surface temperatures, at constant surface activation energy, make the net heat effect less endothermic. Possibly, as in the case of fuel-binders which resist thermal degradation, the net heat effect could change from an exotherm to an endotherm simply by lowering the oxidizer loading. If the imposed flux causes large changes in the burning rate, the net heat effect would be small, according to equation 5.5, *i.e.*, a smaller heat sink would be more easily saturated. Figure 5-3 is a plot of equation 3.3 showing the net heat of gasification as a function of surface temperature and imposed flux-burning rate curve slope.

The principal conclusion here is that because of required assumptions and experimental uncertainties, only order of magnitude values of  $q_s$  may be determined by this technique.

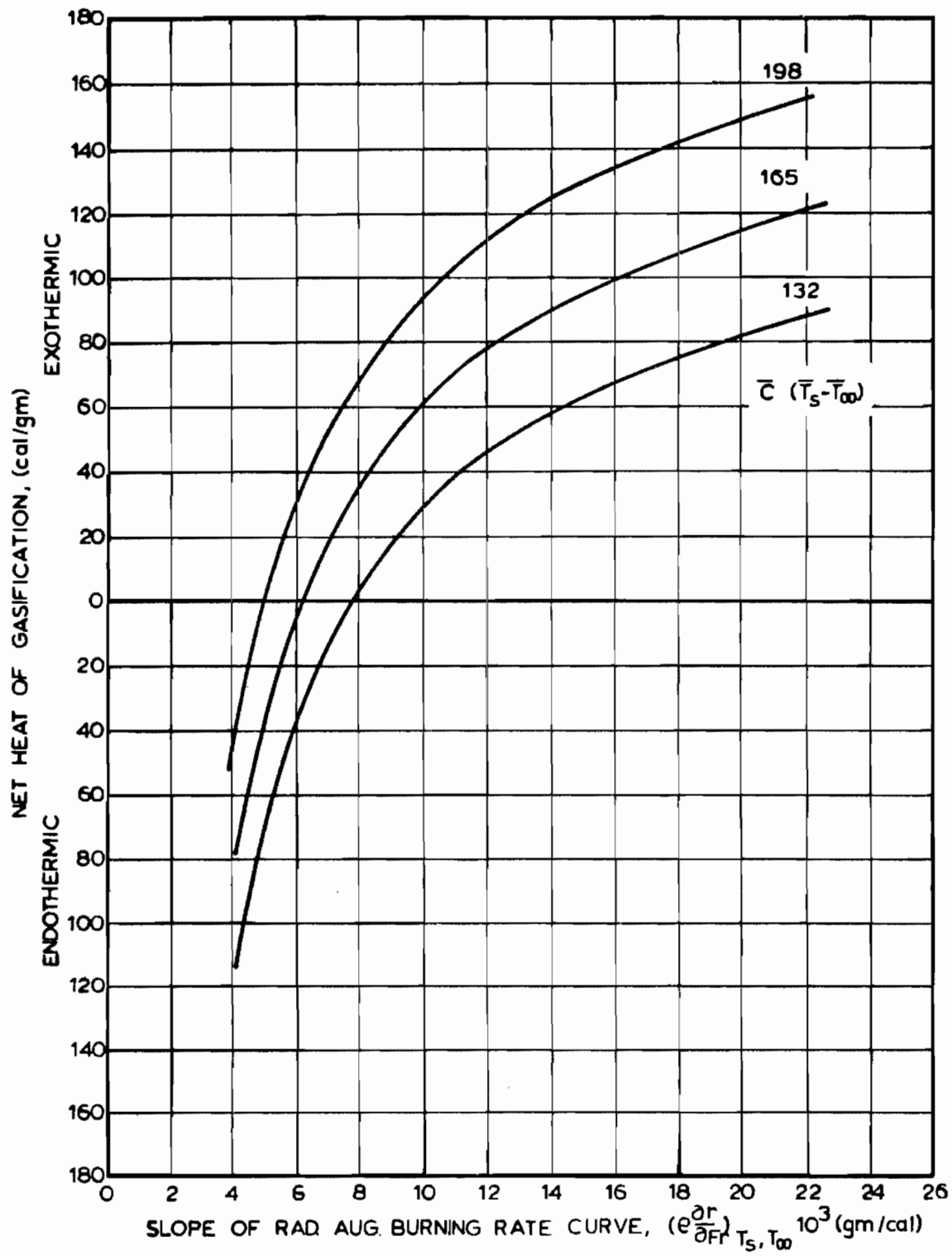


FIG. 5-3. The Effect of Surface Temperature on the Net Heat of Gasification.

## CHAPTER VI: TRANSIENT BURNING RATE EXPERIMENTS

As discussed in Chapter III, several significant questions related to oscillatory combustion remain unanswered. This chapter contains the presentation of an experiment designed to determine the magnitude of the burning rate response to periodic surface heat flux perturbations. The objective of these experiments was to demonstrate the trends in the transient burning rate for a range of imposed thermal radiation frequencies.

### A: EQUIPMENT: MICROPHONE ADAPTED AS A TRANSIENT FORCE TRANSDUCER

The choice of a method for measuring the combustion recoil force discussed in Chapter III, equation 3.48, was made after the performance criteria were set. These criteria are: (1) the sensing element must be capable of detecting the small changes (100 to 2000 dynes/cm<sup>2</sup>) in force produced by the burning rate perturbations stimulated by the radiant heat flux; (2) the response characteristics should be independent of the strand size; and, (3) the response time of the unit must be shorter than the period of driving frequencies used to perturb the burning propellant.

Many techniques for measuring the force created by the recoil of a burning propellant strand were attempted before a suitable method was devised. Among the methods attempted were: (1) a micro-thruster or ballistic pendulum [23,43,44,45,75,76]; (2) a high

quality phonograph cartridge, Shure M44-5, adapted as a force transducer; and, (3) a strain element carrying the burning propellant [43,44].

The successful technique finally devised involved using a sound pressure microphone, Kistler Instrument Corporation Model 717, driven by the burning propellant which was supported by a low-friction load bearing fork.

Figure 6-1 shows the unit used for the dynamic response experiments (transient burning). The transducer used to sense the recoil force was sensitive to changes in recoil force, not steady state values of the force. This feature proved to be advantageous since only the change in force as a consequence of the burning rate change was sought. The transducer response was linear over a wide range of frequencies and had high enough sensitivity to detect the low-level transient forces. Thermal protection of the unit was necessary because it was light and heat sensitive. This required placing the propellant strand support behind heat shields, and connecting it to the transducer with a drive pin. The moment about the low friction bearing created by the strand mount caused the drive pin to rest against the transducer. Ideally, no loss of frequency response should be caused by this arrangement. However, the response time of the transducer with the strand mount in place and the assembled unit placed in a vertical position was found to be between 0.5 and 2 milliseconds and was found to have a decay frequency of about

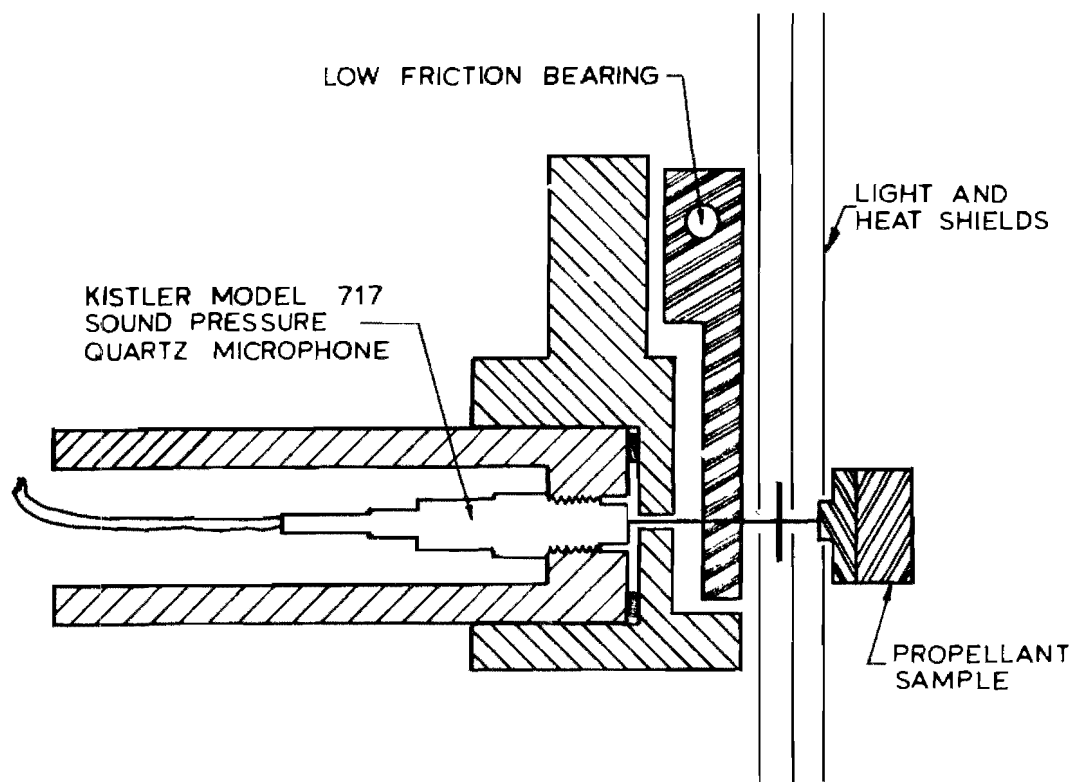


FIG. 6-1. Micro-Force Transducer and Propellant Mount for Transient Burning Rate Experiments.



2500 Hz. This compares with 10 microseconds response time and a frequency range from 2 to 50,000 Hz given by the manufacturer for the transducer. Testing the response time of the assembled unit in the vertical position with weights, 1 to 5 gms., on the pedestal was considered a suitably severe test. In use, the assembled unit was in a horizontal position and was judged to have minimal response time of 1 millisecond and a minimal natural frequency of 2500 Hz. The maximum frequency of the driving heat flux was 200 Hz. There was no need to operate at higher frequencies because the maximum response was observed to have occurred below 100 Hz for all propellants tested. The response time of the vacuum photo diode was on the order of microseconds and was independent of other system variables.

Each of the propellants tested exhibited a diminishing mean value of the transducer signal which approached zero at some high driving frequency, but not the same frequency for each propellant, of course. This particular observation added further supporting evidence that the sensing element was responding to burning rate changes and was not simply an equipment limitation. Propellant samples three times as large as used in the majority of the tests were used to determine whether the transducer sensitivity was mass dependent. If the sensitivity were found to be mass dependent, then one would be back to the nonstationary response problem which the experiment was designed to avoid. Fortunately, the system was

found to be insensitive to the three-fold change in initial sample mass. Several advantages were gained by using this technique: (1) consistent sample mounting was possible; (2) only changes in force are sensed by the transducer; and, (3) the very high spring constant of the transducer minimizes the problem of mass-dependent response characteristics which are unavoidable with more flexible systems. The assembly shown in Figure 6-1 was placed directly inside the combustion chamber shown in Chapter IV. A photo diode, RCA 1P42, was placed next to the transducer to determine the period of sample exposure to the perturbing flux. The transducer and photo diode were along the same axis of the radiation beam so that the photo diode detected essentially the same exposure history as the sample.

#### B: PROPELLANTS USED FOR THE TRANSIENT BURNING RATE

The propellants used in the transient burning rate (dynamic response) experiments contained a high loading of oxidizer in order to produce relatively clean flames which would absorb less of the external radiation. Selection of propellants was dictated by the desire to characterize in detail only a few typical propellants, which would yield general results, rather than performing an extensive study involving many propellants. Table 6-1 contains the list of propellants used in this study. Table C-1 in Appendix C contains the composition data for these propellants as well as those used in related experiments.

TABLE 6-1  
PROPELLANTS TAILORED FOR DYNAMIC RESPONSE EXPERIMENTS

Material Code	Oxidizer Ammonium Perchlorate	Fuel Binder	Additives	Burning Rate cm/sec
UBU	65%, 50% 5 $\mu$	PU <sup>1</sup> , 32%	nbf <sup>2</sup> , 2% 1% carbon black	0.119
UBT	65%, 50% 5 $\mu$	PU, 33%	nbf, 2%	0.247
UAX	80%, 40/40 <sup>3</sup>	PU, 18%	nbf, 2%	0.196
UCX	80%, 40/40	PU, 17%	nbf, 2% 1% carbon black	0.137
UCV	80%, 40/40	PBAA <sup>4</sup> , 18%	copper chromite, 2%	0.317
UCW	80%, 40/40	PBAA, 19%	carbon black, 1%	0.154

<sup>1</sup> Polyurethane.

<sup>2</sup> N-butyl ferrocene.

<sup>3</sup> 50% coarse, +48-100; 50% fine, 50% 5 $\mu$  or less.

<sup>4</sup> Polybutadiene-acrylic acid copolymer.

These propellants represent a suitable range of O/F ratio, binder and catalyst to be representative of many ammonium perchlorate propellants. In addition to the requirements mentioned above, propellants usable in this type of experiment must burn fairly uniformly at moderate pressures, *i.e.*, near atmospheric pressure. The combustion products should permit radiation penetration of the flame zone. This precludes the use of highly metallized propellants and suggests the use of high oxidizer to fuel ratios. The low pressure burning rate should be low enough that the maximum obtainable driving flux frequency can correspond to the frequency of the thermal wave relaxation time,  $\alpha/r^2$ . A dimensionless flux frequency greater than ten should be feasible. With the available equipment, this limited the burning rate to less than 0.3 cm/sec for propellants having a thermal diffusivity of  $10^{-3}$  cm<sup>2</sup>/sec.

#### C: PROCEDURE FOR TRANSIENT BURNING RATE EXPERIMENTS

Propellant cylinders, 1.65 cm in diameter, were cut from cured propellant slabs, sliced to the desired length, usually 0.65 cm, and stored in plastic bags until tested. The pre-selected propellant samples were inhibited along all non-burning surfaces with a thin coating of Kel-F #90 grease. Carbon black was dusted on the exposed surface to aid ignition. The surface of each sample was roughened to promote flame spread over the entire surface. The individual steps for each run were:

1. The inhibited sample was placed on the mounting pedestal. A thin layer of Dow Corning grease on the sample base provided adhesion. The output of the transducer (microphone, hereafter abbreviated K.U.) was checked by manually tapping the sample surface lightly and noting the deflection of the oscilloscope display.
2. The oscilloscope grid was photographed and the shutter left open.
3. The dowser plate of the furnace was opened. The speed of the chopper wheel, which had already been operating at the selected speed, was checked by noting the period of the exposure by use of the time interval meter.
4. A tape recorder (PI Model 2100) was started at a speed of 15 ips and was operated in the record (FM) mode. The photo diode (P.D.) and K.U. signals were recorded simultaneously.
5. The oscilloscope sweep, which was preset at 1 sec/cm, was started.
6. The small shutter between the dowser and the chopper wheel assembly was manually opened, and the sample ignited.
7. After sample burnout, the flux was terminated. The tape recorder was stopped, and the photograph of the oscilloscope trace was developed.

Ordinarily, ten or twenty samples of each propellant were fired

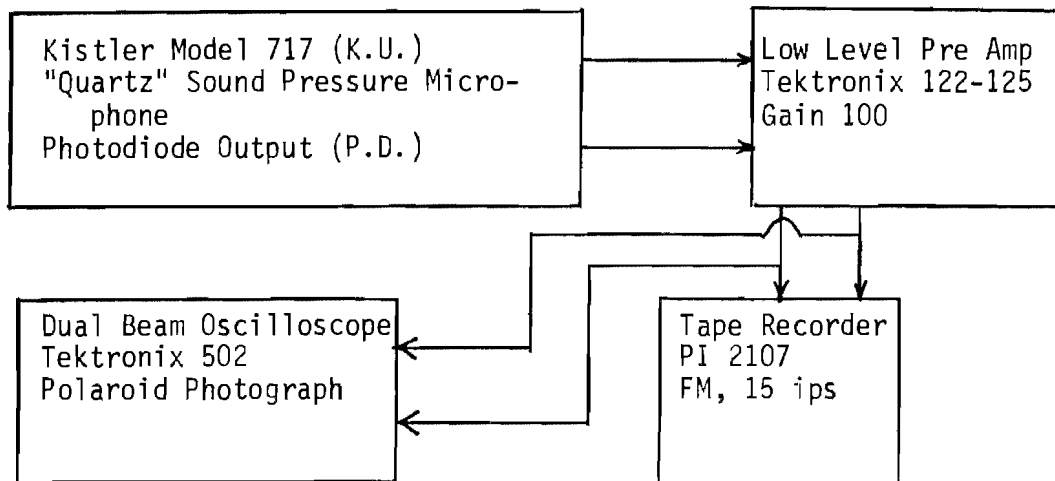
during each of the fourteen series of experiments. A total of 590 tests of this type were performed in the determination of the burning rate response.

#### D: DATA ACQUISITION AND REDUCTION

The data acquisition system is shown on Figure 6-2. Typical output from this system are shown on Figure 6-3. The top trace is the Kistler Unit (K.U.) output and the bottom trace is the photo diode (P.D.) output. Note that no signal from the K.U. is present until the sample ignites. The ignition time was also determined from these photographs and served as a check on the heat flux (as per thermal ignition models). All tests were restricted to atmospheric conditions. Both the transducer and photo diode signal were amplified using the Tektronik type 122 amplifier. The gain setting was 100. The amplified transducer signal was recorded at 15 inches per second on channels #1 and #7 of the PI Model 2107 tape recorder. Channels #3 and #5 were used to record the photo diode signal. Playback was usually at 3 3/4 inches per second, yielding a time expansion of four. The amplifier output was also monitored to provide a check on each test. The taped data formed a permanent record of the tests and was processed after each series of tests.

The frequency of the imposed flux was modified for each test but was maintained at a constant value throughout the test. The frequency was controlled by the setting on a heavy-duty rheostat

# DATA ACQUISITION PROCEDURE FOR DYNAMIC RESPONSE EXPERIMENTS



## DATA ANALYSIS FOR DYNAMIC RESPONSE EXPERIMENTS

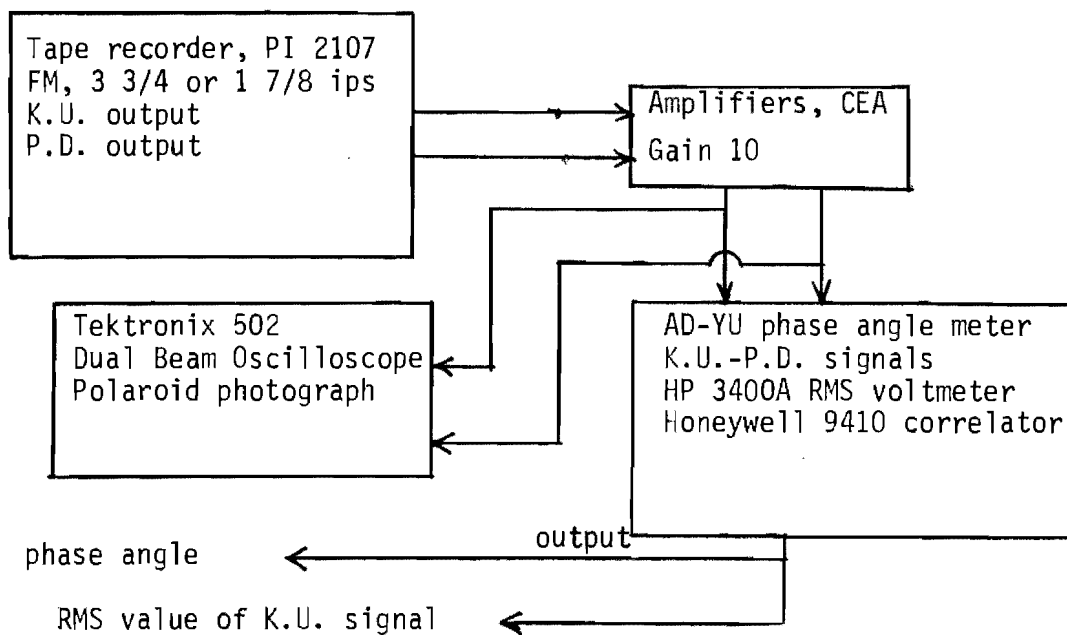


FIG. 6-2. Block Diagram of Data Acquisition and Data Analysis Procedure for Dynamic Response Experiments

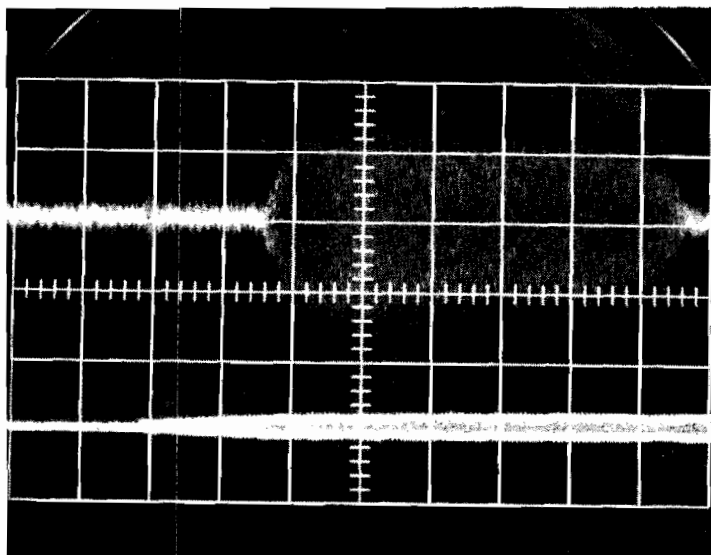


Fig. 6-3a. Transducer Signal from Propellant UBU, Run Number 1402, Frequency 40 Hz.  
 Top Trace: transducer signal, 10 mv/cm.  
 Bottom Trace: photodiode signal, 20 mv/cm.  
 Oscilloscope sweep rate, 1 sec/cm.

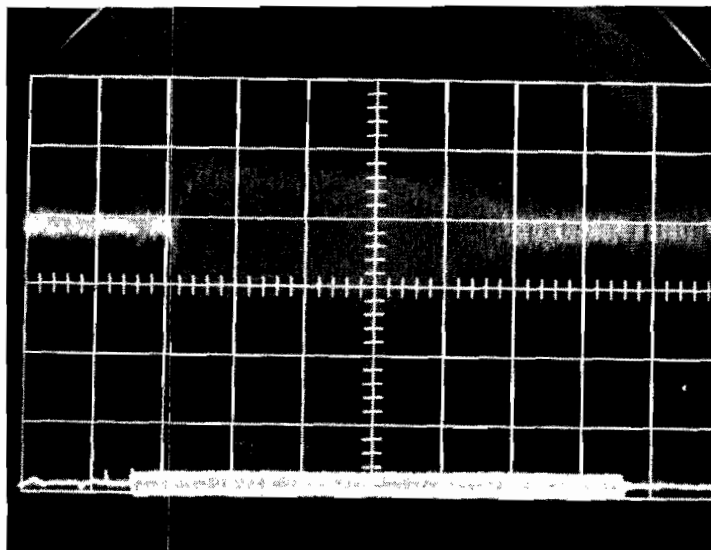


Fig. 6-3b. Transducer Signal from Propellant UCX, Run Number 1147, Frequency 50 Hz.

FIG. 6-3. Typical Output for Transient Burning Rate Experiments.



in the DC power line to the chopper motor. The direct output from channel #1 was fed to the HP 3400 root-mean-square voltmeter and the analog output recorded on a Honeywell Electronik 19, strip chart recorder operating at 5 sec/in, *i.e.*, 0.8 in = 1 second test time. Examples of the results are shown in Figures 6-4 and 6-5. Note that the initially high value of the signal diminishes with the burn time. This was thought to be due to coning of the strand. Only the average over the initial one second of the test was used in preparing the figures. A large number of tests were performed for each propellant, a total of 590 for the five propellants, so complete confidence can be placed in the observed trends of maximum response at the critical frequency. The higher frequency signals observed on the transducer signal were considered to be electronic noise unrelated to the combustion. The possibility of electronic noise in the system causing the signals was checked by recording signals from a HP Model 202A function generator. Playback showed that the amplifiers, tape recorder and strip chart recorder were not coupled in a way to produce a self-amplifying noise. The rms signal levels before and after a run were nearly identical. These signal levels were subtracted from the driven combustion signal to yield the response due to the flux perturbation. The background noise, apparently acoustic disturbances, was a function of the perturbing flux frequency and was traceable to the chopper wheel. At high frequency this acoustic noise became equal to the

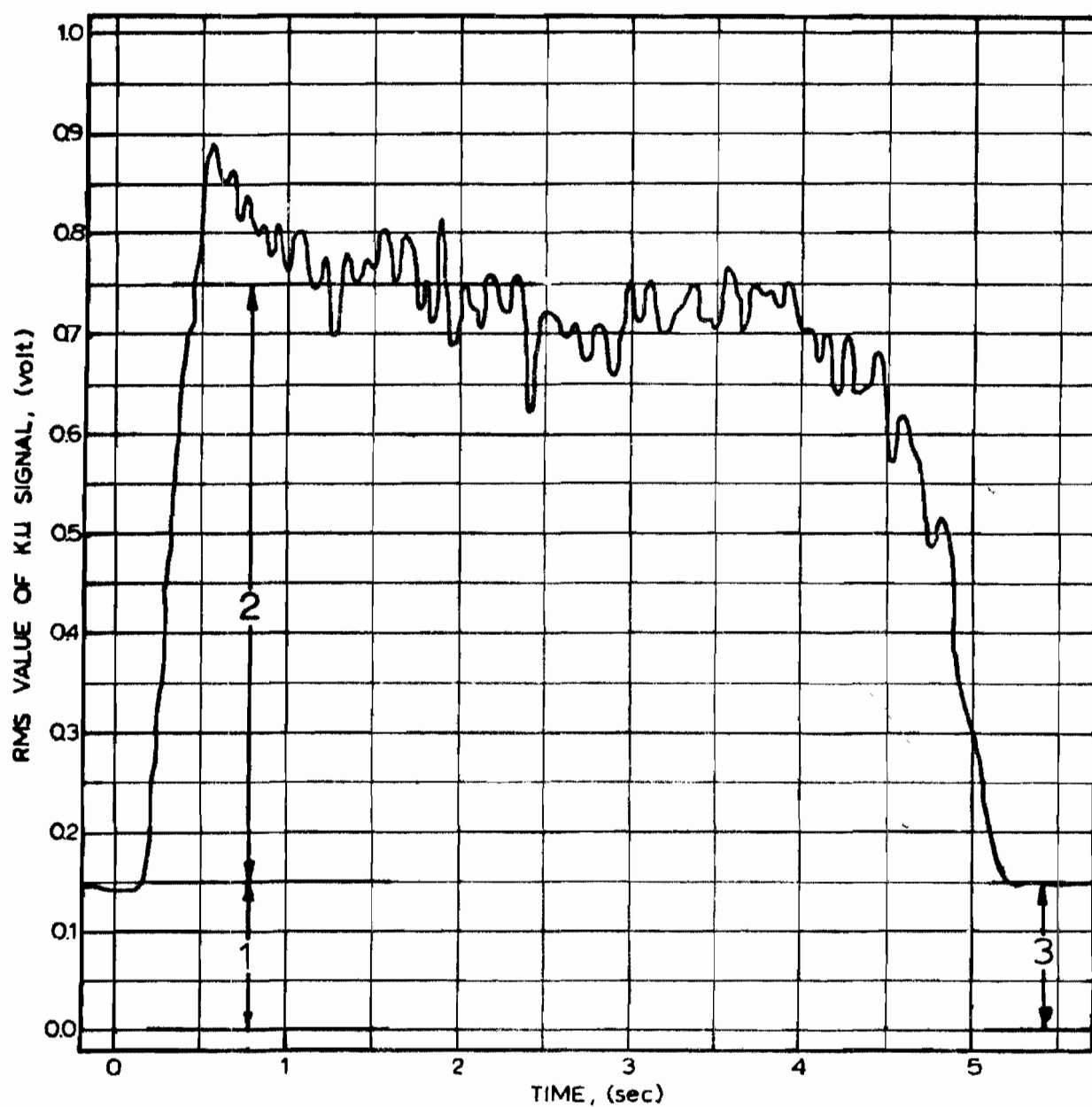


FIG. 6-4 Strip Chart Record of HP rms Voltmeter Signal for Radiation-Driven Combustion as Measured with the Micro-Force Transducer. Run Number 1402, Propellant, UBU, 40 Hz.

1. Background noise before ignition.
2. Signal of driven combustion.
3. Background noise after burnout.

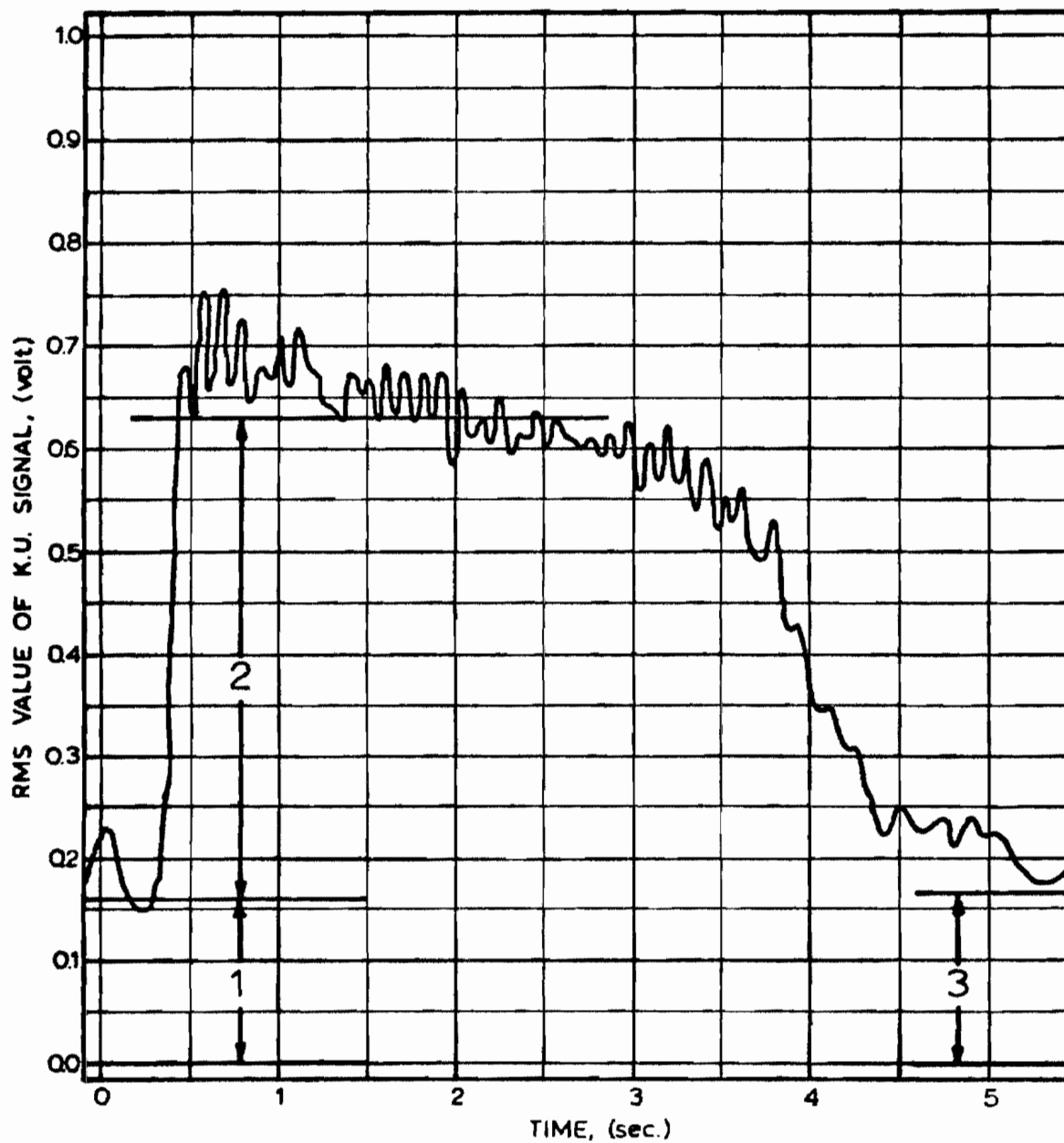


FIG. 6-5. Strip Chart Record of HP rms Voltmeter Signal of Radiation-Driven Combustion as Measured with the Micro-Force Transducer. Run Number 1147, Propellant UCX, 50 Hz.

1. Background noise before ignition.
2. Signal of driven combustion.
3. Background noise after burnout.

intensity of the driven combustion signal. Average values of the corrected transducer signal were determined and plotted as suggested by theoretical considerations. An averaging time of one second, in real time, was chosen for the data reduction. The strand surface tended to become non-planar as it regressed, although a fairly flat surface was maintained for one or two seconds. The effects of the non-flat surface was to cause a loss of signal amplitude during the course of each test. The use of the halocarbon, Kel-F #90 grease, as an inhibitor effectively postponed the coning of the sample long enough that consistent, meaningful data were obtained. For very fast burning propellants,  $\bar{r}$  about 0.5 cm/sec at atmospheric pressure, the transducer and photo diode signal were processed by use of a Honeywell Time Delay Correlator, Model 9410, in an attempt to determine the correlation coefficient between the applied flux and burning rate response. However, because of equipment limitations, it was not possible to obtain uniform signals of long enough duration to determine accurate correlations.

The phase angle between the K.U. signal and the P.D. signal was also measured. A AD-YU Model 405 phase meter coupled to a strip-chart recorder for direct analog output was used. The resultant phase angles determined for each propellant were plotted as suggested by theoretical considerations. Because of the short test times and poor signal quality, an error of  $\pm 10$  degrees existed in these data although high confidence could be placed in the trends observed.

Of all the measurements made in this study, the error in the phase angle was the greatest, although extensive precautions were taken to minimize this error. Experimentally, it was noted that the phase angle tended to increase during nearly all runs. Initially, the angle was the lowest, *i.e.*, strong coupling between the driving flux and the propellant response, but after about one or two seconds, it tended to increase by about ten degrees. Only the time average, one second in real time, values of the phase angle are plotted on the figures. The phase angle measured was always the lag between the K.U. and P.D. signals. None of the tests indicated that the K.U. signal lead the P.D. signal, although a lead angle was predicted on theoretical grounds. Equipment limitations precluded the detection of a lead angle between the K.U. signal and the P.D. signal.

The ordinate on the figures of propellant response is an arbitrary linear scale in units of volts. This happened to be the most convenient way to present the data directly from the data reduction system. To reduce the transducer signals further and relate them directly to the mean transient burning rate, the steady state burning rate measurements and the transducer calibration curve are needed. External thermal radiation increases the propellant burning rate linearly, for all practical purposes (see Chapter V). The transducer had linear response over a wide range of frequencies and since the sample mounting pedestal experiences no displacement during operation, one can confidently claim that the combustion recoil sensing element

exhibits linear response. If points along the transducer mean signal curve are related to the known steady state burning rate change, then one knows the mass burning rate under dynamic conditions. This presumes, of course, that the transient burning rate can be averaged to equal the mean burning rate; which in turn requires the assumption that the chemical kinetics, diffusion of reactive species and the heat transfer under transient conditions are essentially the same as under steady state conditions. Such an assumption must rest primarily on faith because there is no way to experimentally check the difference in these parameters for the steady and unsteady burning. Small perturbations in surface heat flux were used to affect changes in the steady burning so the mode of deflagration is probably near the steady state condition. The principal features of the propellant burning rate response curves are the linear increase at low frequency, the resonance point and the diminishing response at driving frequencies greater than the resonance frequency.

The results from the burning rate response experiments can be conveniently divided into two discussions according to the propellant fuel. The polyurethane propellants exhibited a definite maximum response while the PBAA propellants exhibited lower response to the perturbing flux and the response signal shows only a slight maximum. Experimental results from the polyurethane propellants can be further divided according to the effect of the particle size, the catalyst loading and the oxidizer to fuel ratio. Two PBAA propellants

were studied to determine the effect of the copper chromite burning rate catalyst.

#### E: POLYURETHANE PROPELLANTS

Five polyurethane-fueled propellants were successfully tested under conditions of perturbing heat flux. Three of these propellants, UCX, UAY, and UAX were of relatively high O/F ratio comparable to operational propellants. Thus, results from the determination of the frequency at maximum response should be comparable to the results from T-burner tests for the response of similar propellants. Two polyurethane propellants, UBU and UCX were used to observe the effect of O/F ratio on the critical frequency. The influence of oxidizer particle size, that is surface heterogeneity, can also be inferred from a comparison between propellants UCX and UBU. Comparing the response of propellants UCX, which was opaque, with the translucent propellant, UAX, shows the marked influence of opacity on the magnitude of the propellant response. Figures 6-6 through 6-8 summarize the response curves for the polyurethane-fueled propellants. All data are presented in the Tables in Appendix C.

Another polyurethane propellant, UBT, was tested in thirty runs, but was found to exhibit essentially zero response and was not used in extensive tests. The influence of absorption of radiation in depth was assumed to be the principal reason zero response was measured for propellant UBT and several other propellants having an extinction coefficient less than  $100 \text{ cm}^{-1}$ . A propellant similar to UCX, except it contained 1% n-butyl ferrocene-catalyst, was tested but the results are not shown here. This formulation was found to exhibit similar burning rate response characteristics to propellant UCX with the exception that the magnitude of the peak response was slightly lower.

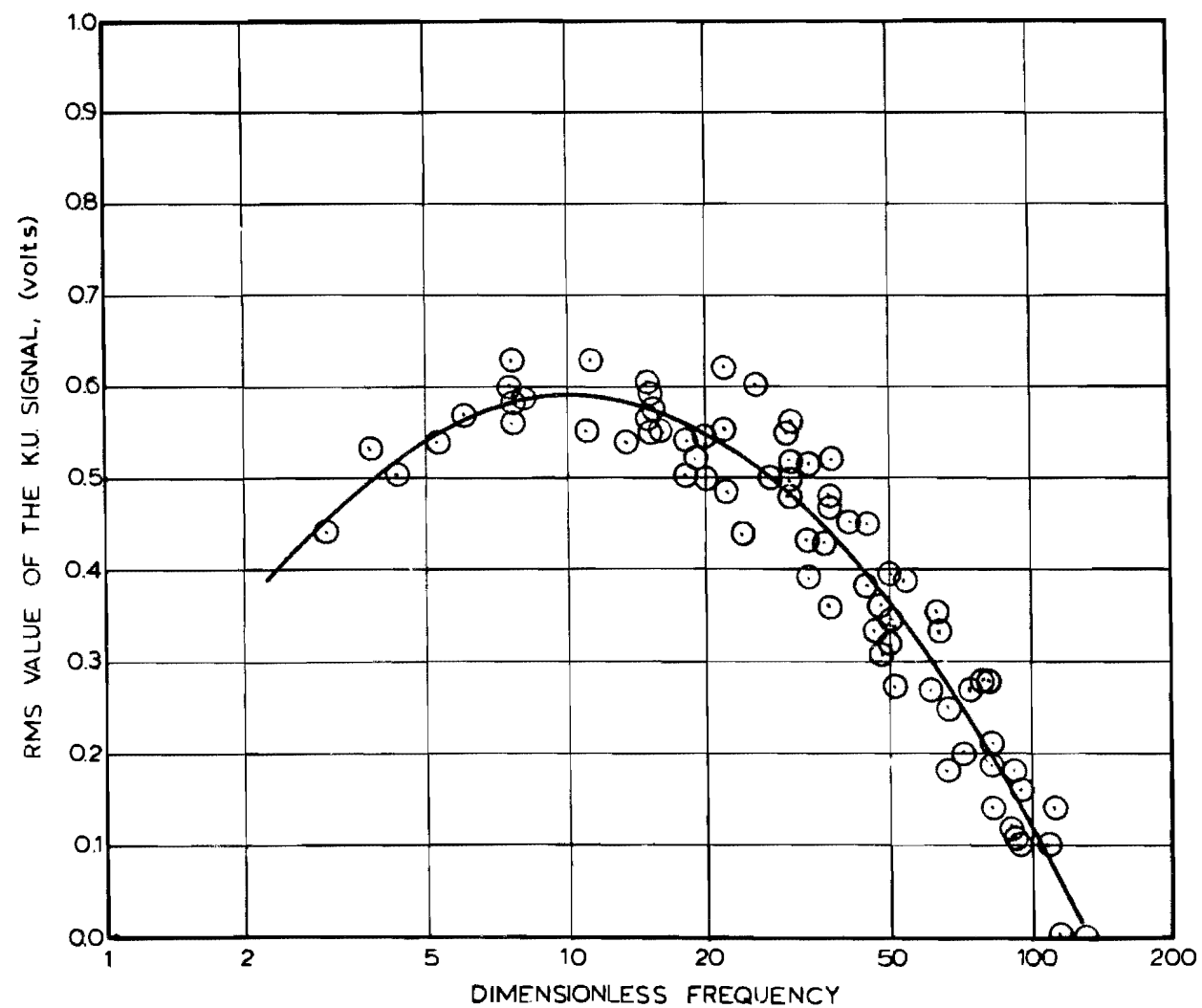


FIG. 6-6. Mean Value of the Transducer Signal for Thermal Radiation-Driven Oscillatory Burning of Polyurethane Propellant UBU.



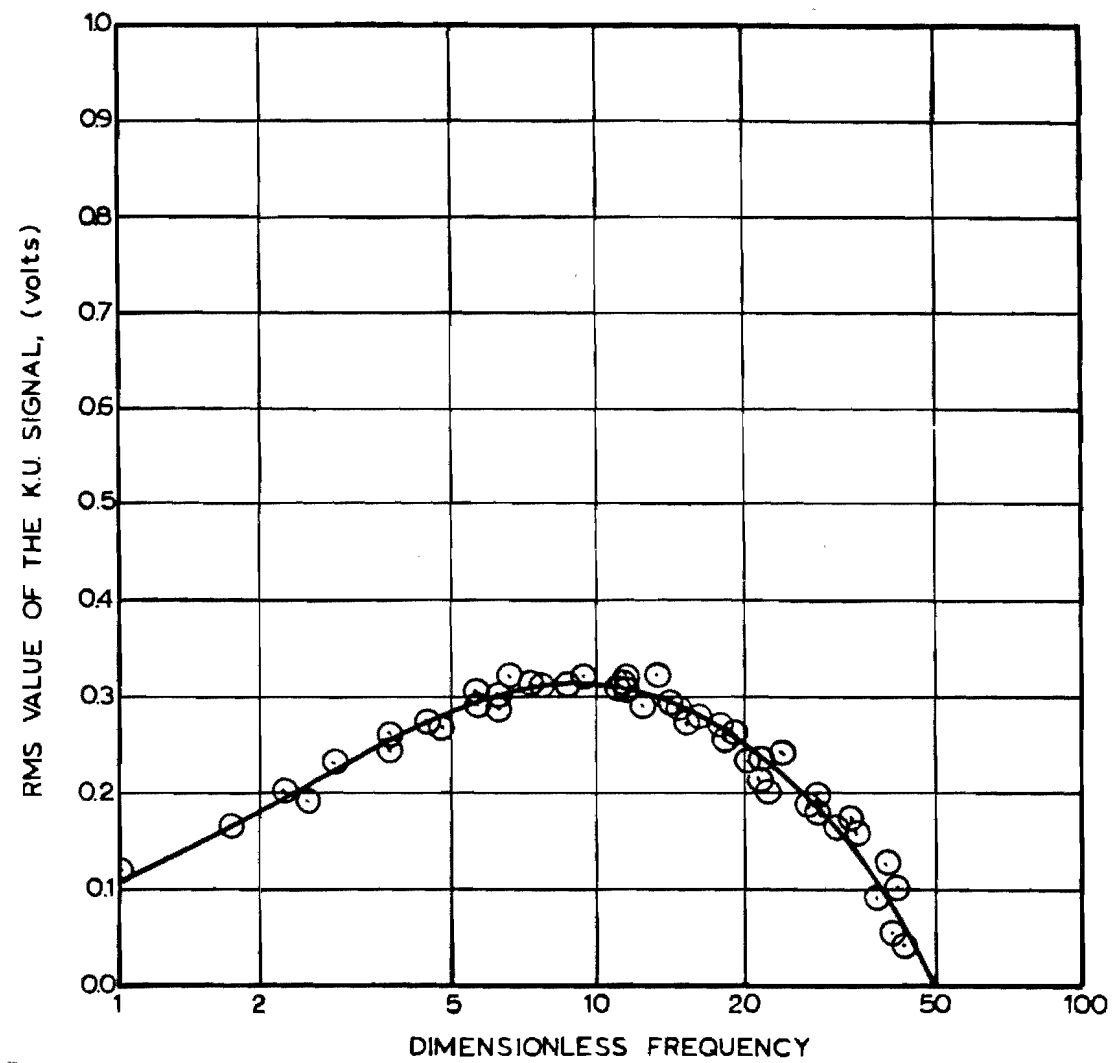


FIG. 6-7. Mean Value of the Transducer Signal for Thermal Radiation-Driven Oscillatory Burning of Polyurethane Propellant UAX.

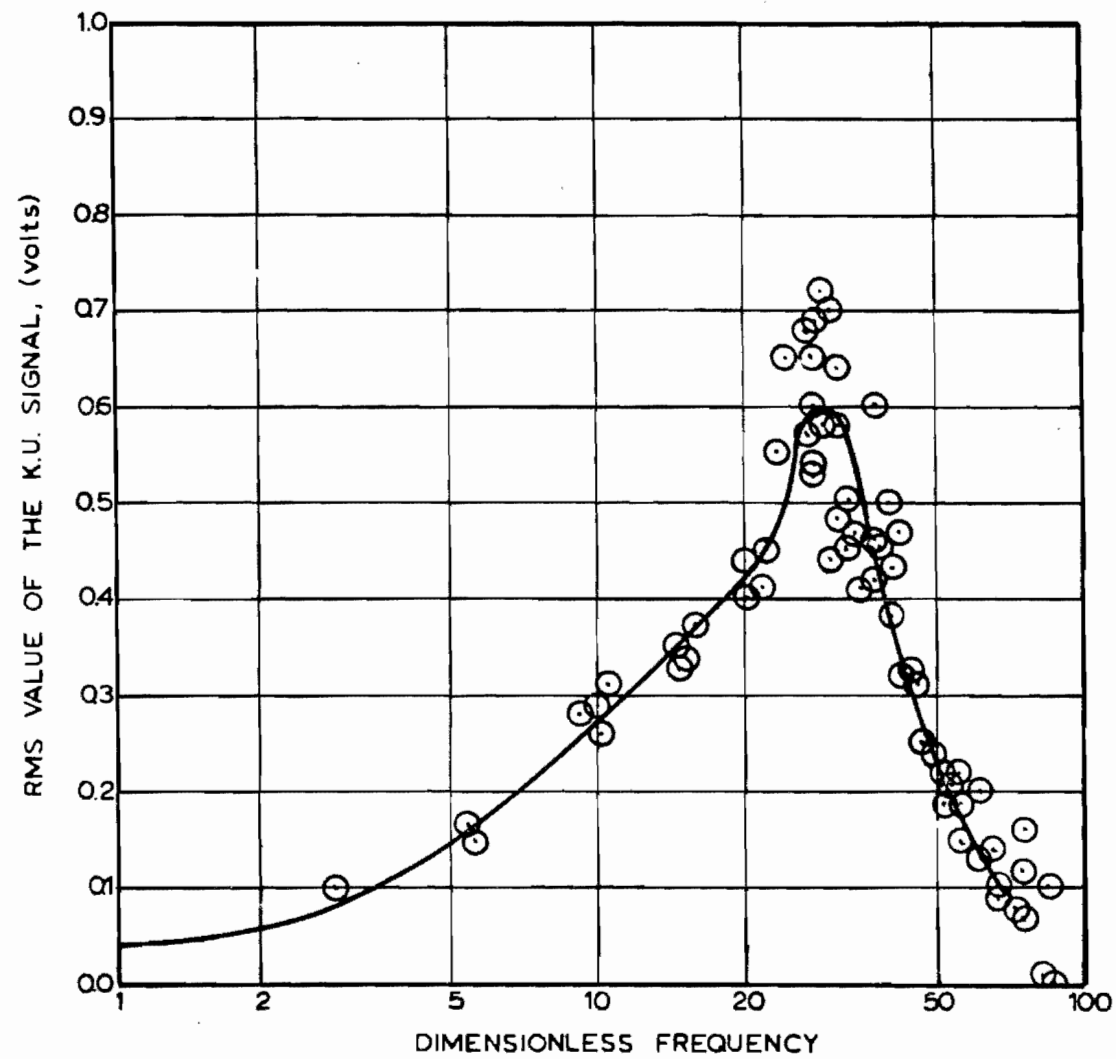


FIG. 6-8. Mean Value of the Transducer Signal for Thermal Radiation-Driven Oscillatory Burning of Polyurethane Propellant UCX.

All of the partially opaque polyurethane propellants showed increased response as the perturbing frequency increased from a low value. As the frequency was then increased, a maximum in the response occurred and at still higher frequencies the magnitude of the periodic response to the heat flux decreased to zero. Since the burning rates of these propellants was only 0.1 to 0.2 cm/sec at 0.85 atms, it was possible to achieve dimensionless frequencies in excess of 100 by use of perturbing frequencies below 200 Hz, and the complete response function at atmospheric pressure could be obtained. Although some scatter is noted, the results shown in Figure 6.6 to 6.8 represent data from three to six individual series of tests which were usually run on different days. In general, significantly different results were observed from day-to-day only near the frequency of the maximum where the response is likely most sensitive to small variations in composition, heat flux, etc.

Figure 6.9 presents the averaged UCX and UAX data normalized to the zero frequency limit and compared to calculated response based upon Eq. 3.46 for the translucent propellant. Since it was not possible to measure the zero frequency response with the microphone force transducer, the zero frequency value was obtained by extrapolation, and fairly significant errors might result from this extrapolation. Since the force transducer yielded the magnitude of the response in Figure 6.9 the calculated values are the magnitude and not the real part of the response function which was the quantity presented in earlier plots.

Perhaps the most significant feature of the UCX results shown in Figure 6.9 is that the maximum response occurred at a dimensionless frequency of about 30. It was necessary to use a very high activation

energy for the surface pyrolysis reaction of 90,000 cal/(g-mole) ( $^{\circ}\text{K}$ ) in Eq. 3.46 to get agreement between observation and calculation for the position of the maximum. The other parameters used ( $E_f/R = 25,000^{\circ}\text{K}$ ,  $q_s = -15 \text{ cal/gm}$ ,  $\bar{r} = .137 \text{ cm}^{-1}$ , and  $\lambda = 500 \text{ cm}^{-1}$  and those of Figure 3.6) were selected on the basis of expected values for the known physical processes and to fit the magnitude of the maximum and the measure phase angle between the flux perturbations and the mass efflux. In the case of the semi-transparent UAX propellant, which was identical to UCX except for the absence of the small quantity of carbon black, an opacity of  $100 \text{ cm}^{-1}$  was assumed and all other parameters were assumed to be the same. The change in the magnitude of the maximum in the response was satisfactorily predicted, but the observed change in the dimensionless frequency at the maximum from 30 to about 10 was not calculated. In fact, no change in the model parameters was found which produced a change in the frequency of the response maximum by variation of the opacity. Possibly, condensed phase reactions which are affected by the energy absorption in depth could be responsible for the experimentally noted change of the frequency of maximum response between propellant UCX and UAX.

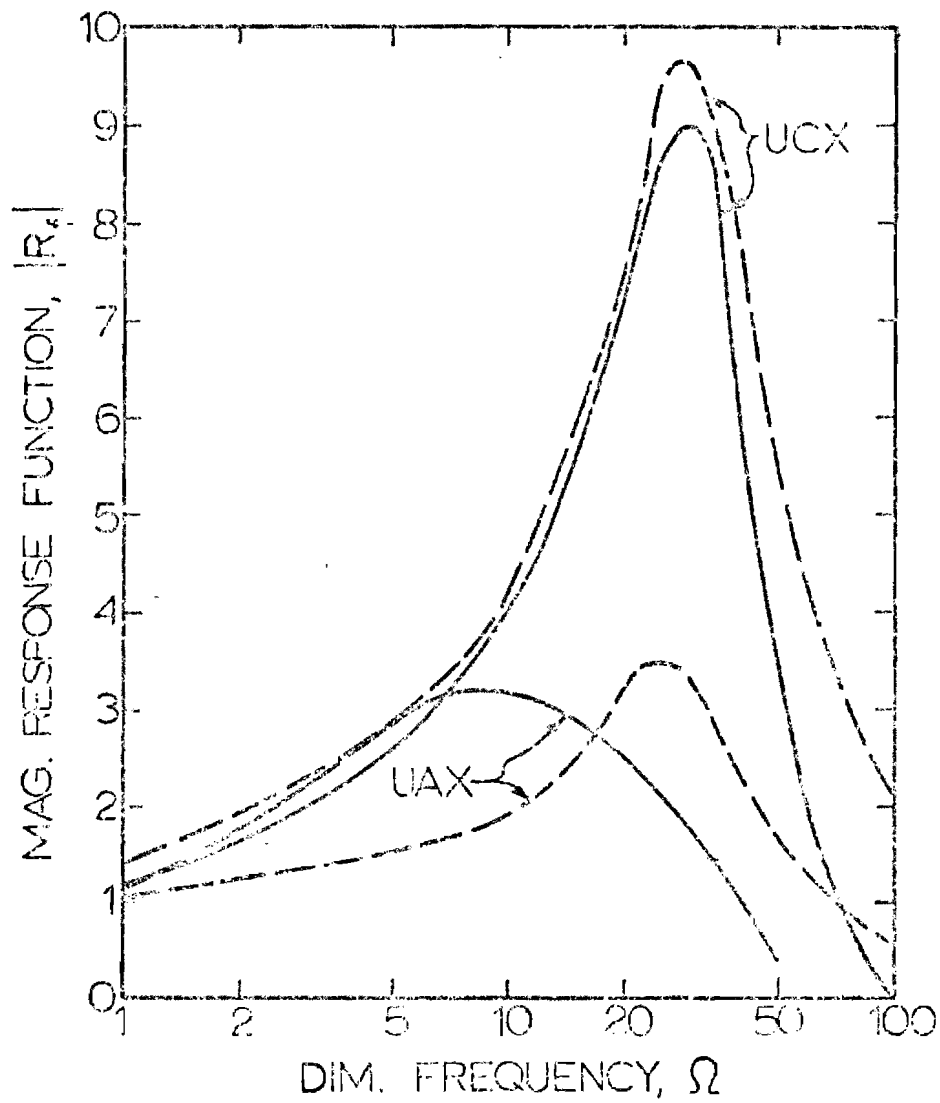


FIG. 6-9 A comparison is shown here between the magnitude of the response functions calculated from the modified conventional theory and experimental values. The dash lines are for the calculated values.

#### F: POLYBUTADIENE PROPELLANTS

Two PBAA-fueled propellants were prepared and tested in the same manner as the PU-AP propellants. The data are plotted on Figure 6-10 and Figure 6-11. Only a small increase in the magnitude of the response with frequency was produced by the external flux, but the response did exhibit a slight maximum.

The differences in behavior of the PBAA and PU based propellants are very great and this result is consistent with observation of such propellants in other test devices. Propellants UCV and UCW correspond closely to Utah F-propellant and Utah BG-propellant previously used in T-burner studies [59] and low  $L^*$ -burner experiments [81].

An interesting feature of the PBAA-AP propellants results is the fact that the uncatalyzed propellant UCW exhibited a response maximum at a higher dimensionless frequency than the catalyzed propellant. The frequency of the catalyzed propellant maximum response is between 80 and 90 Hz for UCV, and between 75 and 85 for UCW. Although the real driving frequencies overlap somewhat, the maximum for the catalyzed propellant did occur at a higher real frequency. Because of its higher burning rate, the transducer signal from the UCV propellant was higher than for any other propellant tested. In general, the magnitude of response was directly related to the mean burning rate as required by Eq. 3.48. Carbon black was included in the formulation of UCW to minimize the problems associated with in-depth absorption of radiant energy.

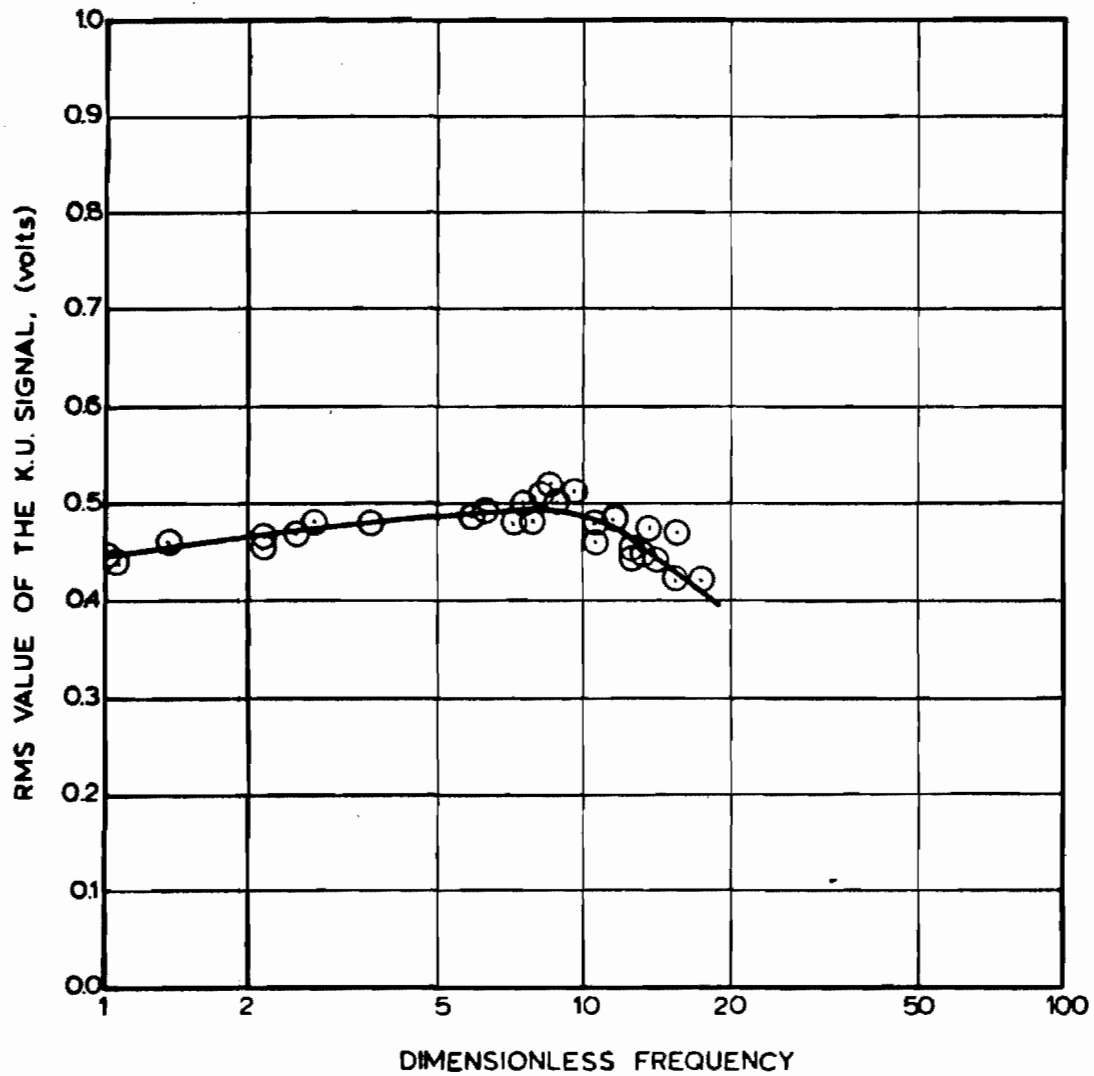


FIG. 6-10. Mean Value of the Transducer Signal for Thermal Radiation-Driven Oscillatory Burning of PBAA Propellant UCV.

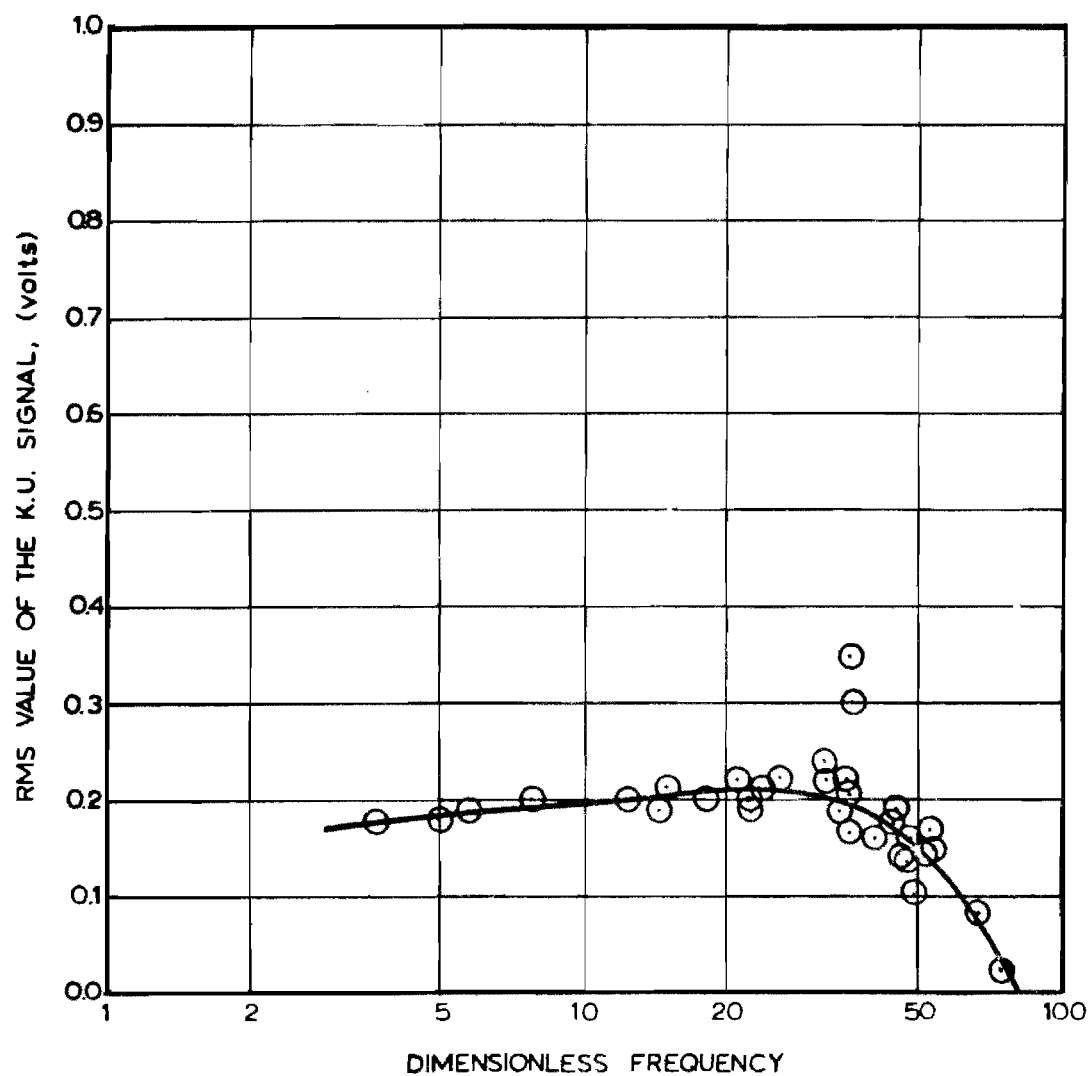


FIG. 6-11. Mean Value of the Transducer Signal for Thermal Radiation-Driven Oscillatory Burning of PBAA Propellant UCW.



Regardless of modifications made in the loading fraction, particle size distribution or type of catalyst, PBAA-AP propellants appeared to exhibit different responses to the perturbing heat flux when compared to PU-AP propellants. The less pronounced maximum response and less distinct increase in burning rate at low frequency, again in comparison to polyurethane-fueled propellants, suggests that the response of the propellant is strongly affected by the polymer reaction processes and that different mechanisms for response may be involved with different systems.

The nature of the response of these propellants was such that a large number of combinations of parameters in the response model could be used to reproduce the experimental results. No unique set could be found and no comparison between experiment and theory is presented here.

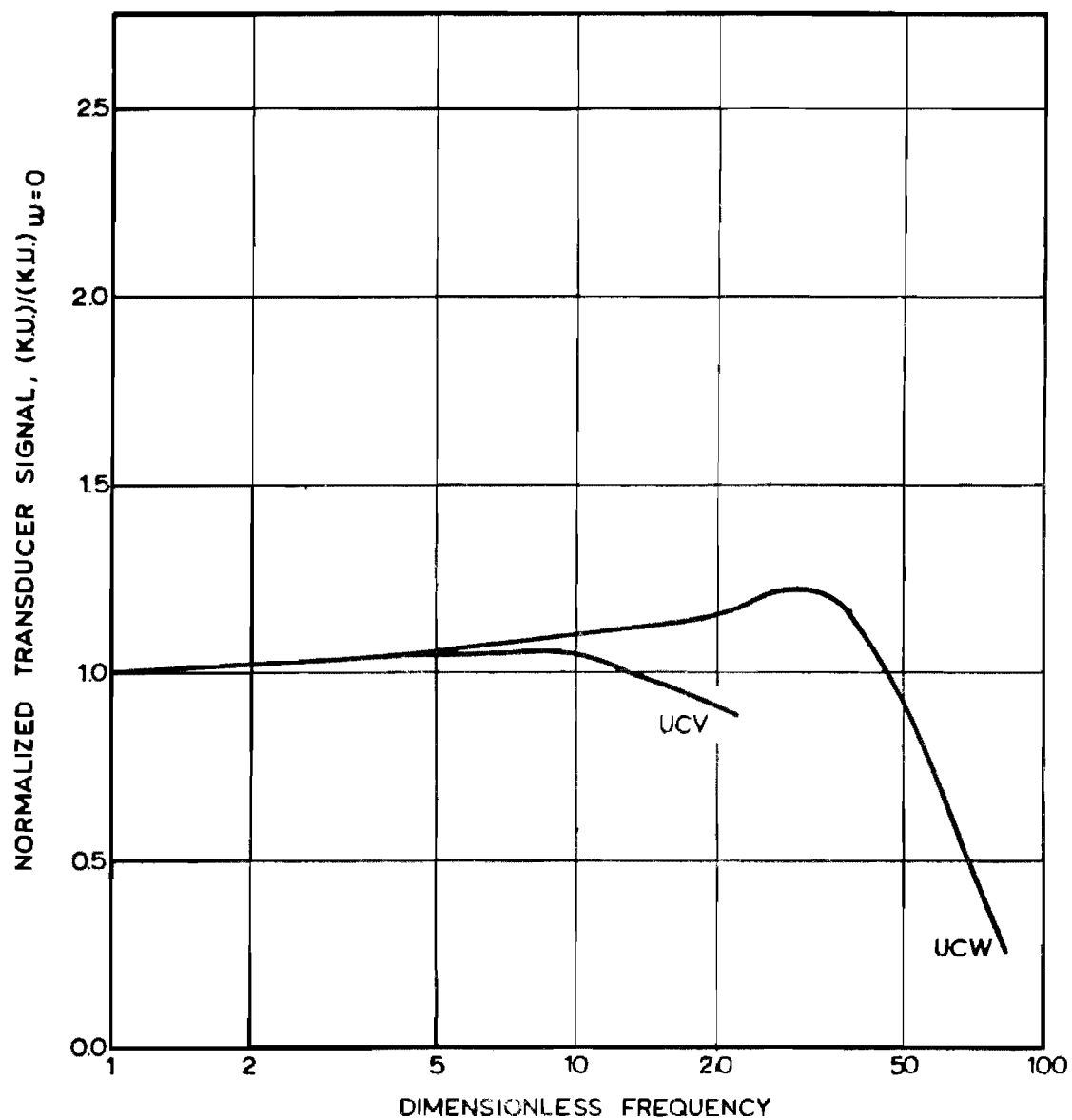


FIG. 6-12. Normalized Mean Value of the Transducer Signal for Thermal Radiation-Driven Oscillatory Burning of PBAA-AP Propellants.

## G: PHASE ANGLE MEASUREMENTS

Figure 6-13 through 6-19 show the measured phase angle between the K.U. signal and the P.D. signal for all the propellants tested. The abscissa on Figures 6-13 through 6-17 is the dimensional frequency. The phase angle data are presented in this way to demonstrate that no resonance with 60 Hz noise was in the signals. Figures 6-18 and 6-19 show the phase angle data plotted against the dimensionless frequency to facilitate the comparison with the response measurements shown on Figures 6-9 and 6-12. No evidence of a lead angle at low frequency was found. This was suspected of being due to the combined limitations of the phase meter and the tape recorder. It should be noted that the inception of the phase angle lag corresponds to the frequency of maximum response shown on Figures 6-9 and 6-12.

Qualitatively, both the burning rate response and the phase angle measurements agree with the theoretical predictions. The differences which exist are possibly due to the imprecision of the experimental data and the invalid assumption used in the model. The one-dimensional analyses and the assumption of quasi static behavior of the gas are most suspect.

Since no comprehensive theory was developed, although one considered to be rather complete has been discussed in Chapter III, and because it was demonstrated that the complete theories do not describe oscillatory combustion adequately, other, more limited,

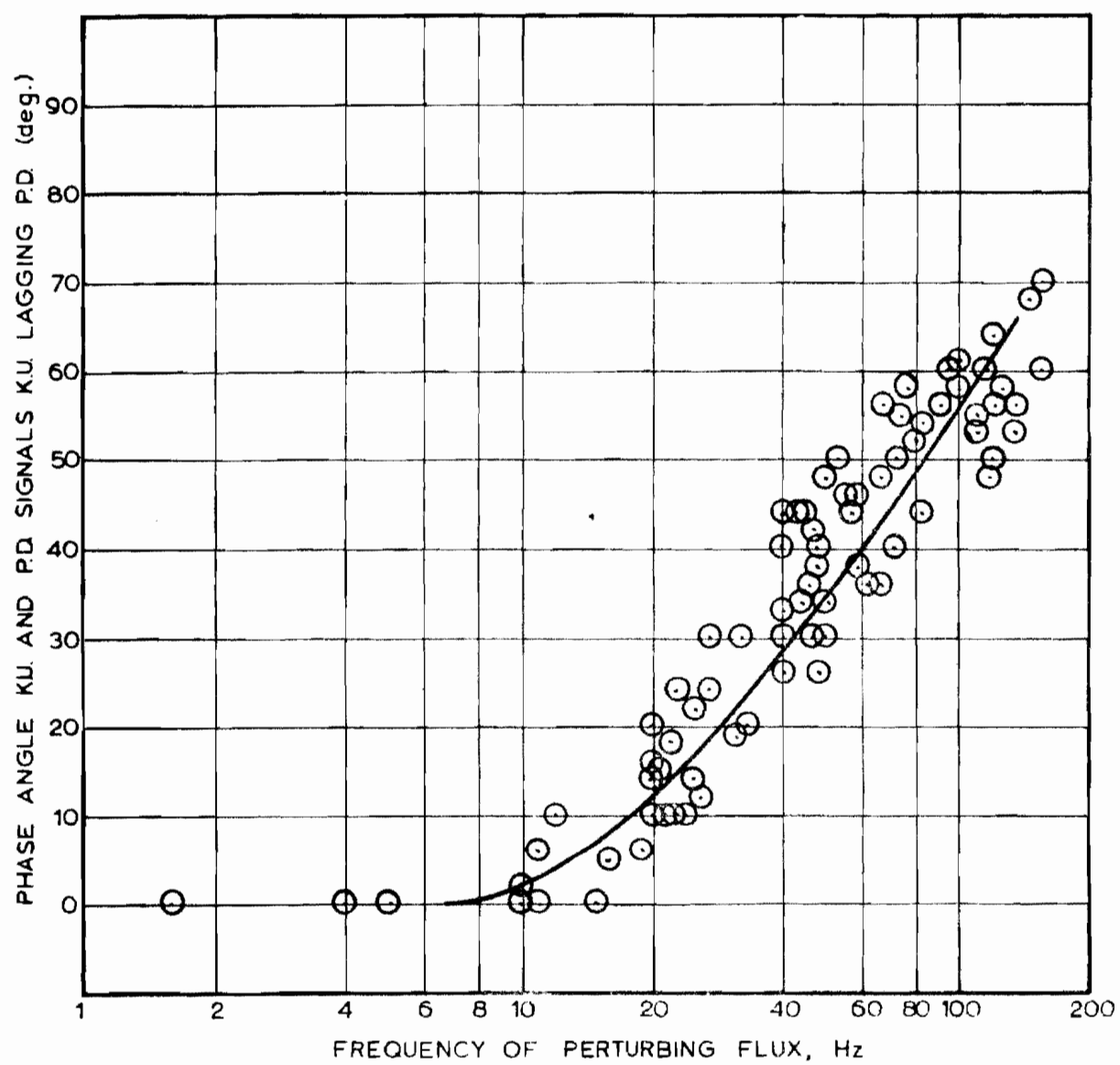


FIG. 6-13. Phase Angle Between Force Transducer Signal and Photodiode Signal for Polyurethane Propellant UBU.

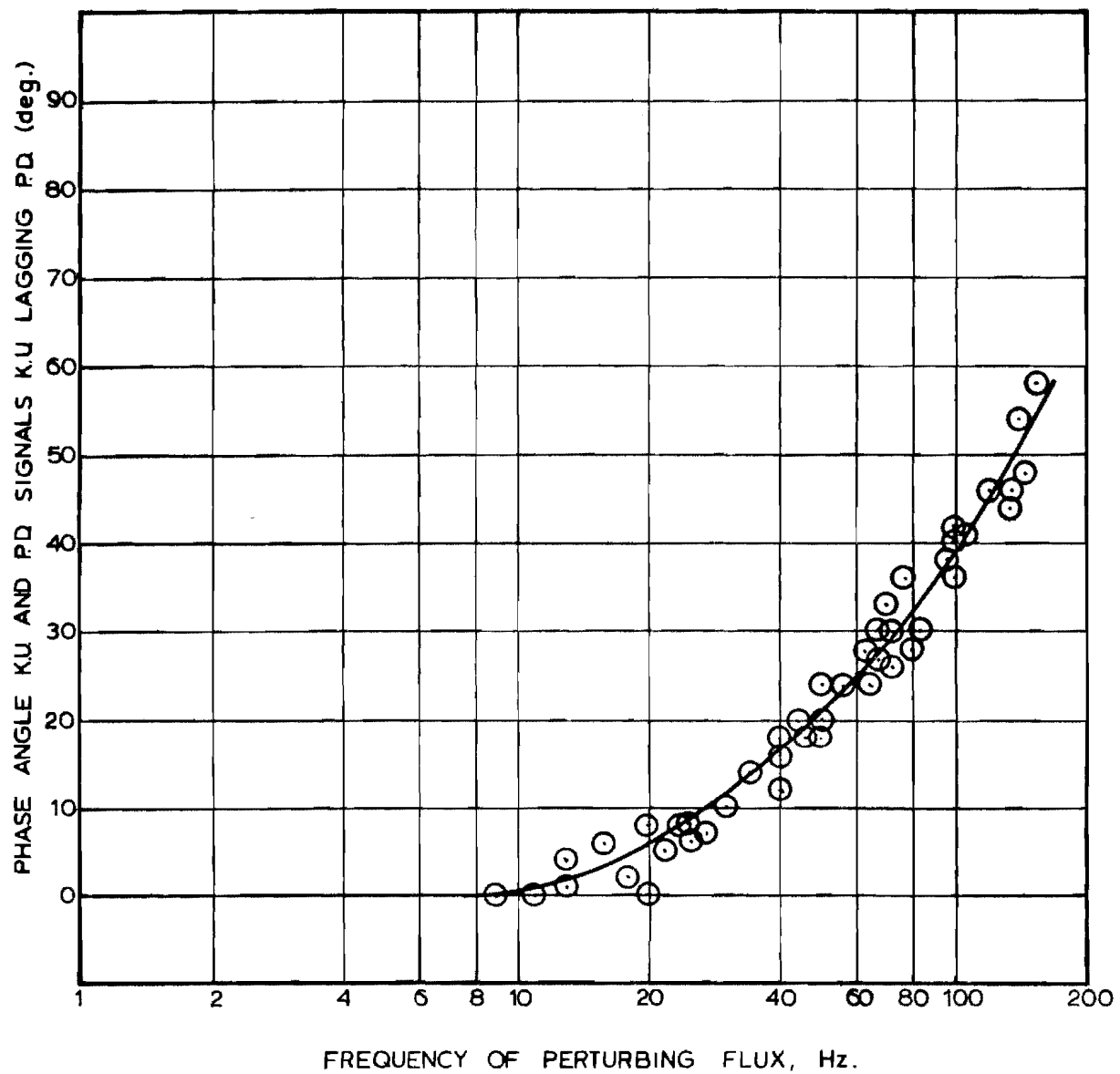


FIG. 6-14. Phase Angle Between Force Transducer Signal and Photodiode Signal for Polyurethane Propellant UAX.

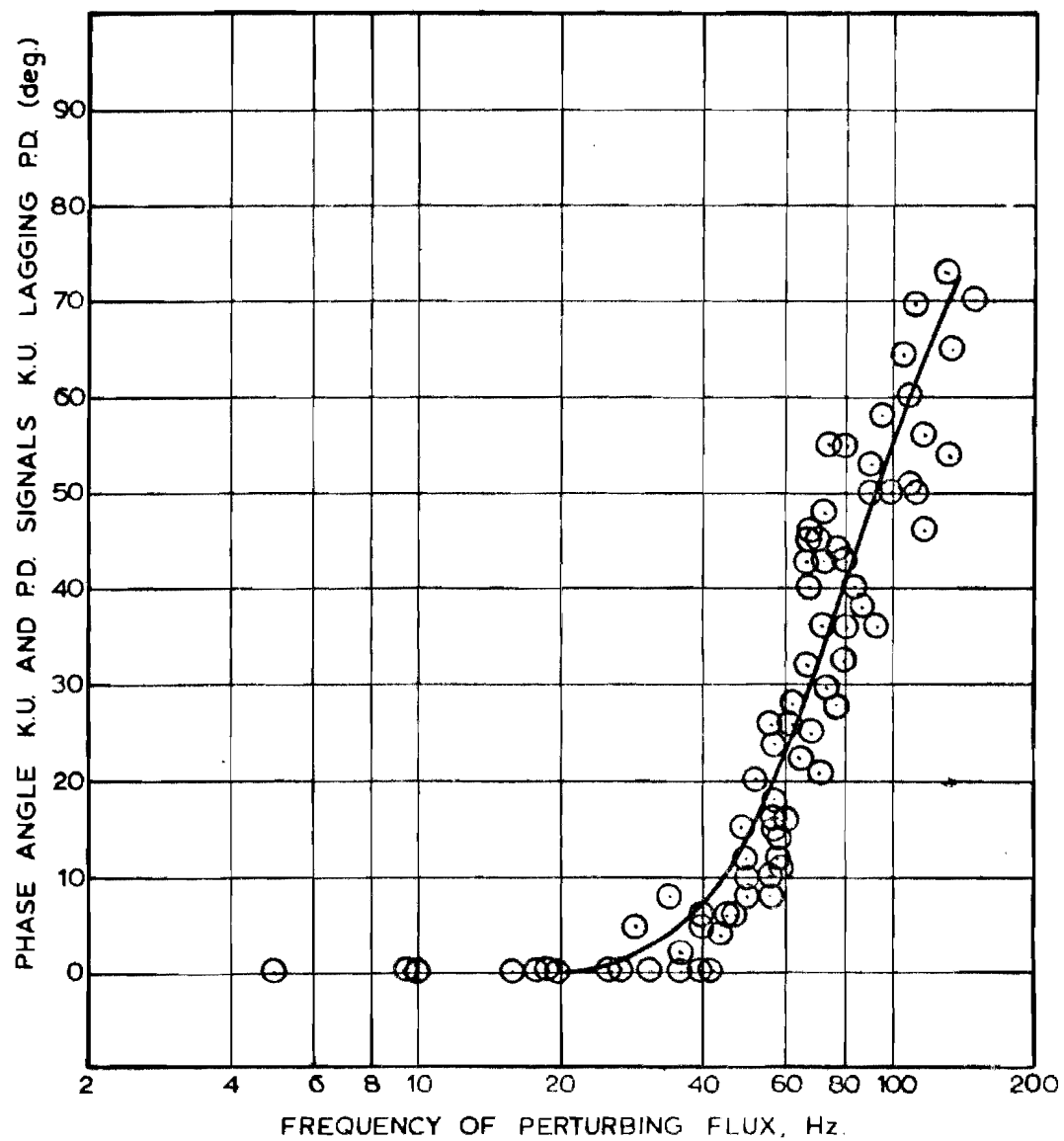


FIG. 6-15. Phase Angle Between Force Transducer Signal and Photodiode Signal for Polyurethane Propellant UCX.

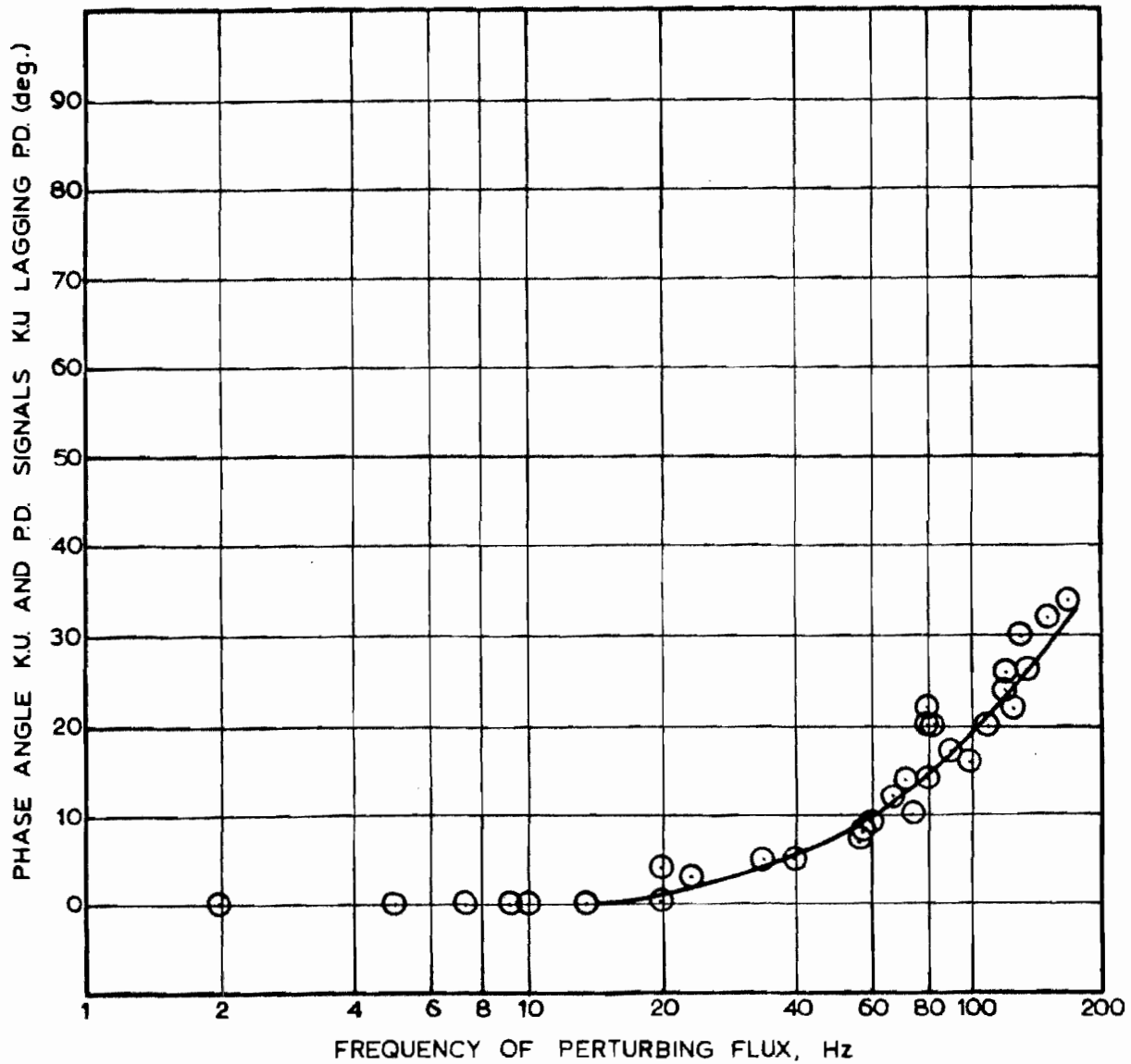


FIG. 6-16. Phase Angle Between Force Transducer Signal and Photodiode Signal for PBA Propellant UCV.

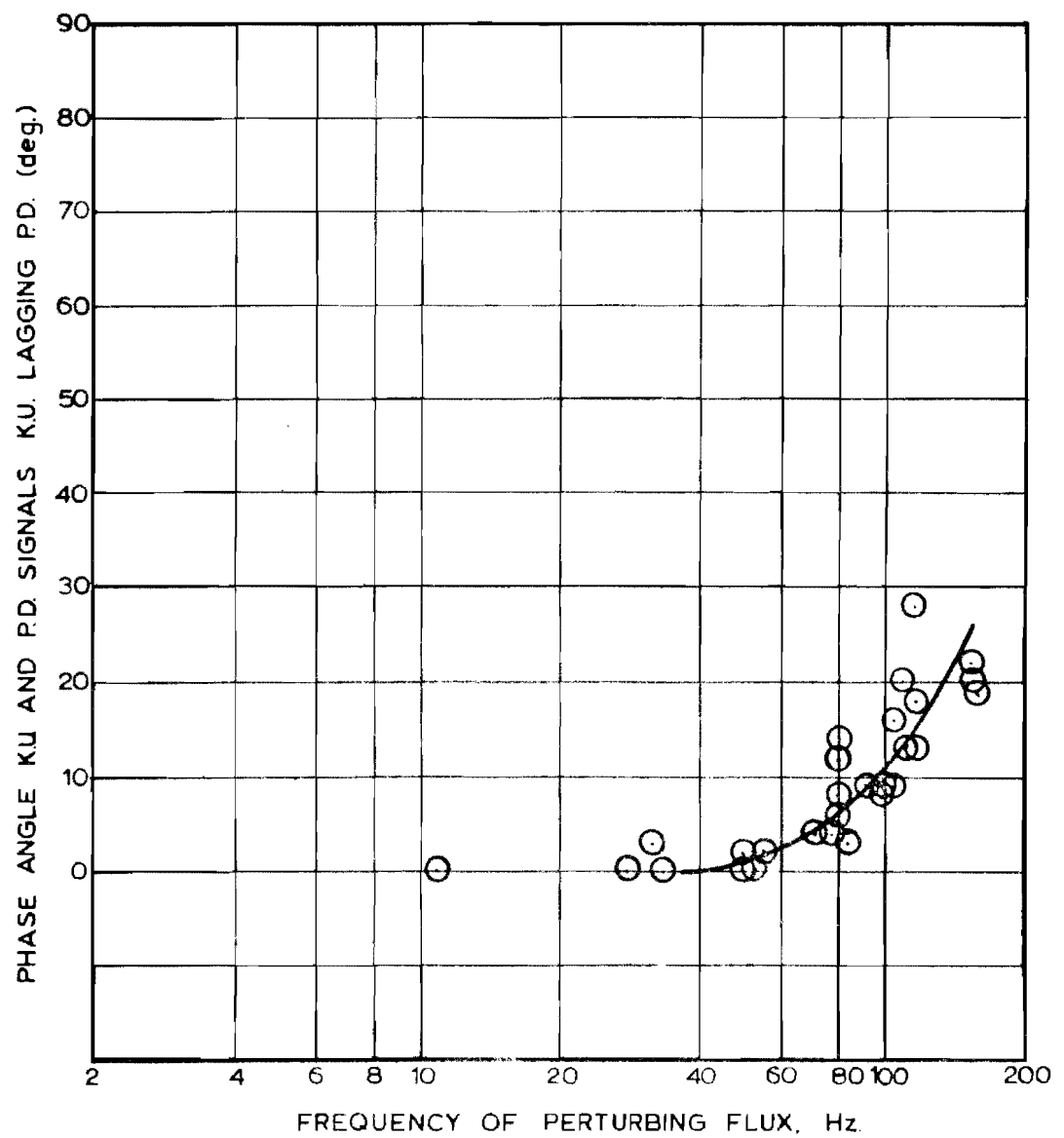


FIG. 6-17. Phase Angle Between Force Transducer Signal and Photodiode Signal for PBAA Propellant UCW.



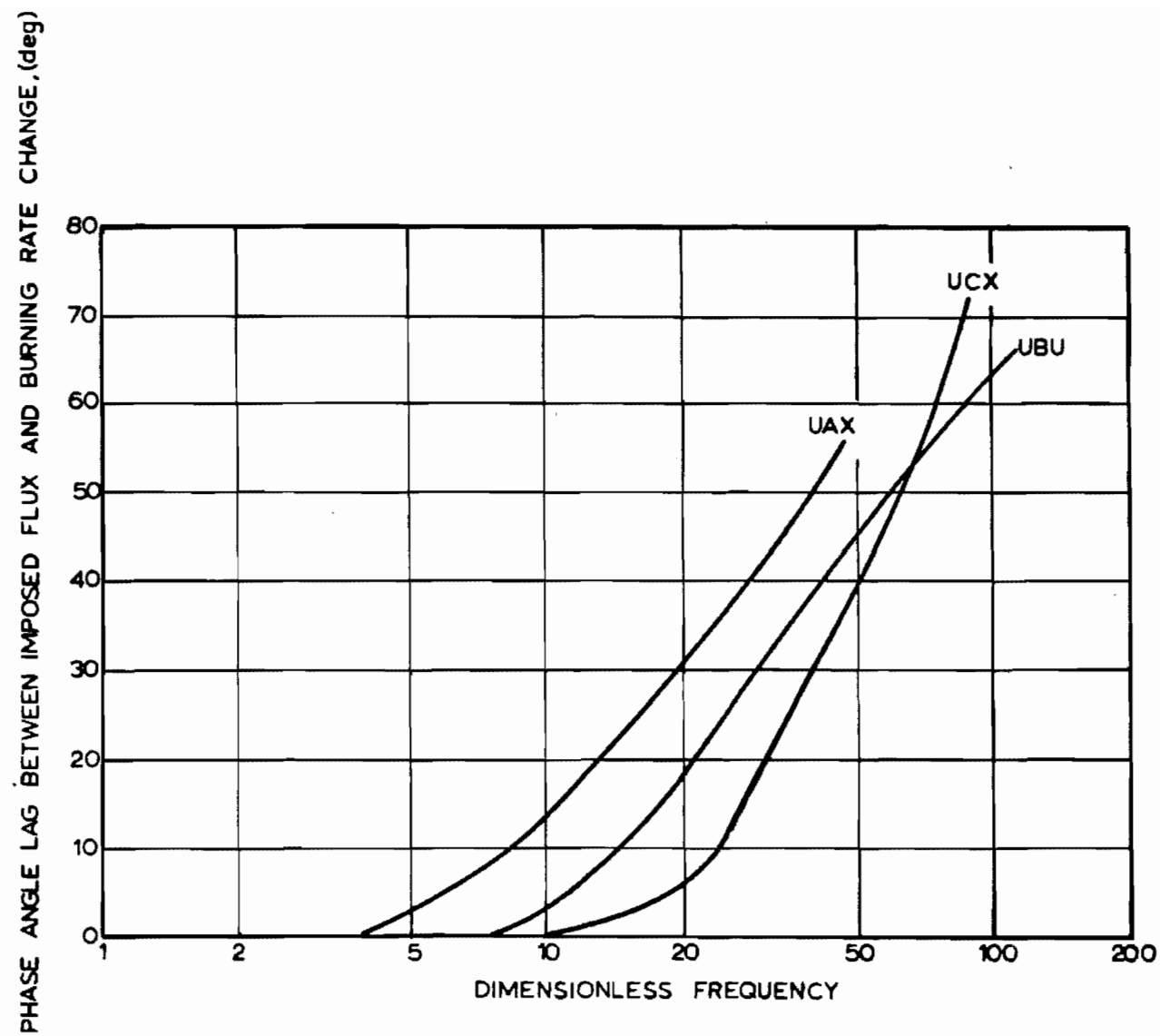


FIG. 6-18. Phase Angle Lag for Polyurethane Propellants.

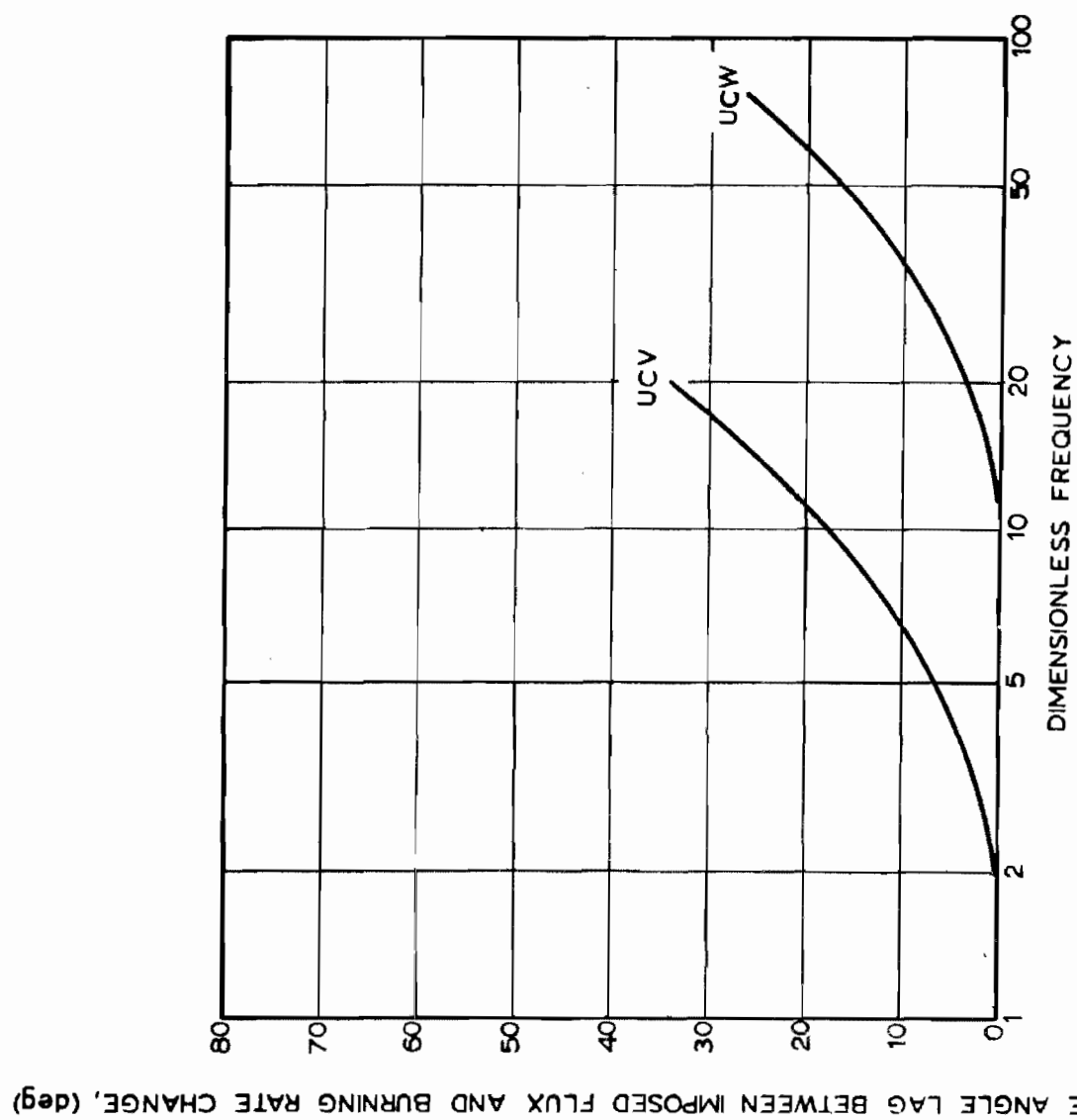


FIG. 6-19. Phase Angle Lag for PBAA Propellants.

points were considered in relationship to the effect of various parameters on the oscillatory burning. These points included: (1) the thermal wave penetration depth in relationship to the AP particle diameter; (2) the AP particle size as a phase correlation parameter; and, (3) the sharp flame front dynamics. An effort was made to correlate the observed resonance frequencies in terms of relaxation times for single, uncoupled processes. However, it was found that no simple process could be used to correlate the data. One must resort to curve fitting schemes to determine the parameters in the response function.

#### H: COMPARISON WITH L\*-BURNER AND T-BURNER DATA

Although no data directly comparable to the results obtained in this study could be found, some interesting comparisons with low L\*-burner and T-burner data can be made. The correspondence between the resonance points determined for the PU-AP propellants and the response functions measured from T-burner and L\*-burner tests can be considered. Although the results from these radiation augmentation studies do not directly yield the response function of the propellant, the presence of the resonance point, containing the ratio  $m'/\bar{m}$ , and the general nature of the burning rate response curves determined experimentally here, suggests that the response function (see Chapter III) could be computed from these results.

First, a few remarks about T-burner and L\*-burner data. An abundance of experimental data on non-acoustic instability has been accumulated from studies at the Naval Weapons Center. A limitation of the L\*-burner data is the narrow range of frequencies at which it occurs, primarily at a dimensionless frequency less than ten. Few of these data are precise enough to determine whether a maximum in the computed response function exists. However, the data on polyurethane propellants lies between the dimensionless frequencies of four and ten, which is encompassed by the range of data of this study. A closer examination of the instability data leads one to believe that the L\*-burner somehow couples the combustor flow characteristics with the propellant response. The equation coupling the propellant response and the combustor-flow system leads to an equation of the form,

$$(\bar{m}'/\bar{m}/\bar{p}'/\bar{p}) = 1 + \alpha\tau_{ch} + i\omega\tau_{tw}, \quad (6.1)$$

where  $\alpha$  = exponential growth constant, and  $\tau_{tw}$  and  $\tau_{ch}$  = time constants of the thermal wave and combustion chamber. Reducing the data is relatively direct, but again the quality of the data leaves much to be desired.

As for T-burner data, the situation is not much better because one is limited by the acoustic characteristics of the chamber. That is, it is not possible to prescribe a wide range of frequencies. Note

the data of Brown, *et al.*, [8] for example. However, it is possible to use the exponential growth rate of the oscillations and the decay rate to compute the propellant response function. The equation generally used is,

$$\operatorname{Re}\left(\frac{\mu}{\epsilon}\right) = \frac{P_o}{4C_D r_o} \left( \frac{\alpha_g}{f_g} - \frac{\alpha_d}{f_d} \right), \quad (6.2)$$

where all terms have the usual meaning [66]. The frequency of the oscillation in the T-burner is higher than in the L\*-burner and one is witnessing the resonator-propellant system in the region of propellant response where diminishing burning rate response is noted, generally from ten to one hundred in dimensionless frequency. Although the T-burner is the most widely used bench-scale device for observing oscillatory combustion in an environment similar to a rocket chamber, it is not without serious shortcomings. These are in the area of imprecise data involving many uncontrollable parameters. It is difficult, if not impossible, to distinguish between the response when subtle changes in propellant formulation are made. Furthermore, it is not possible to operate the T-burner at the resonance point of the propellant as is the case when the driving frequency is a controlled variable.

The results from the present study demonstrate the feasibility of driving the combustion process near the resonance point and that the complete burning rate response *versus* frequency plot has a shape remarkably similar to the response function curves presented from

T-burner and L\*-burner tests. A general plot containing both L\*-burner and T-burner data and the response function determined in this study is shown on Figure 6-20. Note the narrow range of the L\*-burner data as compared to the data of this study. The similarity between the results from different types of experiments is gratifying and demonstrates the superior value of controlling the driving frequency as a means of studying propellant response. The results show that subtle differences between various propellant formulations become apparent by using this technique.

It is desirable to predict the potential instability of rocket propellants from the thermochemistry, chemical reaction rates, heat transfer to the burning surface and the acoustics of the rocket chamber. However, due to the complexity of the interaction between all these factors one must rely on some experiments, preferably a simple, reliable and consistent test to screen propellants for potential instability for the particular application. To date, only the T-burner meets, although only approximately, the criteria of a suitable test for instability. The experimental device developed during the course of this study and applied in a study of five propellants offers another solution to the problem of testing propellant responsivity under laboratory conditions. The advantage of using the perturbing heat flux as the controlled variable is that a wide range of frequencies can be used. The technique is simple and does not require elaborate equipment. Data for the entire response function can be taken in a short time.

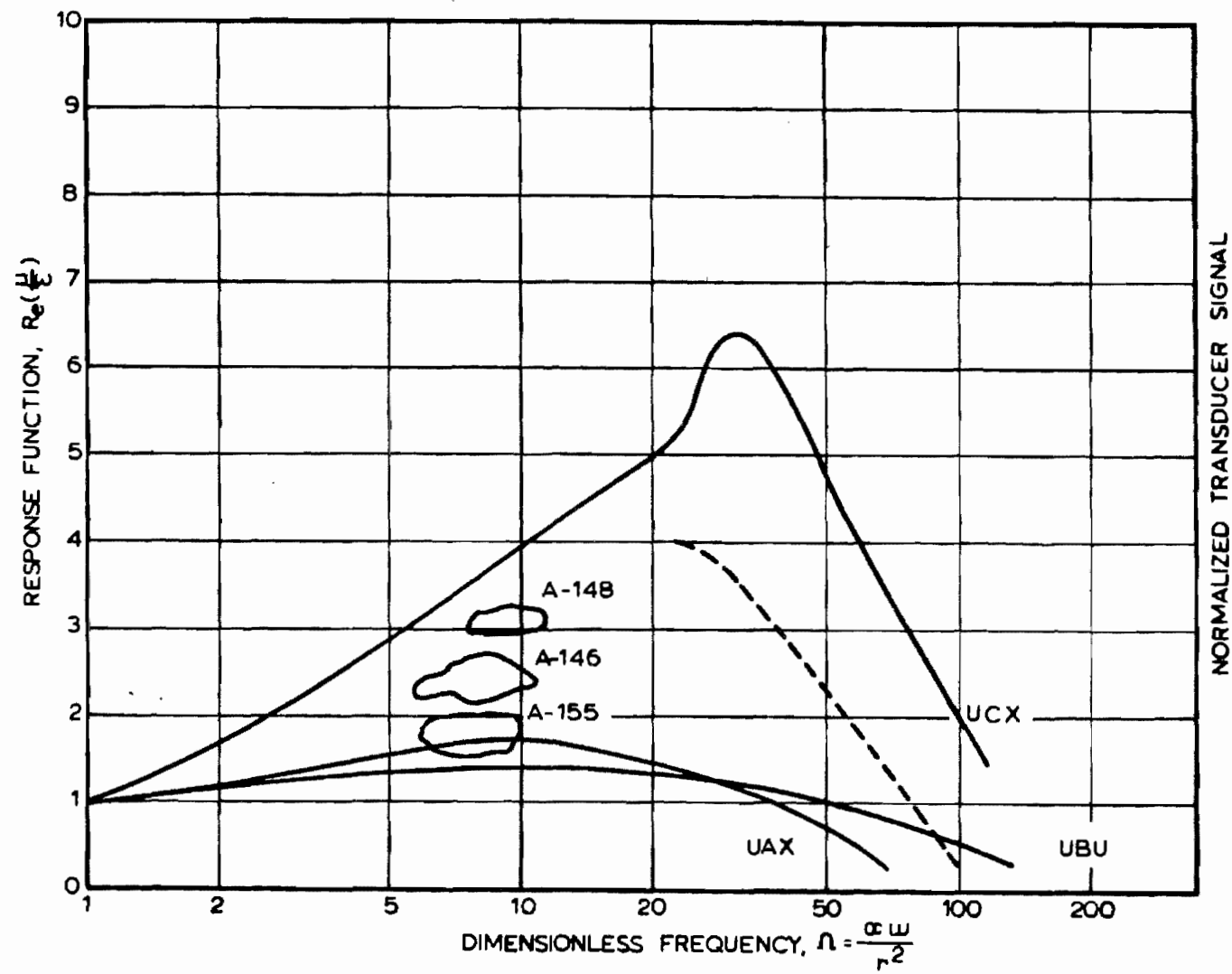


FIG. 6-20. Comparison Between the Mean Value of the Force Transducer Signal and the Propellant Response Function Deduced from T-Burner and L\*-Burner.

TABLE 6-2  
 FORMULATION OF PROPELLANTS USED TO COMPARE  
 L\*-BURNER AND T-BURNER DATA WITH  
 MEAN TRANSIENT BURNING RATES

Propellant Code	Ammonium Perchlorate				Binder % Polyurethane	Carbon Black
	%	μ	%	μ		
A-146	37.5	15	37.5	80	25	
A-155	37.0	45	37.0	400	25	1
A-148	37.0	15	37.0	200	25	1
					CTPB	
UTX-8532		78%		190	22	
A-167	37.0	15	37.0	80	25	1
A-168	37.0	15	37.0	200	25	1



### CHAPTER III: SUMMARY AND CONCLUSIONS

The steady-state burning rates of several PBAA and polyurethane fuel and propellant strands was increased by imposing focused thermal radiation from a xenon-mercury arc lamp on the burning surface. The measured increases for normally burning strands were essentially linearly dependent on the incident heat flux. At a heat flux of about  $15 \text{ cal/}(\text{sec})(\text{cm}^2)$  the increase in burning rate was from 5 to 10 percent. In the case of one high PBAA composition whose low pressure deflagration limit was near to atmospheric pressure, very large increases in regression rate were obtained by use of the external radiant flux.

The fraction of the external radiation which passed through the flame and impinged on the burning surface at atmospheric pressure was measured. Over 80 percent of the radiation reached the surface of high AP loading, clean burning formulations while less than 20 percent of the energy passed through the flame for formulations containing as little as 2 percent of aluminum. The data from these steady-state burning tests were used to estimate the net heat of gasification at the propellant surface, and while the accuracy of the measurements was only adequate to yield approximate values, these values were found to be in accord with previous measurements [49, 52] and with the values assumed in most combustion instability models. Relationships for the pressure driven and heat driven response functions were derived for the same gas phase model and the same set of parameters.

It was shown that the burning rate response to thermal radiation variation is dependent on the same parameters as is the response to pressure fluctuations. Thus, the results of the determination of the response of a burning surface to heat flux perturbations can be used to estimate the response to pressure fluctuations.

A technique was developed and exploited for measuring the burning rate response of several AP-PBAA and AP-polyurethane propellants. Thermal radiation from a xenon-mercury lamp was modulated by a chopper wheel and focused onto the surface of a burning strand. The periodic mass efflux from the surface was determined by measurement of the recoil force by use of a sensitive, quartz-crystal microphone. The magnitude of the periodic-mass efflux was measured at atmospheric pressure over a wide range of frequencies.

The coupling between gas phase process, the thermal wave in the solid and the transient burning rate, which has been the foundation of all theories of solid propellant instability, was experimentally observed and the coupling phenomena confirmed. As the frequency of the perturbing radiant heat flux was increased, the magnitude of the response first increased, passed through a maximum and then decreased in agreement with theoretical predictions. A comparison of the response of the PBAA and polyurethane propellants showed that the character of the response is strongly affected by the nature of the fuel. The measurements were precise enough to show that small formulation changes can produce significant differences in the response.

It was possible to quantitatively describe the experimental results by use of the theoretical model by appropriate selection of parameters. For most propellants, the maxima in the measured response occurred at high values of the dimensionless frequency, and it is necessary to postulate a high activation energy for the pyrolysis reaction of 80 to 90 kcal/(g-mole) to generate experimental and theoretical agreement.

In principal, since the pressure driven and flux driven response functions are dependent on the same parameters, it should be possible to characterize the instability potential of a propellant from the type of measurement made in the study. The principal requirement for such a characterization is adequacy of the response function relationships and which likely requires the essential correctness of the gas phase model employed. An evaluation of the legitimacy of the flux-driven to pressure-driven response transformation should be made; however, the deficiencies of the obvious test devices, the L\*-burner and T-burner, are so great that a meaningful comparison likely cannot be made. The work presented here was limited to operation at atmospheric pressure, the study of very clean burning propellants, and the use of low actual frequencies. The immediate need is the relaxation of these restrictions while retaining the principal advantages of the method, and further work with these objectives in progress.

## REFERENCES

- [1] Adler, J., and Enig, J. W. "The Critical Conditions in Thermal Explosion Theory with Reactant Consumption," *Combustion and Flame*, 8 (June 1964).
- [2] Baer, A. D., and Ryan, N. W. "Characterization of Solid-Propellant Reactions from Hot-Wire-Ignition Data," WSS/CI Paper 68-36.
- [3] Baer, A. D., and Ryan, N. W. "Ignition of Composite Propellants by Low Radiant Fluxes," *AIAA J.*, 3 (1965), 884-889.
- [4] Baer, A. D., and Ryan, N. W. "Evaluation of Thermal-Ignition Models From Hot-Wire Ignition Tests," *Combustion and Flame*, 15(1970), 9-22.
- [5] Beyer, R. B., McCulley, L., and Evans, M. W. "Measurement of Energy Flux Density Distribution in the Focus of an Arc Image Furnace," *Applied Optics*, 3 (June 1964), 131-135.
- [6] Broido, A., and Willoughby, A. B. "Measurement of Intense Beams of Thermal Radiation," *J. Opt. Soc. Am.*, 48 (1958), 344.
- [7] Brown, R. S. Muzzy, R. J., and Steinle, M. E. "Effect of Surface Reactions on Acoustic Response of Solid Propellants," *AIAA J.*, 5 (1967), 1718-1720.
- [8] Brown, R. S., Muzzy, R. J., and Steinle, M. E. "Surface Reaction Effects on the Acoustic Response of Composite Solid Propellants," *AIAA J.*, 6 (1968), 479-488.
- [9] Cantrell, R. H., McClure, F. T., and Hart, R. W. "Effects of Thermal Raditation on the Acoustic Response of Solid Propellants," *AIAA J.*, 3 (1965), 418-426.
- [10] Cavney, L. H., and Pittman, C. U. "Contribution of Solid-Phase Heat Release to AP Composite-Propellant Burning Rate," *AIAA J.*, 6 (1968), 1461-1467.
- [11] Cavney, L. H. "Subsurface Heterogeneity and Ammonium Perchlorate Gas-Phase Decomposition as Composite Propellant Burning Rate Controlling Mechanisms." Ph.D. thesis, University of Alabama, 1969.

- [12] Cheng, J. T. "Reactions of Composite-Propellants." Ph.D. thesis, Department of Chemical Engineering, University of Utah, 1967.
- [13] Coates, R. L. "A Quantitative Experimental Study of Oscillatory Combustion" Ph.D. thesis, Department of Chemical Engineering, University of Utah, 1962.
- [14] Coates, R. L., Ryan, N. W., and Horton, M. D. "The T-Burner Method for Determining the Acoustic Admittance of Burning Propellants," *AIAA Preprint*, No. 64-137, January 1964.
- [15] Culick, F. E. C. "A Review of Calculations for Unsteady Burning of a Solid Propellant," *AIAA J.*, 6 (1968), 2241-2255.
- [16] Culick, F. E. C. "Calculation of the Admittance Function for a Burning Surface," *Astronautica Acta*, 13 (1967), 221-237.
- [17] Culick, F. E. C. and E. W. Price. *Combustion of Solid Rocket Propellants*. AIAA Professional Study Series.
- [18] Culick, F. E. C., and Dehority, G. L. "An Elementary Calculation for the Burning Rate of Composite Solid Propellants," *Combustion Science and Technology*, 1 (1969), 193-204.
- [19] Culick, F. E. C. *Solid Propellant Combustion Instability Studies*. NWC Report TP 4668; China Lake, California: U. S. Naval Weapons Center, December, 1969.
- [20] Culick, F. E. C. "An Elementary Calculation of the Combustion of Solid Propellants," *Astronautica Acta*, 14 (1969), 171-181.
- [21] Culick, F. E. C. *A Review of Calculations of the Admittance Function for a Burning Surface. Appendix A*. NWC Report TP 4244; China Lake, California: U. S. Naval Weapons Center, September, 1967.
- [22] Daverman, L., and Tajima, Y. A. "Thermal Decomposition and Combustion of Nitrocellulose," *AIAA J.*, 6 (1968), 1468-1473.
- [23] Denison, M. R., and Baum, E. "A Simplified Model of Unstable Burning in Solid Propellants," *ARS J.*, (Aug. 1961), 1112-1122.

- [24] Donaldson, A. B. "Extinction of Propellants." M.S. thesis, Department of Chemical Engineering, University of Utah, 1965.
- [25] Fife, W. B. Personal communication, Lockheed Propulsion Company, Redlands, California. August 1968.
- [26] Friedly, J. C., and Petersen, E. E. "Influence of Combustion Parameters on Instability in Solid Propellant Motors. Part I. Development of Model and Linear Analysis. Part II. Nonlinear Analysis," *AIAA J.*, 4 (1966), 1604-1610 and 1932-1937.
- [27] Friedman, R. "Experimental Techniques for Solid Propellant Combustion Research," *AIAA J.*, 5 (1967), 1217-1223.
- [28] Hart, R. W., and McClure, F. T. "Combustion Instability: Acoustic Interaction with a Burning Surface," *J. of Chem. Phys.*, 30 (1959), 1501.
- [29] Hart, R. W., Farrell, R. A., and Cantrell, R. H. "Theoretical Study of a Solid Propellant Having a Heterogeneous Surface Reaction. Part I. Acoustic Response, Low and Intermediate Frequencies," *Combustion and Flame*, 10 (1966), 367-380.
- [30] Hermance, C. E. "A Model of Composite Propellant Combustion Including Surface Heterogeneity and Heat Generation," *AIAA J.*, 4 (1966), 1629-1637.
- [31] Hertzberg, M. "The Free-Laminar and the Laser-Induced Combustion of Ammonium Perchlorate," *Combustion Science and Technology*, 1 (1970), 449-460.
- [32] Horton, M. D., and Rice, D. W. "The Effects of Compositional Variables Upon Oscillatory Combustion of Solid Rocket Propellants," *Combustion and Flame*, 8 (1964), 21-28.
- [33] Horton, M. D. *Testing the Dynamic Stability of Solid Propellants: Technique and Data*. NOTS Report TP 3610; China Lake, California: U. S. Naval Ordnance Test Station, August, 1964.
- [34] Horton, M. D. "Oscillatory Burning of Solid Rocket Propellants." Ph.D. thesis, Department of Chemical Engineering, University of Utah, 1961.

- [35] Huggett, C., Bartley, C. E., and Mills, M. M. *Solid Propellant Rockets*. Princeton Aeronautical Paperbacks, Number 2: Princeton University Press, 1960. p. 37.
- [36] Inami, S. H., Rosser, W. A., and Wise, H. "Adiabatic Decomposition of Ammonium Perchlorate," *Faraday Society Transactions*.
- [37] Inami, S. H., and Shanfield, H. "Nonacoustic Combustion Pulsations of Ammonium Perchlorate Containing Aluminum," *AIAA J.*, 2 (1964), 1314-1318.
- [38] Inami, S. H., Rosser, W. A., and Wise, H. "Heat-Release Kinetics of Ammonium Perchlorate in the Presence of Catalysts and Fuel," *Combustion and Flame*, 12 (1968), 41-44.
- [39] Inami, H., McCulley, L., and Wise, H. "Ignition Response of Solid Propellants to Radiation and Conduction," *Combustion and Flame*, 13 (1969), 531-536.
- [40] Jacobs, P. W. M., and Whitehead, H. M. "Decomposition and Combustion of Ammonium Perchlorate," *Chemical Reviews* (March 1969), 551-590.
- [41] Jacobs, P. W. M., and Russell, Jones A. "Sublimation of Ammonium Perchlorate," *J. of Phys. Chem.*, 72 (January 1968), 202-207.
- [42] Johnson, W. E., and Nachbar, W. "Deflagration Limits in the Steady Linear Burning of a Monopropellant with Application to Ammonium Perchlorate," in *Eighth Symposium (International) on Combustion*. Baltimore: Williams & Wilkins, 1962. pp. 678-689.
- [43] Jonath, A. D. "Gasdynamic Problems in Low Pressure Microthrust Engines," *Astronautics Acta*, 11 (1965).
- [44] Kilpatrick, J. C. Personal communication, Technology development, General Electric, Philadelphia, Pa.
- [45] Kindsvater, H. M. Personal communication, Missiles and Space Division, Organ 55-11/102; Sunnyvale, California.
- [46] Konev, E. V. "Influence of Light Radiation on the Burning Rate of N Powder," *Combustion, Explosion, and Shock Waves*, 1 (1965).

- [47] Konev, E. V., and Khlevnoi, S. S. "Burning of a Powder in the Presence of Luminous Radiation," *Combustion, Explosion, and Shock Waves*, 2 (1969), 21-25.
- [48] Krier, H., T'ien, J. S., Sirignano, W. A., and Summerfield, M. "Non-Steady Burning Phenomena of Solid Propellants: Theory and Experiments," *AIAA J.*, 6 (1968), 278-285.
- [49] Law, B. "Effect of Initial Temperature on Propellant Burning Rates." B.S. thesis, Department of Chemical Engineering, University of Utah, 1968.
- [50] Lee, L. *Third Combustion and Propulsion Colloquium of AGARD*. NATO (March 17-21, 1958).
- [51] Levy, J. B., and Friedman, R. In *Eighth Symposium (International) on Combustion*. Baltimore: Williams & Wilkins, 1962. pp. 663-672.
- [52] Mantyla, R. G. "Extinguishment of Solid Propellants." M.S. thesis, Department of Chemical Engineering, University of Utah, 1968.
- [53] Marxman, G. A., and Wooldridge. "Effect of Surface Reactions on the Solid Propellant Response Function," *AIAA J.*, 6 (1968), 471-478.
- [54] Mayer, S. W., Weinberg, E. K., and Schieler. "Techniques for Controlling Exothermic Decomposition of Ammonium Perchlorate," in *Western States Combustion Institute; Spring Meeting*, 1968.
- [55] Merzhanov, A. S. "Thermal Explosion and Ignition as a Method for Formal Kinetic Studies of Exothermic Reactions in the Condensed Phase," *Combustion and Flame*, 11 (1967), 201-211.
- [56] Muhlfeith, C. M., "Some Experiments on the Effect of Thermal Radiation on Composite Propellants," Ph.D. thesis, Department of Chemical Engineering, University of Utah, 1971.
- [57] Nachbar, W., and Williams, F. A. "On the Analysis of Linear Pyrolysis Experiments," in *Ninth Symposium (International) on Combustion*. pp. 345-357.
- [58] Nachbar, W., and Green, L. J. "Analysis of a Simplified Model of Solid Propellant Resonant Burning," *J. of Aerospace Sciences* (August 1959), 518-526.



- [59] Oberg, C. L. "Acoustic Instability in Propellant Combustion." Ph.D. thesis, Department of Chemical Engineering, University of Utah, 1965.
- [60] Ohlemiller, T. J., and Summerfield, M. *Radiation Augmented Burning of a Solid Propellant*. AMS Report No. 799; Princeton University.
- [61] Olfe, D., and Penner, S. S. "Radiant Energy Emission from the Equilibrated Reaction Products of UPRC Ammonium Perchlorate Pellet," in *Eighth Symposium (International) on Combustion*. Baltimore: Williams & Wilkins, 1962. pp. 293-303.
- [62] Osborn, J. R., Burick, R. J., and Ho, P. Y. *Techniques for the Continuous Measurement of Solid Propellant Burning Rates*. Report No. F-66-3; Purdue University: Jet Propulsion Center.
- [63] Penner, S. S., and Olfe, D. B. "The Influence of Radiant-energy Transfer on Propellant Burning Rates and Ablation Rates Controlled by an Intense Radiation Field," *Astronautica Acta*, 11 (1965), 65-78.
- [64] Pittman, C. U. "Location of Action of Burning-Rate Catalysts in Composite Propellant Combustion," *AIAA J.*, 7 (1969), 328-334.
- [65] Powling, J. "Experiments Relating to the Combustion of Ammonium Perchlorate-Based Propellants," in *Tenth Symposium (International) on Combustion*. Pittsburg: 1965. pp. 447-456.
- [66] Price, E. W. "Experimental Solid Rocket Combustion Instability," in *Tenth Symposium (International) on Combustion*. Pittsburg: 1965. pp. 1067-1082.
- [67] Sabadell, A. J., Wenograd, J., and Summerfield. "Measurement of Temperature Profiles Through Solid-Propellant Flames Using Fine Thermocouples," *AIAA J.*, 3 (1965), 1580-1584.
- [68] Scala, S. M., and Sutter, G. W. "Energy Transfer at a Chemically Reacting or Slip Interface," *ARS J.*, (February 1959), 141-142.
- [69] Schulz, E. M. "Propellant-Flame Spectra During Depressurization." Ph.D. thesis, Department of Chemical Engineering, University of Utah, 1970.

- [70] Sehgal, R., and Strand, L. "A Theory of Low-Frequency Combustion Instability in Solid Rocket Motors," *AIAA J.*, 2 (1964), 696-702.
- [71] Seleznev, V. A., Pokhel, P. F., Maltrev, V. M., and Bavykin, I. B. "An Optical Method of Measuring the Burning-Surface Temperature of Condensed Systems," *Combustion and Flame*, 13 (April 1969), 139-142.
- [72] Selzer, H. "The Unstable Nature of the Burning Mechanism of AP-Propellants," in *AIAA 7th Aerospace Sciences Meeting*. New York: January 20-22, 1969. Preprint No. 69-117.
- [73] Sipowicz, W. W. "Acoustic Instability in the Combustion of Methane-Oxygen-Nitrogen Mixtures." Ph.D. thesis, Department of Chemical Engineering, University of Utah, 1969.
- [74] Steinz, J. A., Stang, P. L., and Summerfield, M. *The Burning Mechanism of Ammonium Perchlorate-Based Composite Solid Propellants*. AMS Report No 830; Princeton University, 1969.
- [75] Suddeth, R. H. Personal communication, Goddard Space Flight Center, Greenbelt, Maryland. February, 1968.
- [76] Sutherland, G. S. Personal communication, Rocket Research Corporation, Seattle, Washington. February, 1968.
- [77] Tipper, C. F. H., Ed. *Oxidation and Combustion Reviews*. Vol. 2. pp. 1-185.
- [78] Waesche, R. H. W., and Wenograd, J. "Calculation of Solid Propellant Burning Rates from Condensed-Phase Decomposition Kinetics," in *AIAA 7th Aerospace Science Meeting*. New York: January 20-22, 1969. Preprint No. 69-145.
- [79] Waldman, C. H., Cheng, S. I., Sirignano, W. A., and Summerfield, M. *Theoretical Studies of Diffusion Flame Structures*. AMS Report No. 860; Princeton University, 1969.
- [80] Wise, H., Inami, H., and McCulley, L. "Role of Condensed-Phase Reactions in Ignition and Deflagration of Ammonium Perchlorate Propellants," *Combustion and Flame*, 11 (1967), 483-488.

- [81] Wong, T. L. "L-Star Instability." Ph.D. thesis, Department of Chemical Engineering, University of Utah, 1969.
- [82] Yang, J. Y. S. "Some Problems in Solid Propellant Combustion Instability." Ph.D. thesis, Department of Mechanical Engineering, University of Utah, 1970.

## APPENDIX A: NOMENCLATURE

<u>Symbol</u>	<u>Definition</u>	<u>Units</u>
A	parameter in the pressure response function	
a	constant in equation 5.3	
$A_b$	area of burning surface	$\text{cm}^2$
B	parameter in the pressure response function	
b	constant in equation 5.3	
C	heat capacity of the solid propellant	$\text{cal/gm}^\circ\text{K}$
$C_{1,2,\dots}$	constants	
$C_p$	heat capacity of the gas phase	$\text{cal/gm}^\circ\text{K}$
E	activation energy	$\text{cal/g-mole}^\circ\text{K}$
F	radiant heat flux	$\text{cal/cm}^2 \text{ sec}$
f	recoil force sensed by transducer	$\text{dynes/cm}^2$
$f_g, f_d$	frequency of growth and decay of pressure oscillations	cycle/sec
H	ratio of heat source to conductive flux in the solid	$\text{cal/g}$
i	indicates an imaginary term	
K	constant in equation for burning velocity	
k	thermal conductivity	$\text{cal/cm}^2 \text{ sec}^\circ\text{K}$
M	molecular weight	$\text{g/g-mole}$
R	gas constant	$\text{cal/g-mole}^\circ\text{K}$

$r$	linear burning rate	cm/sec
$T$	temperature	°K
$t$	time	sec
$\bar{m}$	mean mass flux	$\text{g/cm}^2 \text{ sec}$
$m'$	mass flux perturbation	$\text{g/cm}^2 \text{ sec}$
$n$	burning rate exponent	
$p$	pressure	$\text{dynes/cm}^2$
$Q$	heat of reaction	cal/g
$q$	heat of reaction	
$X$	spacial variable	

### Greek Symbols

$\alpha$	thermal diffusivity	$\text{cm}^2 \text{ sec}^{-1}$
$\alpha_g, \alpha_d$	growth and decay constants of pressure oscillation	
$\beta$	parameter in thermal energy equation	
$\gamma$	extinction coefficient in Beer's law	$\text{cm}^{-1}$
$\epsilon, \mu$	defined by the pressure response function	
$\Omega$	dimensionless frequency	
$\lambda_1, \lambda_2$	roots of complex equation	
$u_{1,2}$	constants in burning velocity, equation 3.9	
$\tau$	time constants in equation 6.1	

$\rho$	density of propellant	gm/cm <sup>3</sup>
$\omega$	angular frequency	rad/sec

### Subscripts and Superscripts

$i, o^-$	condition inside the propellant surface
$-\infty$	condition deep inside the propellant
$o^+$	condition on the gas side of the propellant surface
$g$	gas-phase condition
$s$	surface condition
$f$	flame condition
$+\infty$	condition in the gas phase
$'$	fluctuation of the variable
$-$	overbar indicating the average value
$r$	radiant heat flux component, equation 3.30
$c$	conductive heat flux component, equation 3.40
$op$	designates a condition of an opaque propellant
$TR$	designates a condition of a translucent propellant
$Ch$	designates the combustion chamber condition
$tw$	designates the thermal wave condition

## APPENDIX B: RADIANT HEAT FLUX PROFILES FOR RADIATION FURNACE

Radiant heat flux profile data taken using the total radiation calorimeter described in Chapter IV are tabulated in this Appendix. Three plots of the flux profile data are also presented.

$\diamond = (Z, -1.00, -0.5)$

$\times = (Z, -1.50, -0.5)$

$\odot = (Z, -2.00, -0.5)$

$I_{\max} = 14.86 \text{ cal/cm}^2 \text{ sec}$

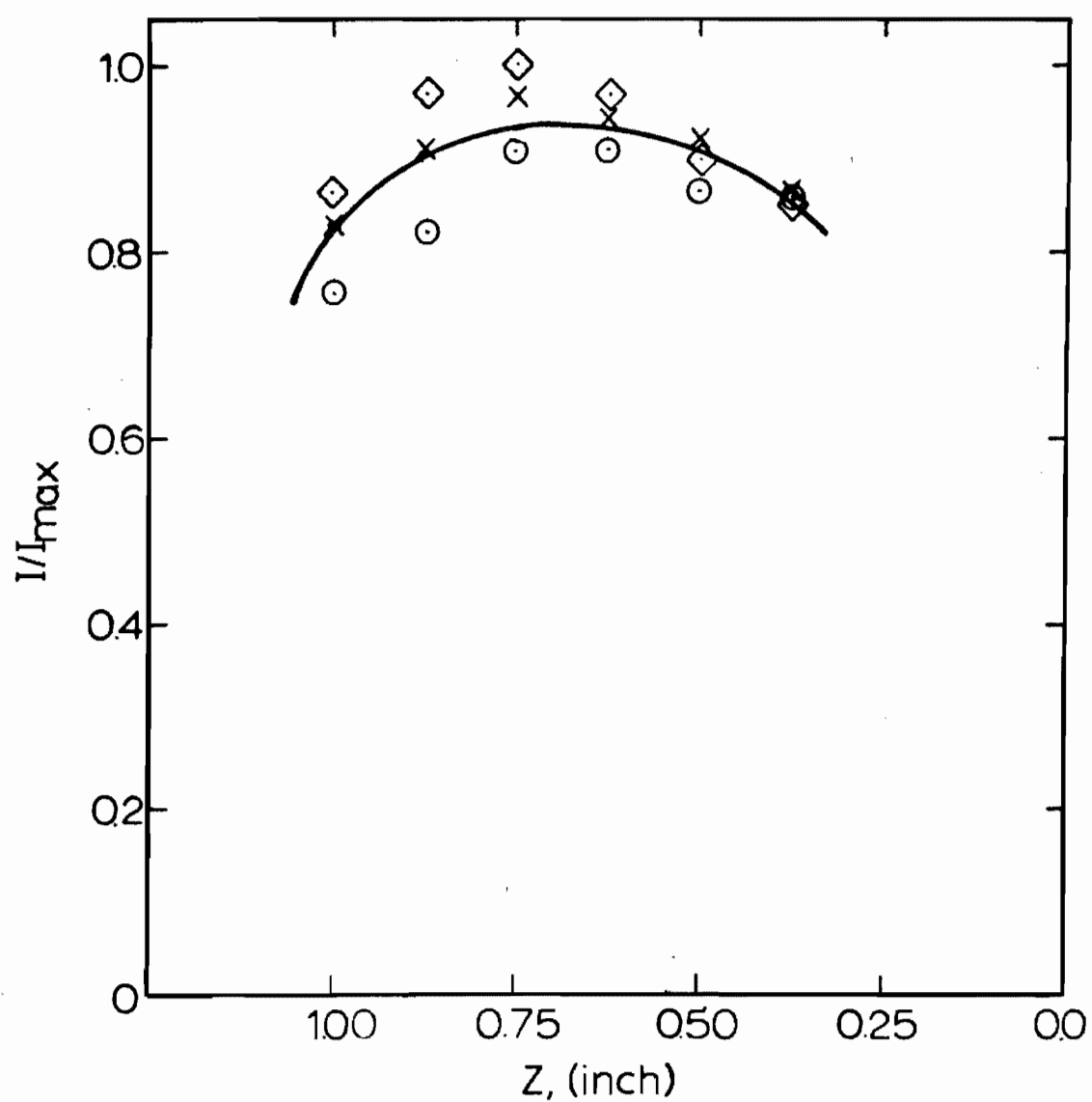


FIG. B-1. Normalized Radiant Flux at Secondary Focus of Radiation Furnace.



$\diamond = (X, -1.00, +0.75)$

$\times = (X, -1.50, +0.75)$

$\circ = (X, -2.00, +0.75)$

$I_{\max} = 14.86 \text{ cal/cm}^2 \text{ sec}$

CALORIMETER #9 MASK #33

RUN #55-72

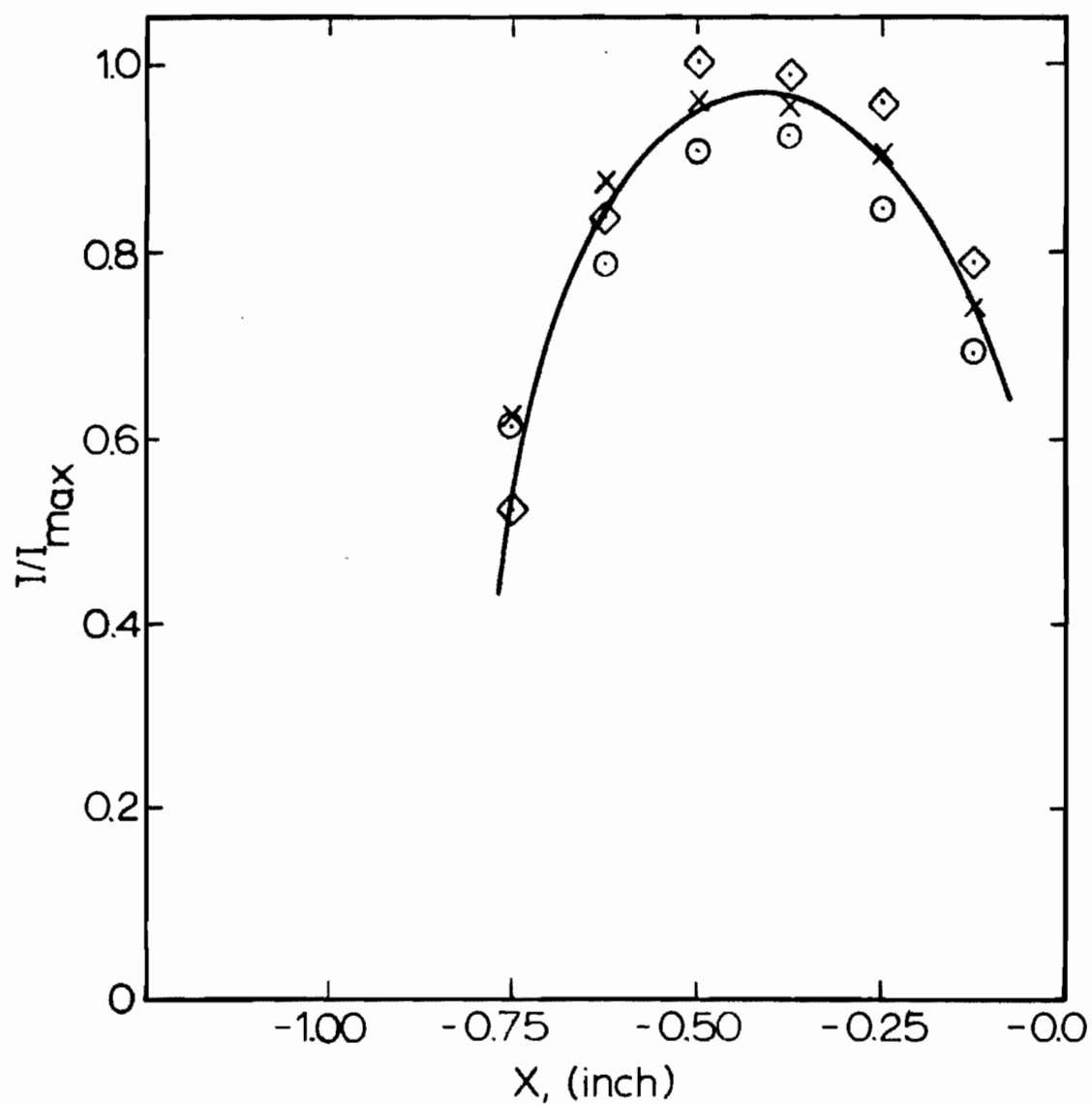


FIG. B-2. Normalized Radiant Flux at Secondary Focus of Radiation Furnace.

$\diamond = (-0.50, Y, +0.375)$   
 $\times = (-0.50, Y, +0.50)$   
 $\odot = (-0.50, Y, +0.625)$   
 $\square = (-0.50, Y, +0.75)$   
 $\triangle = (-0.50, Y, +0.875)$   
 $* = (-0.50, Y, +1.00)$

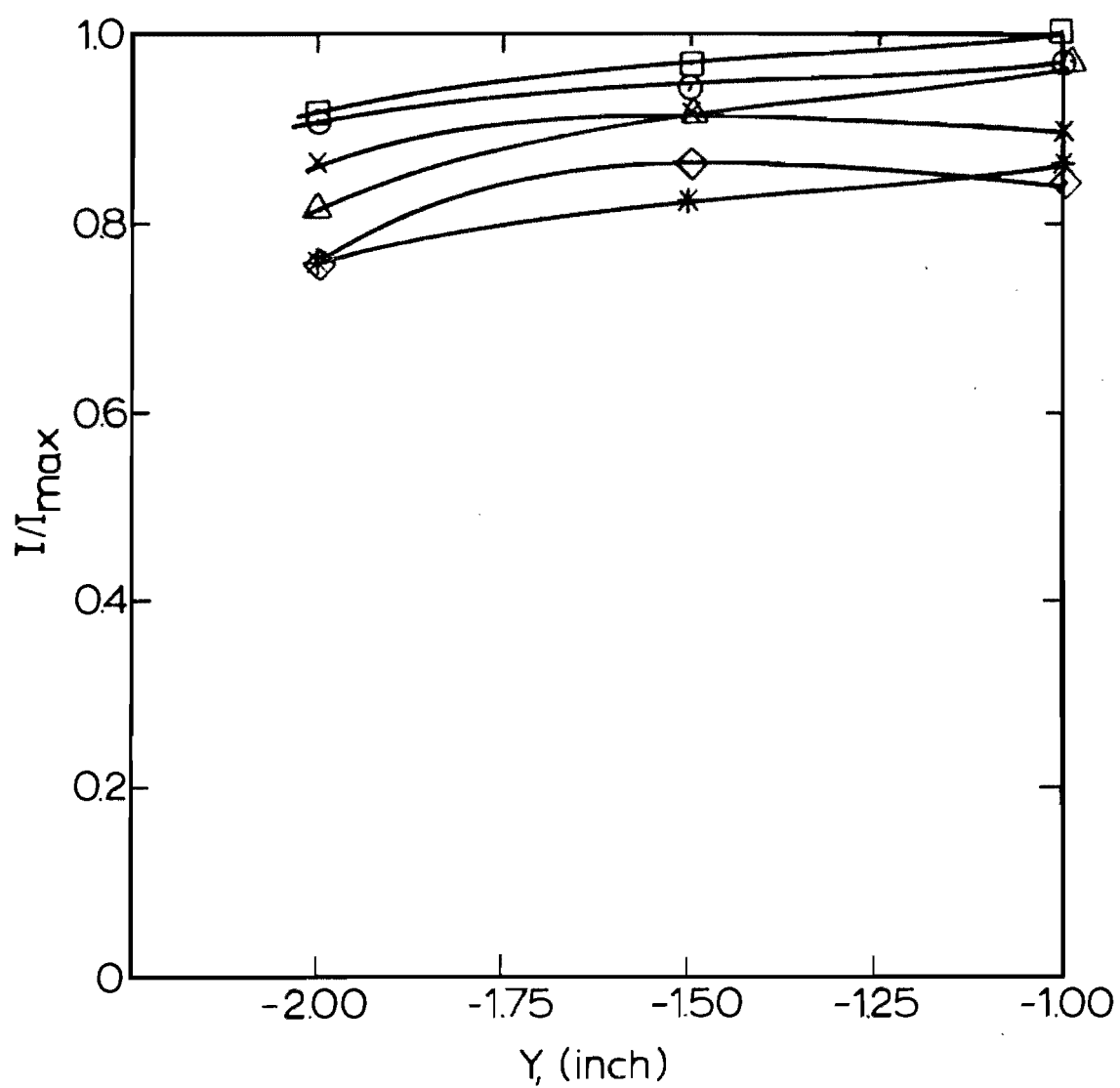


FIG. B-3. Normalized Radiant Flux at Secondary Focus of Radiation Furnace.

APPENDIX C: SUMMARY TABLES OF DATA

TABLE C-1

## SUMMARY OF PROPELLANTS PREPARED, COMPOSITION AND BURNING BEHAVIOR

<u>Code</u>	<u>Oxidizer</u>	<u>Binder</u>	<u>Additives</u>	<u>Burning Behavior at One Atm.</u>
UAP	65% 5 $\mu$ AP	4.2% Epon 23.8% PBAA	2% Copper Chromite 5% AL Reyn. #1-511	Fairly flat interface. Bluish flame zone and jet boundary.
UAO	70% 5 $\mu$ AP	4.2% Epon 23.8%PBAA	2% Copper Chromite	No AP ejected. Flat interface.
UAQ	72% 5 $\mu$ AP	4.2% Epon 23.8% PBAA		No AP ejected. Tended to cone in long samples.
UAX	80% AP 40/40 5 $\mu$ , -48 + 100	18% Estane + Curative	2% n-butyl ferrocene	Larger AP particles were ejected. Slight tendency to cone. Translucent.
UAY	80% AP 40/40 5 $\mu$ , -48 + 100	18% Estane + Curative	1% nbf 1% Carbon Black	Larger AP particles were ejected. Slight tendency to cone. Opaque.
UBT	65% AP 5 $\mu$	33% Estane + Curative	2% nbf	Slow, but fairly uniform burning. Red residue remains on pedestal after burnout. Possibly Fe <sub>2</sub> O <sub>3</sub> . Translucent.
UBU	65% AP 5 $\mu$	32% Estane + Curative	2% nbf 1% Carbon Black	Slow, but fairly uniform burning. Extinguishes easily. Opaque.

TABLE C-1 (CONTINUED).

<u>Code</u>	<u>Oxidizer</u>	<u>Binder</u>	<u>Additives</u>	<u>Burning Behavior at One Atm.</u>
UCX	80% AP 40/40 5 $\mu$ , +48-100	17% Estane + Curative	2% nbf 1% Carbon Black	Larger AP particles were ejected. Flat Interface. Opaque.
UCV	80% AP 40/40 5 $\mu$ , +48-100	18% PBAA + Epon	2% Copper Chromite	Larger AP particles were ejected. Flat interface. Opaque.
UCW	80% AP 40/40 5 $\mu$ , +48-100	19% PBAA + Epon	1% Carbon Black	Larger AP particles were ejected. Flat interface. Opaque.
UBZ	70% AP 5 $\mu$	4.2% Epon 23.8% PBAA	2% nbf	High burning rate, only very slight coning. Translucent.
UBR	60% AP 5 $\mu$	40% Estane + Curative	none	Char layer present on extinguished samples. Slight tendency to cone. Translucent.
UCI	36% AP 5 $\mu$	9.6% Epon 54.5% PBAA		Fizz zone propagates through the sample. Low density ash remains. Initially translucent.

TABLE C-2  
Summary of Radiation Augmented  
Linear Burning Rates

Run #	Propellant	Screen # Flux Ratio	Initial Rate With Rad.	No Radiation	With Radiation
33-1	UBU	None, 1	0.281	0.06	0.275
33-2	UBU	None, 1	0.270	ext.	0.280
33-3	UBU	None, 1	0.255	0.03	0.259
33-4	UBU	None, 1	0.268	ext.	0.265
33-5	UBU	None, 1	0.260	ext.	0.272
33-6	UBU	None, 1	0.272	ext.	0.258
33-7	UBU	None, 1	0.266	ext.	0.263
			0.267	0.045	0.267 $r_{rad} = 0.267$
33-8	UBU	#5, 0.714	0.244	0.04	0.237
33-9	UBU	#5, 0.714	0.215	ext.	0.217
33-10	UBU	#5, 0.714	0.225	ext.	0.223
33-11	UBU	#5, 0.714	0.217	ext.	0.220
33-12	UBU	#5, 0.714	0.230	ext.	0.225
33-13	UBU	#5, 0.714	0.234	0.01	0.238
33-14	UBU	#5, 0.714	0.227	ext.	0.222
			0.227	0.025	0.226 $r_{rad} = 0.2265$
33-15	UBU	#2, 0.508	0.202	ext.	0.209
33-16	UBU	#2, 0.508	0.197	0.05	0.195
33-17	UBU	#2, 0.508	0.208	0.08	0.204
33-18	UBU	#2, 0.508	0.211	ext.	0.205
33-19	UBU	#2, 0.508	0.191	0.06	0.198
33-20	UBU	#2, 0.508	0.206	ext.	0.201
33-21	UBU	#2, 0.508	0.195	ext.	0.206
			0.201	0.063	0.203 $r_{rad} = 0.202$
33-22	UBU	#3, 0.336	0.178	0.07	0.181
33-23	UBU	#3, 0.336	0.186	ext.	0.188
33-24	UBU	#3, 0.336	0.175	ext.	0.172
33-25	UBU	#3, 0.336	0.179	0.09	0.171
33-26	UBU	#3, 0.336	0.170	0.06	0.166
33-27	UBU	#3, 0.336	0.184	0.07	0.192
33-28	UBU	#3, 0.336	0.171	ext.	0.169
			0.178	0.0725	0.177 $r_{rad} = 0.1775$

TABLE C-2 (Continued)

132

Run #	Propellant	Screen # Flux Ratio	Initial Rate With Rad.	No Radiation	With Radiation
34-1	UAO	None, 1	0.357	0.302	0.347
34-2	UAO	None, 1	0.350	0.311	0.342
34-3	UAO	None, 1	0.333	0.292	0.340
34-4	UAO	None, 1	0.354	0.306	0.345
34-5	UAO	None, 1	0.362	0.314	0.357
34-6	UAO	None, 1	0.348	0.308	0.339
			0.351	0.305	0.345
					$r_{rad} = 0.348$
34-7	UAO	#1, 0.656	0.338	0.303	0.332
34-8	UAO	#1, 0.656	0.325	0.296	0.321
34-9	UAO	#1, 0.656	0.343	0.324	0.346
34-10	UAO	#1, 0.656	0.336	0.301	0.329
34-11	UAO	#1, 0.656	0.333	--	0.319
34-12	UAO	#1, 0.656	0.335	0.308	0.331
34-13	UAO	#1, 0.656	0.330	0.309	0.337
			0.334	0.307	0.331
					$r_{rad} = 0.3325$
34-14	UAO	#2, 0.508	0.325	0.315	0.321
34-15	UAO	#2, 0.508	0.335	0.326	0.330
34-16	UAO	#2, 0.508	0.315	0.299	0.314
34-17	UAO	#2, 0.508	0.332	0.320	0.337
34-18	UAO	#2, 0.508	0.338	0.310	0.335
34-19	UAO	#2, 0.508	0.327	--	0.330
34-20	UAO	#2, 0.508	0.323	--	0.318
			0.328	0.314	0.326
					$r_{rad} = 0.327$
34-21	UAO	#3, 0.336	0.311	0.304	0.307
34-22	UAO	#3, 0.336	0.326	0.320	0.329
34-23	UAO	#3, 0.336	0.327	0.308	0.315
34-24	UAO	#3, 0.336	0.319	0.312	0.322
34-25	UAO	#3, 0.336	0.324	0.318	0.322
34-26	UAO	#3, 0.336	0.318	0.309	0.319
			0.321	0.312	0.319
					$r_{rad} = 0.320$

TABLE C-2 (Continued)

Run #	Propellant	Screen # Flux Ratio	Initial Rate With Rad.	No Radiation	With Radiation
35-1	UBT	None, 1	0.275	0.201	0.273
35-2	UBT	None, 1	0.266	0.193	0.268
35-3	UBT	None, 1	0.283	0.207	0.285
35-4	UBT	None, 1	0.280	0.196	0.278
35-5	UBT	None, 1	0.271	0.188	0.259
35-6	UBT	None, 1	0.275	0.198	0.279
			0.275	0.197	0.274 $r_{rad} = 0.2745$
35-7	UBT	#5, 0.714	0.240	0.192	0.245
35-8	UBT	#5, 0.714	0.253	0.185	0.249
35-9	UBT	#5, 0.714	0.254	0.186	0.250
35-10	UBT	#5, 0.714	0.258	0.190	0.254
35-11	UBT	#5, 0.714	0.256	0.200	0.247
35-12	UBT	#5, 0.714	0.235	0.189	0.230
			0.249	0.190	0.246 $r_{rad} = 0.2475$
35-13	UBT	#1, 0.656	0.251	0.197	0.248
35-14	UBT	#1, 0.656	0.253	0.188	0.243
35-15	UBT	#1, 0.656	0.242	0.195	0.240
			0.249	0.193	0.244 $r_{rad} = 0.2465$
35-16	UBT	#2, 0.508	0.231	0.193	0.229
35-17	UBT	#2, 0.508	0.235	0.190	0.233
35-18	UBT	#2, 0.508	0.242	0.198	0.238
35-19	UBT	#2, 0.508	0.237	0.196	0.234
35-20	UBT	#2, 0.508	0.234	0.188	0.237
35-21	UBT	#2, 0.508	0.231	0.201	0.231
			0.236	0.194	0.234 $r_{rad} = 0.235$
35-22	UBT	#3, 0.336	0.232	0.205	0.230
35-23	UBT	#3, 0.336	0.225	0.198	0.228
35-24	UBT	#3, 0.336	0.220	0.193	0.218
35-25	UBT	#3, 0.336	0.206	0.184	0.209
35-26	UBT	#3, 0.336	0.216	0.186	0.213
35-27	UBT	#3, 0.336	0.219	0.190	0.218
35-28	UBT	#3, 0.336	0.221	0.197	0.224
			0.220	0.193	0.220 $r_{rad} = 0.220$



TABLE C-2 (Continued)

134

Run #	Propellant	Screen # Flux Ratio	Initial Rate With Rad.	No Radiation	With Radiation
36-1	UAQ	None, 1	0.232	0.175	0.227
36-2	UAQ	None, 1	0.235	0.185	0.230
36-3	UAQ	None, 1	0.228	0.182	0.230
36-4	UAQ	None, 1	0.225	0.180	0.233
36-5	UAQ	None, 1	0.221	0.173	0.235
			0.228	0.179	0.231 $r_{\text{rad}} = 0.2295$
36-6	UAQ	#5, 0.711	0.220	0.190	0.225
36-7	UAQ	#5, 0.711	0.228	0.188	0.222
36-8	UAQ	#5, 0.711	0.216	0.180	0.221
			0.221	0.186	0.223 $r_{\text{rad}} = 0.222$
36-9	UAQ	#1, 0.656	0.220	0.188	0.217
36-10	UAQ	#1, 0.656	0.224	0.200	0.220
36-11	UAQ	#1, 0.656	0.210	0.175	0.214
36-12	UAQ	#1, 0.656	0.208	0.185	0.216
36-13	UAQ	#1, 0.656	0.215	0.180	0.218
36-14	UAQ	#1, 0.656	0.213	0.168	0.210
			0.215	0.183	0.216 $r_{\text{rad}} = 0.2155$
36-15	UAQ	#2, 0.508	0.206	0.183	0.210
36-16	UAQ	#2, 0.508	0.209	0.175	0.215
36-17	UAQ	#2, 0.508	0.212	0.180	0.209
36-18	UAQ	#2, 0.508	0.207	0.177	0.216
36-19	UAQ	#2, 0.508	0.205	0.172	0.211
36-20	UAQ	#2, 0.508	0.200	0.190	0.214
			0.206	0.179	0.212 $r_{\text{rad}} = 0.209$
36-21	UAQ	#3, 0.336	0.192	0.185	0.204
36-22	UAQ	#3, 0.336	0.195	0.172	0.198
36-23	UAQ	#3, 0.336	0.196	0.183	0.201
36-24	UAQ	#3, 0.336	0.201	0.188	0.205
			0.196	0.182	0.202 $r_{\text{rad}} = 0.199$

TABLE C-2 (Continued)

Run #	Propellant	Screen # Flux Ratio	Initial Rate With Rad.	No Radiation	With Radiation
37-1	UAX	None, 1	0.207	0.172	0.209
37-2	UAX	None, 1	0.222	0.176	0.218
37-3	UAX	None, 1	0.213	0.169	0.214
37-4	UAX	None, 1	0.203	0.158	0.210
37-5	UAX	None, 1	0.212	0.167	0.215
37-6	UAX	None, 1	0.208	0.161	0.202
37-7	UAX	None, 1	0.209	0.171	0.215
			0.211	0.168	0.212
					$r_{rad} = 0.2115$
37-8	UAX	#5, 0.714	0.202	0.164	0.198
37-9	UAX	#5, 0.714	0.200	0.160	0.205
37-10	UAX	#5, 0.714	0.196	0.158	0.193
37-11	UAX	#5, 0.714	0.203	0.167	0.197
37-12	UAX	#5, 0.714	0.191	0.157	0.194
			0.198	0.161	0.197
					$r_{rad} = 0.1975$
37-13	UAX	#1, 0.656	0.193	0.161	0.198
37-14	UAX	#1, 0.656	0.201	0.169	0.197
37-15	UAX	#1, 0.656	0.195	0.160	0.199
37-16	UAX	#1, 0.656	0.191	0.157	0.195
			0.195	0.162	0.197
					$r_{rad} = 0.196$
37-17	UAX	#2, 0.508	0.188	0.172	0.189
37-18	UAX	#2, 0.508	0.193	0.168	0.186
37-19	UAX	#2, 0.508	0.186	0.157	0.190
37-20	UAX	#2, 0.508	0.192	0.165	0.191
37-21	UAX	#2, 0.508	0.195	0.160	0.192
			0.191	0.164	0.190
					$r_{rad} = 0.1905$
37-22	UAX	#3, 0.336	0.185	0.155	0.188
37-23	UAX	#3, 0.336	0.182	0.166	0.183
37-24	UAX	#3, 0.336	0.179	0.164	0.185
37-25	UAX	#3, 0.336	0.181	0.168	0.183
37-26	UAX	#3, 0.336	0.177	0.160	0.175
37-27	UAX	#3, 0.336	0.182	0.163	0.177
			0.181	0.163	0.182
					$r_{rad} = 0.1815$

TABLE C-2 (Continued)

Run #	Propellant	Screen # Flux Ratio	Initial Rate With Rad.	No Radiation	With Radiation
38-1	UAY	None, 1	0.183	0.145	0.182
38-2	UAY	None, 1	0.175	0.136	0.178
38-3	UAY	None, 1	0.180	0.140	0.188
38-4	UAY	None, 1	0.182	0.143	0.176
38-5	UAY	None, 1	0.192	0.148	0.179
38-6	UAY	None, 1	0.170	0.136	0.175
			0.181	0.141	0.180
					$r_{\text{rad}} = 0.1805$
38-7	UAY	#5, 0.714	0.171	0.141	0.166
38-8	UAY	#5, 0.714	0.174	0.146	0.168
38-9	UAY	#5, 0.714	0.169	0.139	0.175
			0.171	0.142	0.169
					$r_{\text{rad}} = 0.170$
38-10	UAY	#1, 0.656	0.167	0.151	0.164
38-11	UAY	#1, 0.656	0.174	0.149	0.170
38-12	UAY	#1, 0.656	0.168	0.145	0.165
38-13	UAY	#1, 0.656	0.160	0.139	0.168
38-14	UAY	#1, 0.656	0.158	0.131	0.163
38-15	UAY	#1, 0.656	0.164	0.145	0.172
			0.165	0.143	0.167
					$r_{\text{rad}} = 0.166$
38-16	UAY	#2, 0.508	0.155	0.135	0.165
38-17	UAY	#2, 0.508	0.160	0.145	0.153
38-18	UAY	#2, 0.508	0.162	0.140	0.163
38-19	UAY	#2, 0.508	0.158	0.138	0.160
			0.159	0.139	0.160
					$r_{\text{rad}} = 0.1595$
38-20	UAY	#3, 0.336	0.157	0.130	0.150
38-21	UAY	#3, 0.336	0.154	0.145	0.149
38-22	UAY	#3, 0.336	0.159	0.152	0.165
38-23	UAY	#3, 0.336	0.152	0.149	0.161
38-24	UAY	#3, 0.336	0.148	0.138	0.147
38-25	UAY	#3, 0.336	0.156	0.137	0.153
			0.154	0.142	0.154
					$r_{\text{rad}} = 0.154$

TABLE C-2 (Continued)

Run #	Propellant	Screen # Flux Ratio	Initial Rate With Rad.	No Radiation	With Radiation
39-1	UBZ	None, 1	0.570	0.530	0.560
39-2	UBZ	None, 1	0.565	0.528	0.568
39-3	UBZ	None, 1	0.555	0.535	0.562
39-4	UBZ	None, 1	0.572	0.545	0.564
			0.565	0.534	0.563 $r_{\text{rad}} = 0.564$
39-5	UCA	None, 1	0.605	0.565	0.595
39-6	UCA	None, 1	0.590	0.570	0.608
39-7	UCA	None, 1	0.610	0.575	0.605
39-8	UCA	None, 1	0.595	0.568	0.607
			0.600	0.569	0.604 $r_{\text{rad}} = 0.602$

TABLE C-3

Summary of Transient Burning Rate  
Data for Propellant UBU

Run Number	Driving Frequency Hz	Transducer Output (volt) RMS	Phase Angle (deg.)	Frequency Parameter Dimensionless
1007	120	0.120	64	90.24
1008	144	0.100	68	109.28
1009	120	0.115	56	90.24
1010	120	0.180	50	90.24
1011	66	0.395	57	49.63
1012	48	0.430	40	36.10
1013	33	0.440	20	24.87
1014	10	0.600	0	7.52
1015	10	0.630	0	7.52
1016	5	0.530	0	3.76
1102	30	0.485	24	22.55
1103	11	0.590	15	8.27
1104	15	0.630	0	11.28
1105	20	0.580	0	15.04
1106	27	0.550	10	20.30
1107	83	0.330	30	64.42
1108	95	0.200	44	71.44
1109	100	0.270	50	75.20
1110	110	0.190	58	82.72
1114	154	-0-	53	115.81
1115	67	0.350	48	50.38
1116	60	0.450	53	45.17
1117	40	0.480	56	30.08
1118	24	0.540	60	18.05
1119	72	0.390	56	54.15
1120	36	0.500	48	27.07
1121	10	0.590	30	7.52
1122	20	0.550	10	15.04
1123	7	0.540	55	5.26
1202	50	0.360	42	37.60
1203	50	0.480	30	37.60
1204	55	0.450	50	41.36
1205	60	0.380	44	45.10

TABLE C-3 (con't)

Run Number	Driving Frequency Hz	Transducer Output (volt) RMS	Phase Angle (deg.)	Frequency Parameter Dimensionless
1206	62	0.330	38	46.62
1207	64	0.360	36	48.13
1208	67	0.320	42	50.38
1209	69	0.270	36	51.89
1210	40	0.490	26	30.08
1211	27	0.500	19	20.30
1212	24	0.500	14	18.05
1213	20	0.570	10	15.04
1214	15	0.550	10	11.28
1215	10	0.560	0	7.52
1216	8	0.570	0	6.02
1218	4	0.440	0	3.01
1220	18	0.540	0	13.54
1221	22	0.550	10	16.54
1222	26	0.520	12	19.55
1223	20	0.590	16	15.04
1301	44	0.390	44	33.10
1310	66	0.310	58	49.60
1311	82	0.270	54	61.60
1312	90	0.180	56	67.60
1313	110	0.210	44	82.70
1314	110	0.140		82.70
1315	125	0.100	58	94.00
1318	45	0.430	34	33.80
1402	40	0.550	--	30.10
1403	30	0.620	--	22.55
1405	50	0.470	48	37.60
1406	50	0.520	58	37.60
1410	90	0.250	60	67.60
1411	85	0.350	52	63.90
1412	110	0.280	60	82.70
1413	128	0.160	61	96.20
1414	150	0.140	70	112.90
1415	105	0.280	60	79.00
1416	70	0.390	40	52.60
1417	40	0.520	46	30.10

TABLE C-3 (con't)

Run Number	Driving Frequency Hz	Transducer Output (volt) RMS	Phase Angle (deg.)	Frequency Parameter Dimensionless
1418	40	0.560	34	30.10
1420	35	0.600	30	26.32
1421	30	0.550	26	22.55
1424	45	0.510	26	33.85
1425	20	0.600	20	15.04
1426	10	0.570	6	7.52
1427	10	0.570	10	7.52

TABLE C-4

Summary of Transient Burning Rate  
Data for Propellant UCX

Run Number	Driving Frequency Hz	Transducer Output (volt) RMS	Phase Angle (deg.)	Frequency Parameter Dimensionless
1027	9.5	0.165	0	5.39
1028	18	0.260	0	10.22
1029	40	0.410	5	22.72
1030	52	0.580	18	29.54
1032	80	0.310	55	45.44
1033	110	0.200	60	62.48
1034	134	0.160	65	76.11
1035	150	0.100	70	85.20
1036	100	0.220	50	56.80
1147	50	0.540	10	28.40
1148	66	0.600	43	37.49
1148b	80	0.320	43	45.44
1149	90	0.220	53	51.12
1150	96	0.210	58	54.53
1151	100	0.185	54	56.80
1152	115	0.140	50	65.32
1153	118	0.100	56	67.02
1154	134	0.070	54	76.11
1155	154	-0-	43	87.47
1156	156	-0-	50	88.61
1157	118	0.090	46	67.02
1158	93	0.190	36	52.82
1159	88	0.240	38	49.98
1160	60	0.470	40	34.08
1161	66	0.420	45	37.49
1162	54	0.700	8	30.67
1163	50	0.530	0	28.40
1164	27	0.330	0	15.34
1165	19	0.290	0	10.29
1166	5	0.100	0	2.84
1225	16	0.280	0	9.09
1226	19	0.310	0	10.79



TABLE C-4 (con't)

Run Number	Driving Frequency Hz	Transducer Output (volt) RMS	Phase Angle (deg.)	Frequency Parameter Dimensionless
1227	27	0.330	0	15.34
1228	29	0.370	5	16.47
1229	36	0.440	2	20.45
1230	40	0.450	0	22.72
1231	42	0.550	0	23.86
1232	48	0.690	15	27.26
1233	50	0.600	15	28.40
1234	50	0.650	10	28.40
1235	48	0.680	8	27.26
1236	43	0.650	12	24.42
1237	52	0.720	20	29.54
1238	56	0.640	24	31.81
1239	56	0.580	18	31.81
1242	72	0.430	43	40.90
1243	75	0.470	55	42.60
1244	84	0.250	40	47.71
1330	58	0.500	15	32.94
1332	66	0.450	14	37.49
1334	72	0.380	30	40.90
1335	102	0.150	45	57.94
1336	134	0.120	50	76.11
1337	110	0.130	45	62.48
1338	125	0.080	51	71.00
1339	66	0.450	42	37.49
1341	77	0.320	43	43.74
1342	58	0.460	44	32.94
1343	56	0.480	11	31.81
1351	62	0.410	16	35.22
1354	54	0.440	20	30.67
1355	66	0.410	32	37.49
1356	62	0.380	26	35.22
1428	10	0.150	0	5.68
1432	26	0.350	0	14.77
1436	36	0.400	0	20.45
1440	48	0.570	6	27.26
1444	56	0.590	26	31.80
1452	72	0.500	32	40.90
1456	77	0.470	48	43.74

TABLE C-5

Summary of Transient Burning Rate  
Data for Propellant UAX

Run Number	Driving Frequency Hz	Transducer Output (volt) RMS	Phase Angle (deg.)	Frequency Parameter Dimensionless
1037	6	0.165		1.71
1038	22	0.300		6.27
1039	40	0.310	18	11.40
1040	84	0.240	30	23.94
1041	100	0.200	36	28.50
1042	120	0.160	46	34.20
1043	140	0.125	54	39.90
1044	144	0.100	52	41.04
1045	100	0.195	42	28.50
1046	40	0.315	12	11.40
1047	20	0.290	0	5.70
1048	8	0.200	0	2.28
1167	33	0.320	14	9.41
1168	31	0.310	10	8.84
1169	13	0.245	1	3.71
1170	3.3	0.120		0.94
1171	25	0.310	8	7.13
1172	27	0.305	10	7.70
1173	50	0.290	24	14.25
1174	67	0.260	30	19.10
1175	72	0.230	33	20.52
1176	77	0.215	36	21.95
1177	80	0.200	32	22.80
1178	96	0.195	38	27.36
1179	110	0.160	42	31.35
1180	118	0.170	44	33.63
1181	133	0.090	46	37.91
1182	143	0.050	48	40.76
1183	154	0.040	58	43.89
1184	45	0.290	20	12.83
1185	22	0.285	8	6.27
1186	8.8	0.190	0	2.51
1187	17	0.265	2	4.85
1188	54	0.275	18	15.39
1189	75	0.245	30	21.38

TABLE C-5 (con't)

Run Number	Driving Frequency Hz	Transducer Output (volt) RMS	Phase Angle (deg.)	Frequency Parameter Dimensionless
1245	13	0.250	4	3.71
1246	16	0.270	6	4.56
1247	20	0.300	8	5.70
1248	27	0.320	6	7.70
1249	40	0.310	16	11.40
1250	42	0.310	17	11.97
1251	47	0.320	18	13.40
1252	50	0.290	20	14.25
1253	56	0.280	24	15.96
1254	63	0.270	28	17.96
1255	65	0.260	24	18.53
1256	66	0.270	27	18.81
1257	70	0.245	26	19.95
1258	80	0.230	28	22.80
1259	100	0.190	40	28.50
1260	105	0.180	41	29.93
1261	133	0.090	44	37.91
1262	50	0.290	21	14.25
1263	27	0.315	7	7.70
1264	10	0.230	0	2.85

TABLE C-6

Summary of Transient Burning Rate  
Data for Propellant UCW

Run Number	Driving Frequency Hz	Transducer Output (volt) RMS	Phase Angle (deg.)	Frequency Parameter Dimensionless
1059	40	0.200		18.08
1060	11	0.180	0	4.97
1061	28	0.200	0	12.66
1062	50	0.190	2	22.60
1063	80	0.170	12	36.16
1064	80	0.220	8	36.16
1065	120	0.150	16	54.24
1066	110	0.160	20	49.72
1067	116	0.145	28	52.43
1068	80	0.210	14	36.16
1069	32	0.190	3	14.46
11-112	100	0.180	8	45.20
11-113	77	0.190	4	34.80
11-114	50	0.200	0	22.60
11-115	53	0.210	0	23.96
11-116	72	0.220	4	32.54
11-117	80	0.300	6	36.16
11-118	100	0.180	9	45.20
11-119	105	0.150	9	47.46
11-120	110	0.100	13	49.72
11-121	118	0.170	13	53.34
11-122	105	0.140	16	47.46
11-123	90	0.160	9	40.68
11-128	83	0.350	3	37.57
11-129	56	0.220	2	25.31
11-130	33	0.210	0	14.92
11-131	17	0.200		7.68
11-132	8	0.180		3.62
11-133	13	0.190		5.88
11-134	47	0.220		21.24
1460	71.4	0.240		32.27
1461	110	0.160		49.72
1462	154	0.080		69.61
1463	167	0.020		75.48

TABLE C-7

Summary of Transient Burning Rate  
Data for Propellant UCV

Run Number	Driving Frequency Hz	Transducer Output (volt) RMS	Phase Angle (deg.)	Frequency Parameter Dimensionless
1049	20	0.465	0	2.128
1050	10	0.450	0	1.064
1051	34	0.480	5	3.620
1052	56	0.485	7	5.960
1053	80	0.500	22	8.510
1054	80	0.520	20	8.510
1055	120	0.455	24	12.770
1056	120	0.450	26	12.770
1057	130	0.475	30	13.830
1058	150	0.470	32	15.960
1190	70	0.500	14	7.450
1191	74	0.480	10	7.870
1192	83	0.500	20	8.830
1193	100	0.470	0	10.640
1194	110	0.480	20	11.700
1195	125	0.450	22	13.300
1196	134	0.440	26	14.260
1197	167	0.420	34	17.770
1198	148	0.420	0	15.750
1199	100	0.480	16	10.640
11-100	91	0.510	17	9.680
11-101	67	0.480	12	7.130
11-103	24	0.470	0	2.550
11-105	20	0.460	4	2.130
11-106	13	0.460	0	1.380
11-107	5	0.440	0	0.532
11-108	9	0.450	0	0.958
11-109	20	0.480	0	2.730
11-110	57	0.490	8	6.060
11-111	80	0.510	14	8.512

UNCLASSIFIED

Security Classification

## DOCUMENT CONTROL DATA - R &amp; D

(Security classification of title, body of abstract and indexing annotation must be entered when the overall report is classified)

1. ORIGINATING ACTIVITY (Corporate author) <b>University of Utah Chemical Engineering Department Salt Lake City, Utah 84112</b>		2a. REPORT SECURITY CLASSIFICATION <b>UNCLASSIFIED</b>	
		2b. GROUP	
3. REPORT TITLE <b>The Response of a Burning Solid Propellant Surface to Thermal Radiation</b>			
4. DESCRIPTIVE NOTES (Type of report and inclusive dates) <b>Scientific Interim</b>			
5. AUTHOR(S) (First name, middle initial, last name) <b>Mihlfeith, C. Max; Baer, Alva D.; Ryan, Norman W.</b>			
6. REPORT DATE <b>1 August 1971</b>		7a. TOTAL NO. OF PAGES <b>146</b>	7b. NO. OF REFS <b>82</b>
8a. CONTRACT OR GRANT NO. <b>AF-AFOSR-1656-69</b>		9a. ORIGINATOR'S REPORT NUMBER(S)	
b. PROJECT NO. <b>9711-01</b>			
c. <b>61102F</b>		9b. OTHER REPORT NO(S) (Any other numbers that may be assigned this report)	
d. <b>681308</b>		<b>AFOSR-TR-71-2664</b>	
10. DISTRIBUTION STATEMENT			
11. SUPPLEMENTARY NOTES <b>Tech, Other</b>		12. SPONSORING MILITARY ACTIVITY <b>AF Office of Scientific Research (SREP) 1400 Wilson Boulevard Arlington, Virginia 22209</b>	
13. ABSTRACT <p>A new technique for the study of processes related to propellant combustion instability has been employed in which burning rate variations produced by a periodic radiant heat flux are measured. The phase angle between the perturbing flux and the burning rate response and the dependence of the magnitude of the response on the driving frequency are obtained. As the frequency of the perturbing flux increases, magnitude of the reaction is observed to first increase and then to pass through a maximum.</p> <p>In general, the experimental results tend to confirm the theoretical models for transient burning rate response, although the observed maximums in the response functions appear to occur at higher frequencies than is predicted by the simpler gas-phase models. The technique for measuring the response function by periodic input of energy to the burning surface holds great promise as a method for characterizing a propellant. Not only are the results reproducible for a given propellant, but minor formulation variations produce measurable changes in the response. This technique has a great advantage over test-burner methods because the driving frequency can be varied over a wide range and the total response function can be obtained.</p>			

DD FORM 1473  
1 NOV 65

UNCLASSIFIED

Security Classification

UNCLASSIFIED

Security Classification

14	KEY WORDS	LINK A		LINK B		LINK C	
		ROLE	WT	ROLE	WT	ROLE	WT
	<p>Solid Propellant Combustion</p> <p>Combustion Instability</p> <p>Propellant Response Function</p> <p>Solid Propellant Response to Thermal Radiation</p>						

UNCLASSIFIED

Security Classification